METHODOLOGY FOR FAULT DETECTION AND DIAGNOSTICS IN AN OCEAN TURBINE USING VIBRATION ANALYSIS AND MODELING

by

Mustapha Mjit

A Thesis Submitted to the Faculty of

The College of Engineering and Computer Science

in Partial Fulfillment of the Requirements for the Degree of

Master of Science

Florida Atlantic University

Boca Raton, Florida

December 2009

METHODOLOGY FOR FAULT DETECTION AND DIAGNOSTICS IN AN OCEAN TURBINE USING VIBRATION ANALYSIS AND MODELING

by

Mustapha Mjit

This thesis was prepared under the direction of the candidate's thesis advisor, Dr. Pierre-Philippe Beaujean, Department of Ocean and Mechanical Engineering, and has been approved by the members of his supervisory committee. It was submitted to the faculty of the College of Engineering and Computer Science and was accepted in partial fulfillment of the requirements for the degree of Master of Science.

SUPERVISORY COMMITTEE:

Pierre-Philippe Beaujean, Ph.D.
Thesis Advisor

Nikolaos Xiros, Ph.D.

Frederick Driscoll, Ph.D.

David Venditti, Ph.D.

Mohammad Ilyas, Ph.D.
Chair, Department of Ocean and Mechanical Engineering

Karl K. Stevens, Ph.D., P.E.
Dean, College of Engineering and Computer Science

Barry T. Rosson, Ph.D.
Dean, Graduate College

November 25, 2009
Date

ACKNOWLEDGEMENTS

First, I would like to thank my advisor Dr. Pierre-Philippe Beaujean for his inestimable guidance and personal support since the beginning of my research work. His invaluable suggestions at difficult times have contributed a lot towards the success of this thesis.

I would like to thank Dr. Vendittis for his constant support, motivation, and valuable advice. I have benefited immensely from his knowledge and experience.

I would also like to thank Dr. Xiros and Dr. Driscoll for their guidance and constructive criticism during the preparation of this thesis.

I am very grateful to my colleagues khaled Kaiser and Mico Pajovic for their support and friendship. I also want to thank Caitlin Slezycki, who was always available and willing to help with the laboratory experimental setup.

Lastly, I am eternally grateful to my parents for the love, support, and encouragement that have helped to make everything I have accomplished possible.

ABSTRACT

Author: Mustapha Mjit

Title: Methodology for fault detection and diagnostics in an ocean turbine using vibration analysis and modeling.

Institution: Florida Atlantic University

Thesis Advisor: Dr. Pierre-Philippe Beaujean

Degree: Master of Science in Ocean Engineering

Year: 2009

This thesis describes a methodology for mechanical fault detection and diagnostics in an ocean turbine using vibration analysis and modeling. This methodology relies on the use of advanced methods for machine vibration analysis and health monitoring. Because of some issues encountered with traditional methods such as Fourier analysis for non stationary rotating machines, the use of more advanced methods such as Time-Frequency Analysis is required. The thesis also includes the development of two LabVIEW models. The first model combines the advanced methods for on-line condition monitoring. The second model performs the modal analysis to find the resonance frequencies of the sub-systems of the turbine. The dynamic modeling of the turbine using Finite Element Analysis is used to estimate the baseline of vibration signals in sensors locations under normal operating conditions of the turbine. All this information is necessary to perform the vibration condition monitoring of the turbine.

METHODOLOGY FOR FAULT DETECTION AND DIAGNOSTICS IN AN OCEAN TURBINE USING VIBRATION ANALYSIS AND MODELING

LIST OF FIGURES

List of Tables

1. INTRODUCTION AND OBJECTIVES

This thesis discusses traditional and more advanced approaches, procedures and techniques to evaluate the health of ocean turbines, such as the 20 KW turbine developed at Florida Atlantic University, based on monitored vibration data. Such methods have shown to be efficient for evaluating equipment component health, provided the data are properly acquired and the thresholds are properly set. The thesis work is a sub-component of the ocean energy project at the Center of Ocean Energy and Technology at FAU (COET).

The overall thesis objective is to develop a proper methodology of combining numerical Finite Element Modeling and modern vibration techniques for condition monitoring and faults diagnosis of the 20 KW turbine. A LabVIEW model for on-line vibration condition monitoring that contains the most advanced diagnostic techniques features was developed. A Finite Element Modeling (FEM) and simulation of the ocean energy turbine was performed to study state condition; the modeling was used to determine the baseline of the vibration data in its normal operating conditions and to determine the resonance frequencies of its sub-components.

The specific efforts discussed in this thesis are:

- The development of a LabVIEW model that acquires the vibration data from accelerometers and encoders and normalizes and analyzes these data in real time.

This model includes time domain signal, power spectrum, power cepstrum, fractional octave, Time-Frequency analysis, kurtosis analysis, RMS value and crest factor. This model contains threshold for alarm criteria for each technique mentioned above that allows comparing the actual acquired vibration data to the baselines for inception fault detection.

- The development of a LabVIEW model that performs the modal analysis testing in order to find the resonance frequencies and mode shapes of the structures.
- To perform finite element modeling and simulation on ANSYS of the ocean energy turbine. This simulation leads to an estimation of a baseline for the vibration data under the normal operating conditions of the turbine.
- The modeling on ANSYS of the sub-systems (shaft, motor, shell among others) of the turbine to estimate their resonance frequencies and mode shapes.
- The demonstration of the vibration condition monitoring strategy and diagnostic techniques proposed in this thesis on a simple "fan" system as an intermediate step for the test bench (dynamometer). Real time data patterns, profiles and trends are obtained by processing vibration signals acquired from various points on the test bench. The purpose of this experiment is to test and demonstrate the diagnostic techniques implemented in the LabVIEW model.
- The analysis of vibration data collected and interpretation of results.
- To diagnose system problems using time domain, frequency domain, time-frequency domain, crest factor, kurtosis analysis and resonance testing.

Vibration condition monitoring using a LabVIEW model and data acquisition systems indicates the mechanical state of the equipment and allows to accurately identify the

trends of a developing component problem in advance of catastrophic failure. This assumes that the changes in the structural vibration response are caused by deterioration in the condition of the turbine. However, due to changing rotational speed, the measured signal may be non-stationary and difficult to interpret. For this reason, the ordering (normalization) technique - which relates the vibration to the machine speed - is introduced and implemented in the LabVIEW program. The advantage of this ordering technique is the ability to clearly identify non-stationary vibration data from data caused by the inception of anomalies in the system.

In this thesis, a vibration data acquisition and fault diagnostic techniques are introduced and tested on a simple system ”fan” for eventual use on the dynamometer which mimics the prototype of the 20KW turbine. The vibration data acquisition system based on LabVIEW program is described in detail, six vibration sensors and one encoder are used. The vibration data acquisition system includes 8 channels for the accelerometers and 8 for encoders. The LabVIEW model can accomplish real-time data acquisition and analysis, off-line data analysis, trend analysis, fault detection. The common vibration faults such as unbalance and misalignment of the shaft and gears faults maybe detected on the prototype (dynamometer) if they exist.

This thesis is organized in 8 Chapters: Chapter 1 introduces the statement of the problem, background and objectives of the thesis. Chapter 2 provides a literature review of the state-of-the-art in vibration monitoring techniques. Chapter 3 describes of the two LabVIEW programs. One program contains the advanced diagnostic techniques and is used for dynamic vibration acquisition and analysis. The second program is used to perform the modal analysis testing of the structures. Chapter 4 introduces and describes

faults detection and diagnostic techniques for condition monitoring of the 20 KW turbine, their advantages and disadvantages. In this chapter, an efficient method for fault detection based on Short Time Fourier Transform (STFT) is presented. This method can be used for non-stationary rotating machines. Chapter 5 provides a brief description of the mean components of the turbine and their failure modes analysis, procedures for data acquisition and analysis using LabVIEW model and data acquisition system. Chapter 6 presents the results of the modal analysis testing on the small scale cylinder of the 20 KW turbine and validation with FEM results. Also, the modal analysis of the cylinder with different masses of the accelerometers was performed to determine the effects of the added mass on the modes. Chapter 7 presents the results of the simulation in ANSYS of the 20 KW turbine to approximate the baseline of the vibration data in normal operating condition in steady state. Conclusions and suggestions for future work are discussed in Chapter 8.

2. LITERATURE REVIEW

The 20 KW turbine is designed to generate electrical power from mechanical power in steady-state, and vice-versa in transient state: the turbine acts as a motor that transform the electrical power to mechanical power that is needed to rotate the blades at certain rpm to reach the steady-state. It is designed to work under variable dynamic loads, or in most cases under periodic loads. Thus, it is subjected to forced vibrations and hence dynamic stresses. Any change in the mechanical condition of the machine affects its dynamic conditions and thus the vibration behavior. Much has been written about vibration of electrical motors in many books and papers.

Nandi et al. [31] have classified the major faults in electrical machines: Bent shaft, bearing and gearbox failures. These faults produce one or more of the following symptoms: vibrations, increased torque pulsation, decreased average torque, increased losses and reduction in efficiency, excessive heating.

Tavner & Penman [31] and Rao [32] confirm that in many applications, the overall vibration levels are sufficient to diagnose mechanical failures in the machine. To diagnose a vibration problem, it is important to understand the root cause of the vibration: (1) How those forces are generated, (2) the resonance frequency that amplifies the response, and (3) how the motor react to transmit this force.

Some parameters can be monitored, such as oil debris analysis, temperature, pressure, flow, to determine the condition of the machine. One of the most powerful approaches to monitor rotating machinery is to monitor vibrations (Table 1). There is a large amount of information contained in the vibration signals that are obtained by monitoring at the various key points of a machine. These signals, however, can be very complex and even with today's state-of-the-art measurement techniques, there is still much to learn in order to be able to measure, display, and utilize the vibration data to its fullest potential for predictive maintenance purposes.

Parameter **Machine Fault**	**Vibration**	**Temperature**	**Pressure**	**Flow**	**Oil Analysis**
Unbalance	✓				
Misalignment/ Bent shaft	✓	✓			
Damaged Rolling Element Bearings	✓	✓			✓
Damaged Journal Bearings	✓	✓	✓	✓	✓
Damaged or Worn Gears	✓				✓
Mechanical Looseness	✓				

Table 1: Machine Fault vs. Parameter [12].

It is recommended that the monitoring of the health of the machine should be used using the combination of the techniques above, because sometimes the use of only vibration measurements will not perfectly assess the condition of the machine due to a

lack of understanding of machine dynamics and signal processing techniques. The measurement of vibration is still a very effective tool to determine machine condition, especially since it can detect abnormal operating conditions long before there is any permanent damage to the machine. This feature is often not possible when other more traditional techniques are used.

Predictive or condition based maintenance requires regular checks of key performance parameters, e.g. vibration, temperature, pressure and oil analysis. The signals from the accelerometers are measured, stored and trended to predetermine warning and alarm levels before remedial action is taken. The alert and alarm threshold levels are obtained from statistical data derived from a population of machines functioning correctly, or in the case of new types of equipment, from standards related to the size and horsepower of the machine.

Two papers by C.A.W. Glew [13] [14] describe the results obtained by the Canadian Navy using a portable octave Constant Percentage Band (CPB) analyzer for predictive maintenance. Vibration in general and octave CPB analysis in particular, still ranks as one of the best techniques for fault detection and it is fundamental to the machine-condition monitoring approach described in this thesis. Vibration analysis is the dominant technique used for predictive maintenance programs. This technique uses the noise or vibration created by mechanical equipment to detect machine problems. The gear mesh frequency is the rate at which gear teeth engage together and it is equal to the number of teeth on the gear times the revolutions-per-second (rps) of the gear. A gearbox always has a strong vibration component at the gear mesh frequency, which is usually the one observed in machinery monitoring to detect failures [40].

Faults detection and diagnostics techniques used for on-line vibration and health monitoring can be classified into the time and frequency domain methods based on the time signal and frequency spectrum, the Joint time-frequency domain methods, such as the Wigner-Ville Distribution (WVD) [29, 30].

Joint time-frequency domain methods include the Short Time Fourier Transform (STFT), and the Wigner-Ville Distribution (WVD) [29, 30]. The joint time-frequency methods provide an interactive relationship between time and frequency during the period of the time data window, and detect the damage of elements. The Wigner-Ville Distribution (WVD) could easily show instantaneous information of vibration energy changes. This advanced signal processing technique is well suited for faults detection in transient state or for non-stationary rotating machine.

The use of the cepstrum for fault detection and diagnostic has been found to be very efficient for detecting gearboxes and bearings faults, gearbox and bearing tend to produce many families of sidebands in their vibration spectra, due to the variety of the meshing frequencies and shaft speeds that may be present. The detection of many sidebands present in a complicated signal may be practically impossible using spectrum analysis, but using cepstrum, they can easily be determined. Randall [22] provides an example of the use of cepstrum applied to the gearbox.

The vibration monitoring is the key technique of fault detection and diagnostics, Caryn [23] proposes a method to enhance on-line vibration monitoring in induction machines by monitoring its electrics parameters (current, voltage and power).

The ordering technique is one of the important vibration analysis techniques for rotating machinery. The advantage of this technique consists of analyzing non-stationary noise

and vibration which may vary in frequency and amplitude with rotational speed of the shaft. For this purpose, a tachometer is needed to acquire the rotational data. The order technique allows to easily determining the fundamental rpm and its harmonics [22]. The ordering method can be performed in generally three different ways: 1) Fourier Transform based order tracking "FT-OT" suggested by Blough [25]. 2) Angle domain sampling based order tracking "AD-OT" proposed by Potter and Hewlett Packard [26]. 3) Vold-Kalman filter based order tracking "VKF-OT" [24]. The first order tracking method is most commonly used method, the disadvantage of this method is due to the frequency changing as function of time. Beside the three methods mentioned above, there is also the Gabor order tracking proposed by Pan et al. and Albright and Qian in 2006 [27]. We conclude that the order tracking approach is not a very effective tool to deal with the non-stationary vibration and noise, which vary in frequency and amplitude and is linked to the rpm of the shaft. However, VKF-OT is one of the best available techniques for performing OT.

Some faults are not mentioned above cause random or non-periodic vibration, these non-cyclic-faults are generated typically by severe wear, contaminants in or inadequate lubrication and sliding of the bearing and gearbox components [32].

3. LABVIEW MODELS DEVELOPED FOR ON-LINE VIBRATION CONDITION MONITORING

3.1. LabVIEW Model for Dynamic Measurements and Modal Analysis

The LabVIEW programs that have been developed can be easily configured and used for on-line vibration condition monitoring and rapidly processing large amounts of data to highlight new or unusual events like high vibration level that may signify a problem. This LabVIEW model in Figure 1 offers powerful, engineer-friendly features that users can apply systematically to monitor the health of the rotating machine. The user interface is simple and does not require the user to possess extensive process knowledge and an in-depth technical understanding of the code used. Also many other features can easily be added to the program if needed. Vibration analysis techniques used in this LabVIEW model are described in Chapter 4.

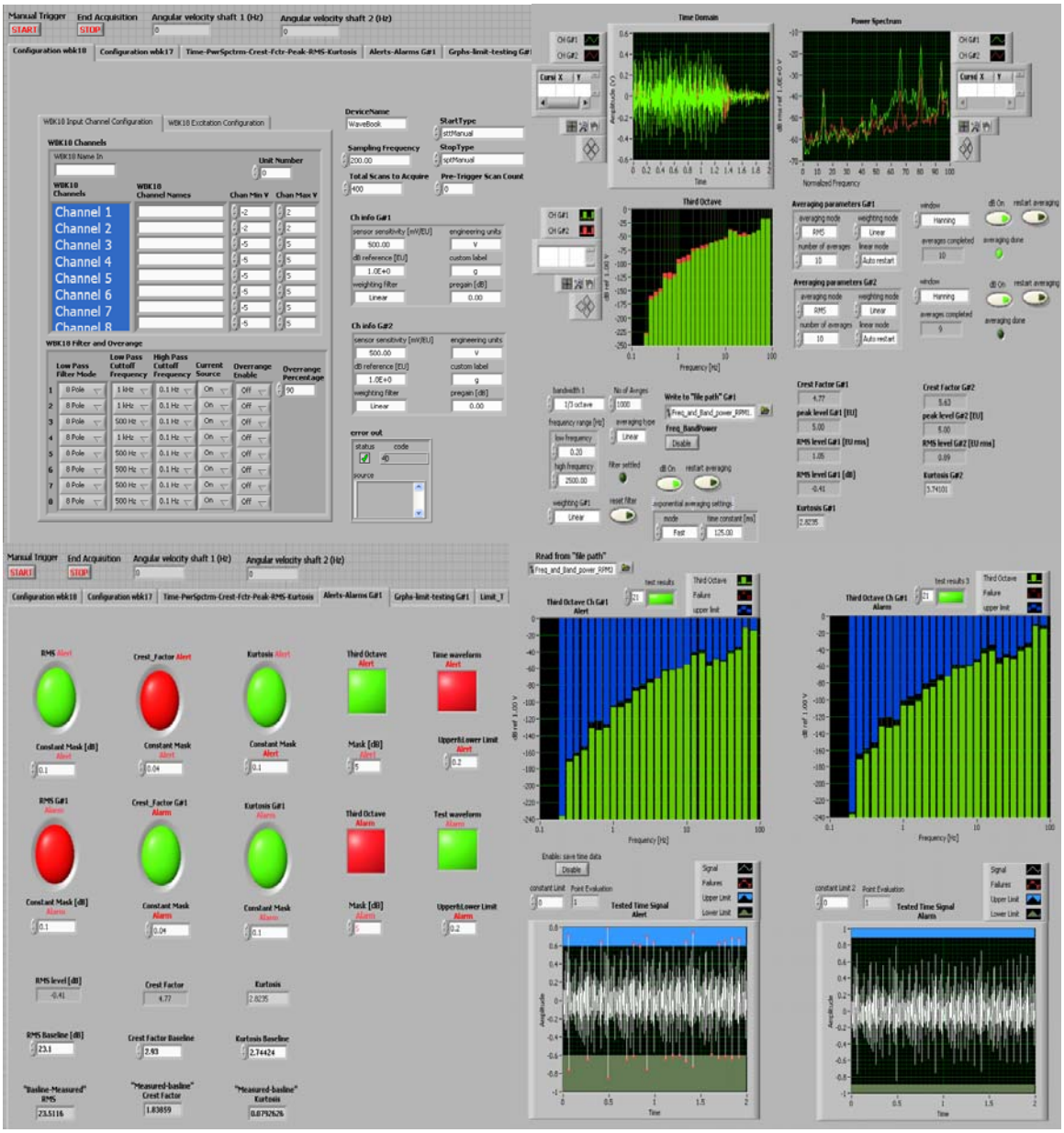

Figure 1: Overall system monitoring features of the LabVIEW model.

The first phase of the workflow is the data acquisition. This model includes a simple configuration designed with LabVIEW GUIs. The acquired data then can be saved in a variety of formats for post-processing, or can be processed in real time using powerful preprocessing tools. These tools allow the data to be analyzed, filtered, and refined to

precisely capture the characteristics of normal behavior and optimize the ability of this model to discriminate abnormalities.

The LabVIEW model performs the calculation of the overall vibration level (RMS, peak, crest factor, kurtosis), the computation of angular velocity using an analog tachometer signal and acquire the real-time spectral order analysis, apply the application of set points to the time data, power spectra and third octave (Figure 1).

The vibration data acquired from the accelerometers: RMS value, peak level, crest factor and spectra are calculated in real-time. If those vibrations exceed the baselines, a vibration alert is activated and stays on until the vibration levels decrease. The configuration window allows the setting of vibration limits that encompasses a normal working range, so that the power plant must shut down if this range is exceeded. While there is a natural spread of the vibration level around the baseline, this limit must be based on a suitable margin above the highest allowable vibration. This means that subtle changes in vibrations, due to noise, are much more difficult to detect.

In the configuration window, it is also possible to impose tighter threshold limits based on normal behavior. These tighter limits allow discriminating abnormalities (alert) before they become significant (alarm). This allows the identification of faults even when other variables are within the normal working range.

The vibration monitoring techniques mentioned above assume that the changes in the vibration data are caused by the deterioration in the condition of the rotating machine. However, due to the changes of the rotational speed, the vibration data measured by the accelerometers may be non-stationary and difficult to interpret, for this reason the order tracking technique was introduced. The order tracking relate the vibration data to the

machine speed and it allows to clearly identifying non-stationary vibration data excluding the influences from varying rotational speed.

A LabVIEW program has been developed to perform the resonance testing on any structure. This program acquires “raw” time domain data generated from the acquisition system, perform the required signal processing on the data and calculate the FRF for each test trial, then performs automatically the averages of the tests trials chosen.

3.2. LabVIEW Model for Tachometers Data Acquisition

The “IH 120” Incremental quadrature shaft encoder and WBK17 acquisition system are used to acquire the angular velocities of the shaft. The encoder has six outputs, A, B, Z and their complimentary. The signals A and B contain 1024 pulse per revolution and are in quadrature of phase. This phase relationship between A and B determines the direction of rotation of the shaft.

The signal Z contains one pulse per revolution, is used to measure the RPM. It can also be used as a reference to define the zero position. The output is a pulse signal that is generated when the encoder disk rotates, due to the rotation of the turbine shaft.

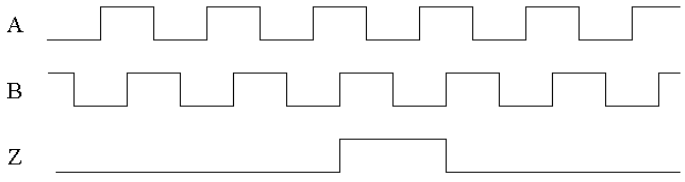

Figure 2: Quadrature encoder output: A, B and Z.

From those signal the angular velocity is calculated using the methods mentioned below [16, 18, and 19].

- **Method to measure the angular velocity: Frequency counting**

If p pulses are counted over the scan period T_s, then:

$$w(rad/s) = (2\pi \times p)/(1024 \times M \times T_s). \quad (3.1)$$

Where M is the encoder measurement mode, M=1, 2 or 4 for X1, X2 or X4 mode respectively.

In the encoder mode X1, only one rising or falling edge of signal A is used, in the encoder mode X2, both rising and falling edge of signal A are used. And encoder mode X4 uses rising and falling edge of both signal A and B.

The velocity resolution of the encoder using this method is:

$$dw_f = 2\pi/(1024 \times M \times T_s). \quad (3.2)$$

Where M=1, 2 or 3 for encoder measurement mode X1, X2 or X4, respectively. The details of the LabVIEW function for the encoder is given in Appendix-A.

4. VIBRATION ANALYSIS, FAULTS DETECTION AND DIAGNOSIS TECHNIQUES FOR ON-LINE CONDITION MONITORING OF THE 20 KW TURBINE

A practical system for on-line machine health monitoring of the 20 KW turbine comprises the sub-steps shown in Figure 3.

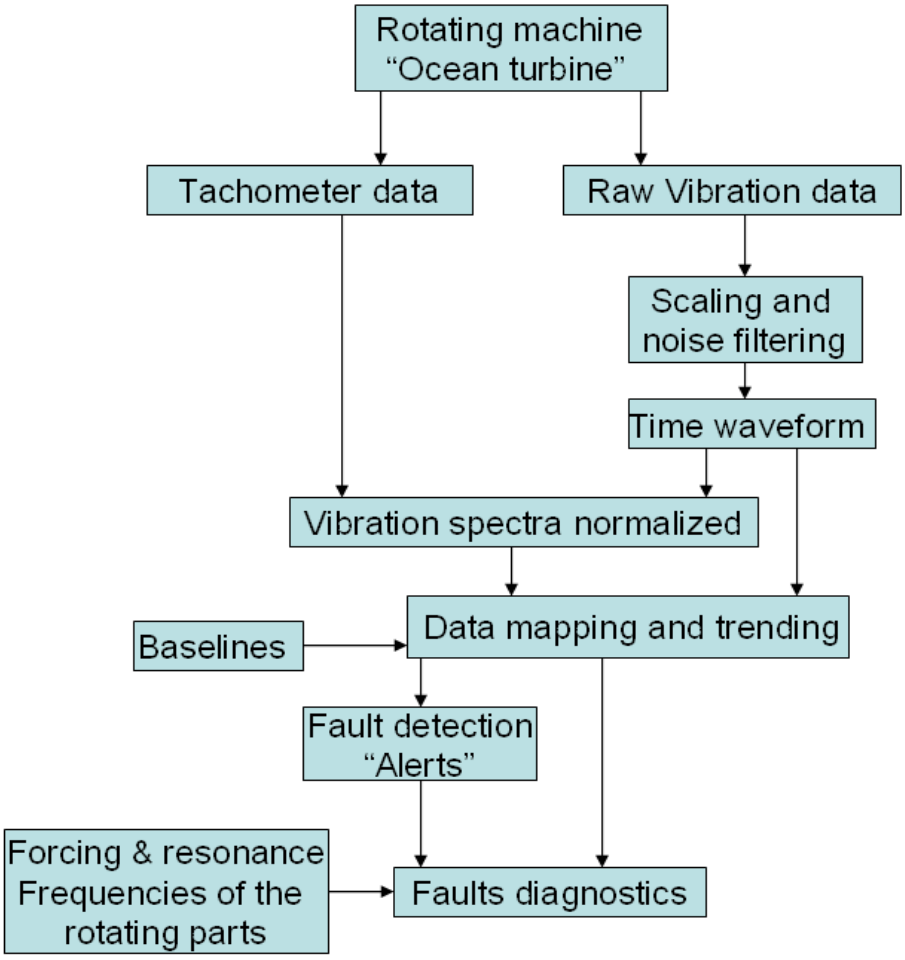

Figure 3: Subtasks for On-line Vibration Condition Monitoring.

After measuring machine vibration acceleration with accelerometers, the low pass filters can be used to filter the noise from the signal and to improve the signal-to-noise ratios. Then, the vibration signal should be ordered "normalized" with respect to the fundamental shaft speed using the data from the tachometer, this will allow to clearly identifying the non-stationary vibration data from the vibration caused by the presence of any anomalies. Taking several measurements of the turbine that operate normally in varying operating condition "steady state, transient state, when using the mechanical brake etc …" and using the vibration severity level standardized charts leads to a description of the normal behavior of the machine "baselines", baselines can also be estimated from the Finite Element Modeling. These baselines "signals and indicators" will be used to detect deviating vibration patterns "fault detection" by mean of alerts and alarms thresholds. Knowledge about the forcing frequencies of the rotating parts can be used for fault diagnostics "type, location, severity of the faults".

Vibration condition monitoring system can be accomplished using Fault detection and diagnostic methods. Fault detection is mainly concerned with detecting abnormal conditions in running machines. Fault diagnostics is the process of analyzing the data in order to determine precisely the type of the fault, its severity and its location.

This distinction between detection and diagnosis is very important, some analysis techniques mentioned below are well adapted for diagnosis but not for fault detection and vice-versa. Measurement techniques for fault detection are especially important as they indicate when to start the diagnosis, a time consuming process. However, some faults do not necessarily result in an increase of the overall level thresholds: a strong vibration component from another source can mask a change and the machine could very well fail

long before the fault can be detected, as shown in Figure 4 [12]. Therefore it is highly desirable to compare and trend the vibration data to a baseline spectrum. A baseline spectrum is derived by either measuring the vibration levels on a machine in its normal operating conditions or derived statistically from a population of similar machines.

Faults can be detected, and identified, by trending over equal intervals of time variations.

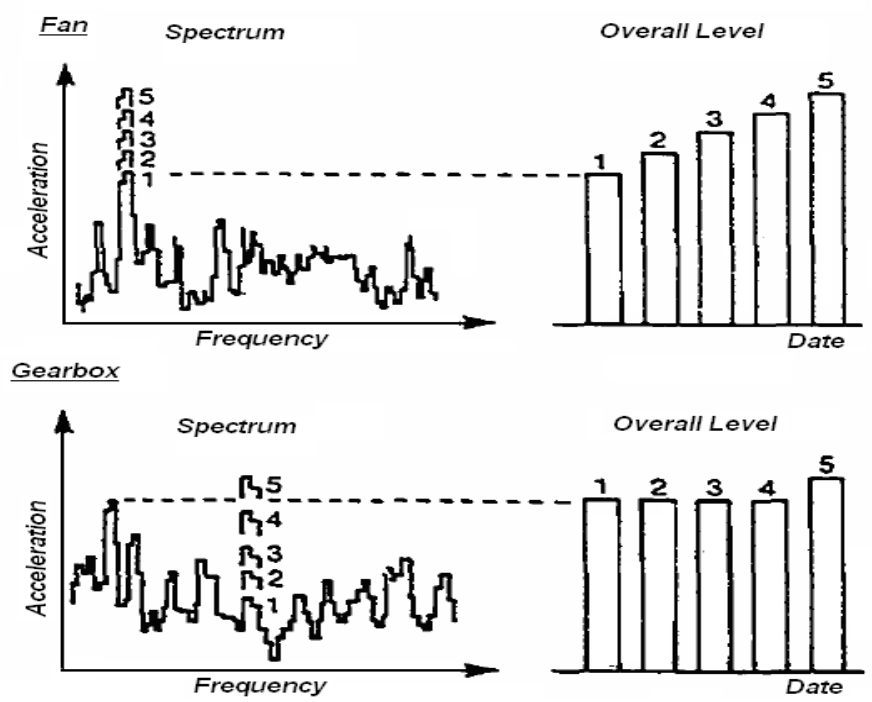

Figure 4: Vibration components at the gear mesh frequency masked by the component at the rotational frequency [12].

4.1. Time Based Vibration Analysis Techniques

Time-based analysis techniques currently available will be used for faults detection and diagnostic, as described in papers [15, 16]. All the analysis techniques used for faults detection and diagnostic are applied on the acquired acceleration of the vibration signal.

4.1.1. RMS Level Measurements

Overall level measurements using the root mean square (RMS) are the most common vibration measurement in use. It is important to measure true RMS and not the mean. The interpretation of RMS levels of vibrations can be performed using the ISO "International Standards Organization" vibration severity level standardized charts (Figure 5). In practice, the measurement parameter for this technique is the vibration velocity. Thus, the acceleration is converted to velocity by single integration in order to compute the RMS velocity and to use the vibration standardized chart below.

R.m.s. vibration velocity mm/sec	up to 15 kW Class I	15 to 75 kW Class II	> 75 kW (rigid) Class III	> 75 kW (soft) Class IV
0,28 (89 dB)	A	A	A	A
0,45 (93 dB)				
0,71 (97 dB)				
1,12 (101 dB)	B			
1,8 (105 dB)		B		
2,8 (109 dB)	C		B	
4,5 (113 dB)		C		B
7,1 (117 dB)	D		C	
11,2 (121 dB)		D		C
18 (125 dB)			D	
28 (129 dB)				D
45 (133 dB)				

Figure 5: Criteria zone vibration magnitude for different type of machines [17] [26].

Note that zone A, B, C and D refer to good, allowable, just tolerable and not permissible zones respectively.

The greatest limitation of this approach is the lack of sensitivity and information available in the data. Unless a problem is severe, the overall level measurements may not change significantly. Unfortunately the machine monitoring community has relied too heavily in the past on these measurements alone, resulting in unanticipated machine failure [17].

The RMS level is calculated over a time period analysis that should be set in the configuration window in the LabVIEW program. RMS level should be calculated over different time periods to separate the various faults components.

4.1.2. Peak Level Measurements

As an alternative to overall level, the peak level of the acceleration signal can be used. This is particularly useful for monitoring the change in the amount of impulsiveness, possibly due to increased bearing damage. However, on its own this method is not reliable, as other effects can also increase the peak level of a signal, but in conjunction with RMS level measurements it is a useful technique to identify bearing faults. A useful way of showing the data is shown in Figure 6.

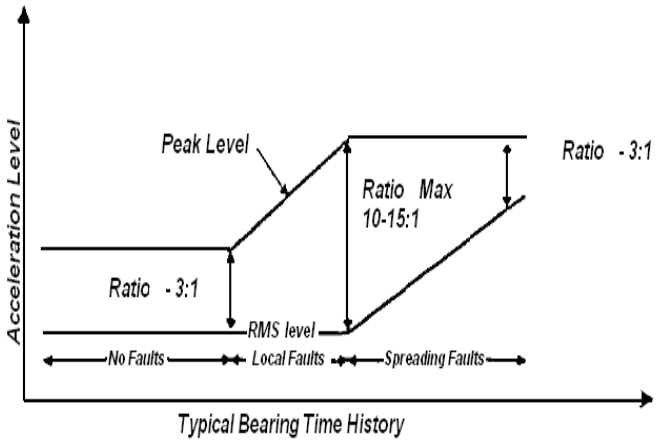

Figure 6: Trending Overall and Peak Level Acceleration for Bearing Fault Detection [17].

4.1.3. Crest Factor

The time waveform of a bearing in good health is mostly random. As bearing damage increases, the waveform becomes far more impulsive, with higher peak levels. The crest factor (CF) is the ratio of the peak level to the RMS level. A useful chart for showing

developing faults is shown in Figure 7. The chart may also be used for showing the distribution of a population of similar bearings.

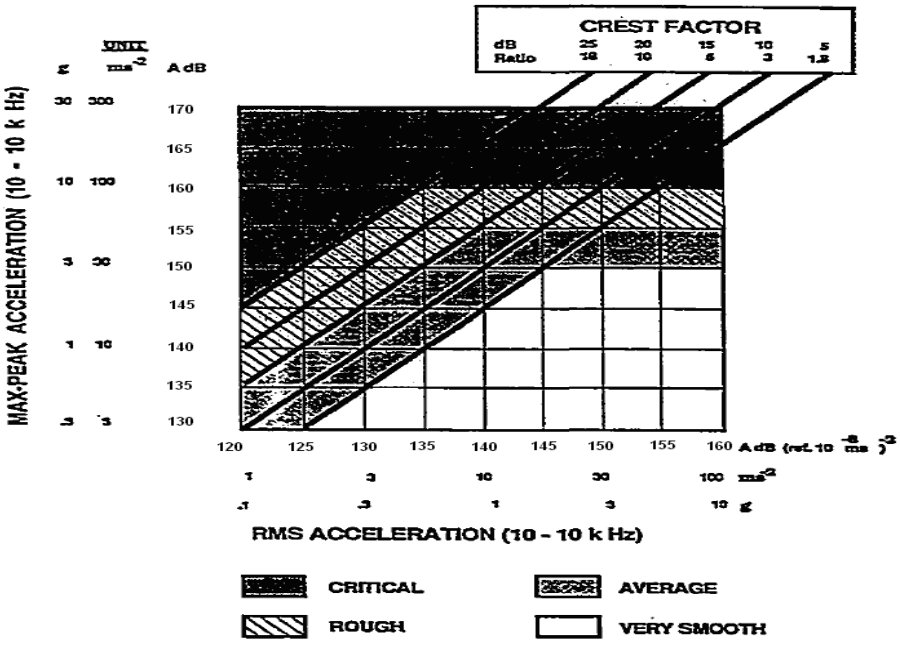

Figure 7: Bearing severity chart [17].

4.1.4. Time Waveform

Most of the defects encountered in the rotating machinery give rise to a distinct vibration pattern (vibration signature) and hence most faults can be identified using vibration signature analysis techniques. It is difficult to use this technique in isolation; however it can be a very helpful tool in combination with others. The frequency components of the fault can be determined from the time spacing between the impacts (f=1/T). However, the sampled time period should be set so that it is greater than at least two revolutions of the shaft to be measured (generally 6 to 10 revolutions per sampled period is good enough). The formula to calculate the sampled time period is:

$$T_s[s] = \frac{60 \times N}{RPM}. \tag{4.1}$$

Where T_s the total sample period in second, N is generally between 6 to 10 revolutions, RPM is the number of revolutions per minute of the shaft. This method has been found to be a reliable technique for identifying bearing faults [20]. Time waveform can be used effectively to enhance spectral information in the following applications:

- Low speed applications (less than 100 RPM).
- Indication of true amplitude in situations where impacts occur such as assessment of rolling element bearing defect severity.
- Different faults will cause high vibrations at the same frequency.
- Lot of noise is present in the signal.

Time waveform can be used especially to detect bearings and gearbox faults, but does not give accurate result for unbalance and misalignment anomalies. In this case, other techniques such as power spectrum analysis of the signal are preferred.

4.1.5. Kurtosis

Kurtosis is a statistical parameter, derived from the fourth statistical moment about the mean of the probability distribution function of the vibration signal and is an indicator of the peakedness of that function. The kurtosis technique has the major advantage that the calculated value is independent of load or speed variations. The kurtosis analysis is a good parameter for faults and transient effect detection, but it does not give any indication of the diagnosis of the problem [18, 19]. The kurtosis will be equal to 3 for healthy machine and greater than 3 if the machine presents some faults. The general definition of the kurtosis is,

$$Kurtosis = \frac{\sum_{i=1}^{n}\left(x_i - \bar{x}\right)^4}{(n-1)\times\sigma^2}. \quad (4.2)$$

Where $x_1, x_2 .. \ x_n$ are the population data of the signal, $\bar{x}$ is the mean of x, and σ is the variance of x. n is the number of samples.

4.2. Frequency-Based Vibration Analysis Techniques

The following is a description of frequency based vibration analysis techniques available for fault detection and diagnostic. Typical frequencies associated with common faults are shown in Table 2 [16, 21].

This technique is quite useful for analyzing stationary signals whose frequency components do not change over time. In other words, this technique is very accurate if the rpm of the shaft does not change over time or does not change at least during each updated duration of time analysis.

Forcing Frequency	Fault
1 x RPM	Imbalance-Misalignment-Bent shaft
2 x RPM	Misalignment-Bent shaft
Harmonics of RPM	Loose bearing caps
Non-integer multiples of RPM	Rolling bearings-Gears
Number of teeth time RPM and harmonics	Gear faults

Table 2: Common faults with their corresponding frequencies.

4.2.1. Power Spectrum and Constant Percentage Band Analysis (CPB)

The power spectrum is derived from the vibration waveform by performing a Fast Fourier Transform (FFT) or a Constant Percentage Band (CPB) filtering function. Given

that the running speed of the machine is directly proportional to the frequency measured, the power spectrum will be normalized with respect to this fundamental frequency (measured by the encoder) and will be equal to order 1, and the peaks in the spectrum will be related to machine components. Because the speed of the shaft can slightly change over time and in order to have accurate results, the LabVIEW program created here for vibration acquisition and analysis allows normalizing the power spectrum after each iteration using the data from the encoder before the synchronous averaging process. In order to have accurate results, the sampled time period should be set so that it is a little longer than the period of revolution of the shaft.

The FFT spectrum is well-suited to analysis and diagnosis, as it shows more clearly the harmonics and the side-band patterns in the signal. The CPB spectrum is well-suited for trending and detection, as it covers a larger frequency range, and is easier to use for comparison purposes, especially if there is a small speed variation.

The direct analyses of the spectrum, and of indices derived from it, have been found to be the best vibration based indicators of machine condition. A wide frequency range is required to detect all types of faults as may be seen in Table 3:

Frequency Range	Low	Medium	High
Faults to be detected	Unbalance, Misalignment, bent of the shaft 2	Wear faults in gears 1 and 2	Unbalance, Misalignment, bent of the shaft 1 (Rolling element bearings faults)

Table 3: Wide vibration frequency range is required to detect all types of faults [12].

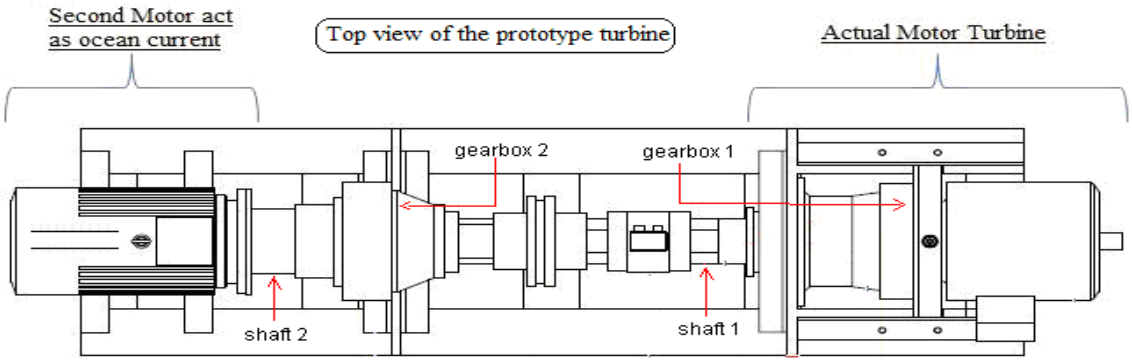

Figure 8: The rotating components of the dynamometer "prototype of the 20 kW turbine".

4.2.2. Cepstrum Analysis

The power cepstrum is the spectrum of the logarithm of the power spectrum, it is used to highlight periodicities in the vibrations spectrum, in the same way that the spectrum is used to highlight periodicities in the time waveform. Thus, harmonics and sidebands in the spectrum are

summed into one peak in the cepstrum (called rahmonic), allowing simplified identification and trending of specific fault frequencies. It has been found to be useful in bearing and gearbox analysis [22].

$$C(\tau) = \xi^{-1}\{\log(\ F(f))\} = \int_{+\infty}^{-\infty} \log(\ F(f)) \times e^{j2\pi f\tau}\, df \ . \qquad (4.3)$$

Where ξ is the Fourier transform operator and $F(f)$ is a power spectrum, τ is the quefrency in second unit.

The cepstrum is very good indicator for bearing and gearbox faults, is used for both faults detection and diagnostic: for fault detection point of view, the data of harmonics and sidebands are reduced to one line and is not subjected to amplitude and frequency modulation.

For fault diagnostic point of view, the cepstrum gives an accurate spacing between the peaks, and it can be used on specified section of spectrum.

4.2.3. Trending of Spectral Data and Comparison with the Baseline

Trending the current spectrum and comparing it with the baseline spectrum, was found to be a good indicator of many problems, including unbalance and misalignment in lower frequency band, and growing bearing damage in higher frequency bands. The use of logarithmic scaling for the amplitudes was found to be very useful.

4.3. Time-Frequency "Short Time Fourier Transform" Based Vibration Analysis Techniques

When the rpm of the shaft is changing over time due to short transient effects or due to variances in load, or the shaft begins to develop a fault, the frequency changes over time and the FFT is not very accurate. In other words two different signals, one stationary and the other with transient effects can have the same spectrum, as shown in Figures 9 and 10.

In this case, the Time-Frequency Technique using "Short Time Fourier Transform" is used. The Time Frequency Analysis (TFA) is the process of taking multiple FFT's of small portions of data (equation 4.4), rather than taking the FFT of short period of time. These FFT's can then be combined to see how the power spectrum of a signal changes over time. Time-frequency Analysis results are displayed in a spectrogram, which shows how the energy of a signal is distributed in the time-frequency domain. A spectrogram is an intensity graph with two independent variables: time and frequency. The color intensity shows the power of the signal at the corresponding time and frequency.

Narrow-band, periodic signals, transients and noise appear very differently on a spectrogram.

In Figure 9, the two signals are similar with signal 2 containing transient effect. Despite the presence of the transient, the power spectra of both signals are almost identical because the energy of this transient "spike" is low and spread over a wide range of frequencies but the two signals have not the same histogram.

In Figure 10, the top signal's frequencies increase with time while the bottom signal's frequencies decrease with time. Although the frequency behavior of the two signals is different, the two signals produce the same power spectrum because the energy at individual frequencies in each signal is the same; but, the two signals do not have the same histogram.

$$PS(t, f) = \left|STFT(t, f)\right|^2 = \left|\int_{-\infty}^{+\infty} s(t')w(t'-t)e^{-j2\pi ft'}dt'\right|^2 . \quad (4.4)$$

Where PS is power spectrogram of the signal $s(t)$ and $w(t)$ is a real and symmetric window translated by t.

t and f are the instantaneous time and frequency. t' is a variable.

The resolution in time and frequency of the STFT depends on the selected window type and its size (Rectangle, Blackman, Hamming, Gaussian, Hanning, etc.). A very good resolution is achieved by using the Gaussian window.

$$w(t) \approx e^{-18t^2} . \quad (4.5)$$

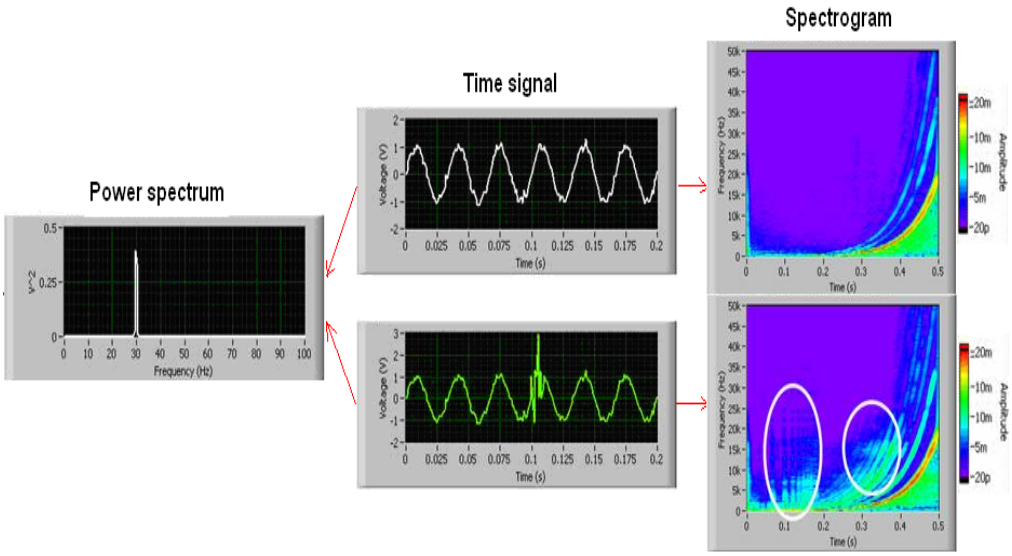

Figure 9: The transient in the bottom's signal cannot be seen in the frequency analysis of the signal but can be clearly seen in the spectrogram.

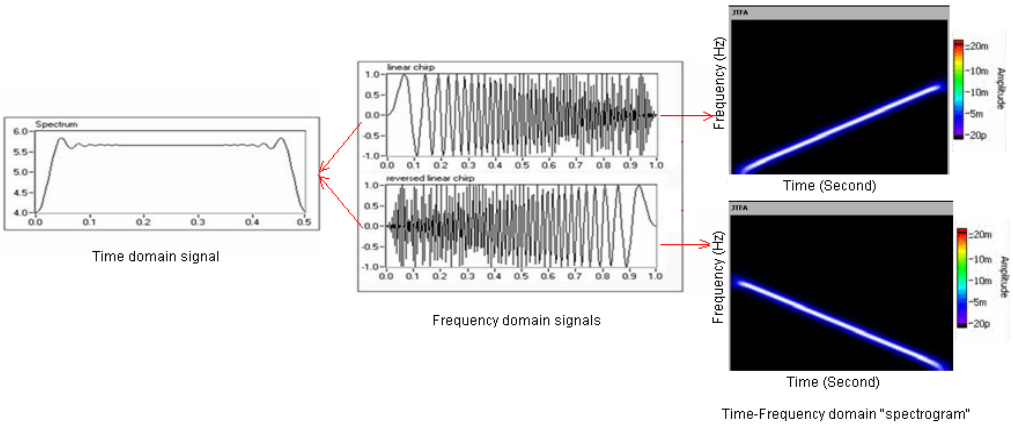

Figure 10: A signal and its reverse both produce the same frequency spectrum but not the same spectrogram.

5. EXPERIMENTAL VIBRATION MEASUREMENT ON THE TEST BENCH USING THE LABVIEW MODEL

5.1. Description of the System Components and its Failure Modes

The main components subject to failure in the turbine are the gearbox and the bearings. Figure 11 shows a picture of the cycloidal gearbox of the 20 KW turbine.

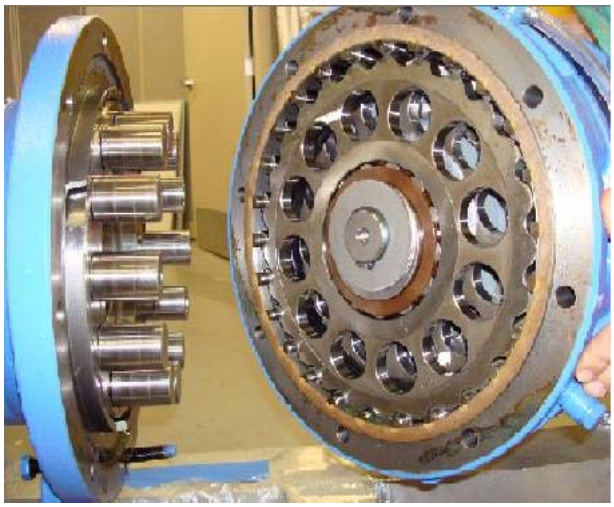

Figure 11: Gearbox of the actual turbine.

The gears are used to transmit power between shafts rotating at different speeds. Its task is to increase the low rotational speed of the rotor blades to the generator rotation speed. The gearbox may have also the secondary function of supporting the main shaft bearings [27]. The main components of this cycloidal gearbox are illustrated in the Figure 11 above:

- An interior toothed gear wheel (ring gear).
- A smaller toothed gear wheels (planet gear).

- A common carrier arm (planet carrier).
- A centrally placed toothed gear wheel (sun gear).

The ring gear is stationary while the planet carrier is mounted on the rotor shaft which rotates with the same rotational speed as the rotor blades. The planet carrier transmits the driving torque to the planet gears, which move within the inner circumference of the ring wheel. The rotational speed of the centrally placed sun gear wheel is increased. The speed-up ratio for this configuration can be expresses by the following [27]:

$$\frac{n_s}{n_p} = \frac{D_r}{D_s}. \tag{5.1}$$

n_s and n_p are respectively the rotational speed of the sun and the planet carrier, D_r is the diameter of the ring wheel and D_s is the diameter of the sun. The gear ratio for this planetary gearbox is 1:25. Note that the number of teeth in each gear is a linear function of the diameter. The gear-mesh frequency can be calculated as follow:

$$f_{gmf} = n_t \times \frac{rpm}{60}. \tag{5.2}$$

n_t is number of teeth.

The main sub-systems that interact with the gearbox and can contribute to its failures are the bearings, shafts, coupling, mechanical break and lubrication.

The main function of bearings is to reduce the frictional resistance between two surfaces with relative rotational motion. Bearings are in many cases responsible for gearbox failures [4] [25] [26]. The majority of bearing failures is due to imbalance, improper lubrication or manufacturing errors.

Fault location	Fault Frequency
Rolling element bearing	$f_{rol} = \frac{d}{D}\left[1-\left(\frac{D}{d}\right)^2\right]\times s.$ (5.3)
Outer race	$f_{or} = \frac{n_r}{2}\left[1-\frac{D}{d}\right]\times s.$ (5.4)
Bearing cage	$f_{cage} = \frac{s}{2}\left[1-\frac{D}{d}\right].$ (5.5)

Table 4: Bearing faults and their corresponding frequencies.

Where s is the shaft speed (Hz), n_r is the number of rolling elements, D is the roller diameter and d is the pitch diameter as shown in Figure 12.

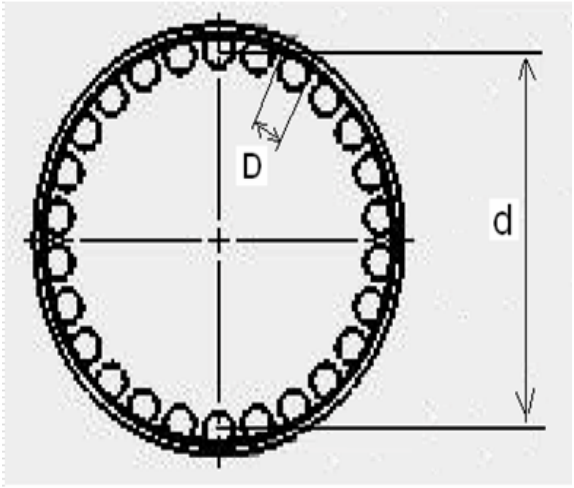

Figure 12: Needle bearing of the 20 KW turbine.

Shafts are cylindrical elements designed to rotate with the function of transmitting torque. Shafts (low speed on the blade side and high speed on the generator side) are mechanically coupled in the gearbox housing. The shafts are subject to faults that can lead to potential failure modes of the gearbox and the bearings. An anomaly in the shaft rotation (unbalance) is associated with a fault (misalignment), which if not repaired will lead to potential failure modes (gears and rolling element damage).

Couplings are elements used to connect two shafts together for the purpose of transmitting torque between them. Damaged couplings can lead to misalignment of the shaft and gears and rolling element faults.

A mechanical friction brake and its hydraulic system are used to stop the turbine blades from turning in emergency cases or during maintenance. Use of brakes can also introduce dynamic loads on the gearbox and can lead to its failures.

The function of the lubrication system is to maintain an oil film on gear teeth and the rolling elements of bearings, in order to minimize surface pitting and wear. Improper lubrication can lead to potential failure modes of the gearbox and the bearing. Low quality oil or oil temperatures which are too high can cause damage of the gearbox and the bearing. Oil coolers and filters are indispensable and so is the careful observance of oil change intervals [29].

5.2. Procedure

Based on the maximum observable frequency of interest and the smallest difference between two successive frequencies (bearing tones), the sampling frequency F_s is set to 25000 Hz and the frequency resolution is 0.01Hz. This resolution is achieved using a period of observation of 100 seconds. This choice is based on the following relationships:

$$F_{\max} = \frac{F_s}{5}. \tag{5.6}$$

$$df = \frac{1}{T_s} = \frac{F_s}{n}. \tag{5.7}$$

Where $F_{\max}$ is the maximum frequency of interest (5000Hz in the case of the actual turbine), F_s is the sampling frequency (should be greater than at least five times the

maximum frequency of interest), df is the frequency resolution, T_s is the total sampled period and n is the number of samples.

Thus, the data will be recorded during a long period of time to be able to perform the average. The number of averages is determined using this rule of thumb: record two spectra, the first one with m averages and the second with 2m averages. If the spectra are significantly different, the number of averages should be doubled again and another spectrum recorded. If the latter two spectra are similar, then the previous number of averages is adequate for this machine.

The low pass filter has a cut-off frequency of 5000 Hz to avoid aliasing. An 8-pole low pass filter is selected to achieve good attenuation in the stop band and minimal distortion in the pass-band.

Channel 1, 2, 3 and 4 are connected to low-frequency accelerometers of sensitivity 500 mv/g, with a frequency range of [0.2, 3000 Hz] and resonance frequency of 12000 Hz. Channel 5 and 6 are connected to high-frequency accelerometers of sensitivity 100mv/g, frequency range of [0.5, 10000 Hz] and resonance frequency of 22000 Hz.

The power spectrum, displayed in decibel (dB) is computed using a Hanning window (to minimize the frequency distortion due to block averaging), RMS averaging mode and exponentially-weighted time averaging.

5.2.1. Accelerometers

An accelerometer is a seismic device that generates an output voltage signal proportional to the acceleration of the body being measured. The accelerometers used for the experiments are:

- AC136-1A: low noise, low frequency, sensitivity of 500 mV/g, frequency response between 0.2 and 3000 Hz, and very low noise PSD of 1.7 µg/√Hz at 10 Hz.
- AC104-1A: low-noise, high-frequency, frequency response between 0.5 and 10000 Hz, RMS noise of 200 µg between 2.5 and 25000 Hz.

5.2.2. Location and Mounting Method of the Accelerometers on the Test Bench

The accelerometers are mounted near each bearing where excessive vibration is expected. Figure 13 shows the location of the high and low frequency accelerometers.

When performing measurements on the test bench, many temporary measurements on different locations of the accelerometers are expected. Adhesive (glue) is used to mount the accelerometer on the surface of the system. However, when monitoring these accelerometers on the actual turbine, a permanent stud should be used, as the resonance frequency of this permanent stud is much greater than the maximum frequency of interest. In addition, unlike the adhesive, the permanent stud integrity does not depend on the fluctuations of temperature.

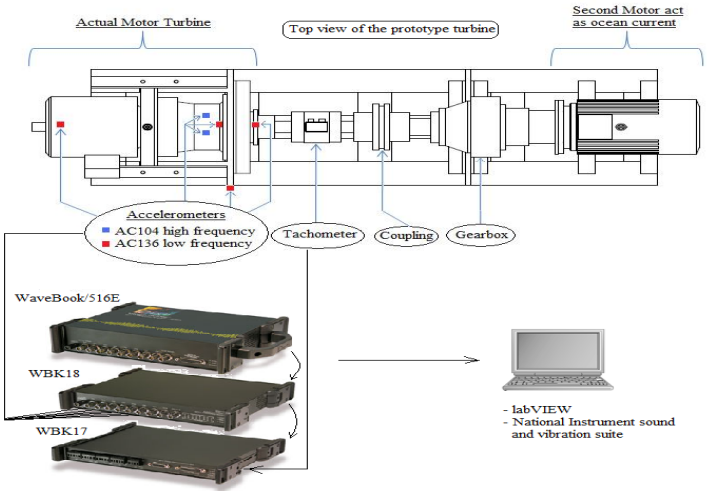

Figure 13: Schematic of the test bench.

5.3. Data Analysis

The purpose of this experiment is to record the data both in the time and frequency domain, then relate and compare the observe forcing frequency spikes to those calculated theoretically. If some spikes do not correspond to any forcing frequency, they should be compared to the resonance frequencies of the components. The common vibration faults such as unbalance and misalignment of the shaft and gears faults maybe detected on the prototype (dynamometer) if they exist.

Also the values of the kurtosis and crest factor should be acquired and compared to their expected values in normal operating conditions of the system. This test will also be used to estimate the baseline data in time and frequency domain to do the trending; narrow-band spectra trending as a third octave trending is used for this test bed and octave trending for the actual turbine.

Initially, a set deviation will be used as a threshold setting for alerts. Three rotation speeds of the motor 2 will be used in the experiment 35rpm, 44rpm, 60rpm.

5.3.1. Theoretical Forcing Frequencies

The theoretical forcing frequencies are stored in a spreadsheet as a function of rotational speed. Table 5 shows the forcing frequencies measured at 44rpm. The governing equations are:

$$f_{gmf} = n_t \times \frac{rpm}{60}. \tag{5.8}$$

$$f_{or} = \frac{n_r}{2}\left[1 - \frac{D}{d}\right] \times s. \tag{5.9}$$

$$f_{cage} = \frac{n_r}{2}\left[1 - \frac{D}{d}\right]. \tag{5.10}$$

$$f_{rol} = \frac{n_r}{2}\left[1-\left(\frac{D}{d}\right)^2\right]\times\frac{d}{D}. \tag{5.11}$$

Where n_t is the number of teeth, D is the roller diameter, d is the pitch diameter, n_r is the number of rolling elements and s is the shaft speed (Hz).

The multiplication ratio of the gearbox 1 and 2 are 25 and 28 respectively.

Shaft 2 speed (rpm)			Theoretical frequency (Hz)	Theoretical frequency normalized
	Shaft 2	$1\times rpm$	0.73333333	1
		$2\times rpm$	1.46666667	2
	Gearbox 2	$1\times f^*_{gmf}$	20.5333333	28
		$2\times f^*_{gmf}$	41.0666667	56
		$3\times f^*_{gmf}$	61.6	84
		$4\times f^*_{gmf}$	82.1333333	112
	Gearbox 1	$1\times f_{gmf}$	513.333333	700
		$2\times f_{gmf}$	1026.66667	1400
		$3\times f_{gmf}$	1540	2100
44		$4\times f_{gmf}$	2053.33333	2800
	Needle roller bearing	f_{or}	7.62666667	10.4
		f_{rol}	3.432	4.68
		f_{cage}	0.29333333	0.4

Table 5: Theoretical forcing frequencies of the rotating components of the turbine.

In theory, if the vibrations process is linear, the spectrum should only contain the forcing frequencies. If the process is not linear, the vibration generated at those forcing frequencies (especially rpm) is distorted, causing harmonics to appear in the spectrum. If the degree of non-linearity increases, the forcing frequencies interact between each other causing amplitude and frequency modulation and this result in sidebands in the spectrum.

If the rotation speed presents small change (±0.1 Hz for example), the 4th harmonic of the shaft 1 will change significantly (±280 Hz) and the FFT of the signal will have several peaks in a frequency band of 560 Hz after averaging the signal instead of having only one peak as expected. Thus, the importance of normalizing the signal before averaging it.

In order to detect most machine faults, a broad frequency range must be used to include low-frequency components (such as a sub-harmonic of the shaft rpm) and high frequency components (such as the harmonics of tooth mesh and structural resonances excited by rolling element defects). The theoretical forcing frequencies calculated above indicate that a sampling frequency of 10000 Hz is required to display all the essential information in a vibration spectrum obtained with a good quality correctly mounted accelerometer.

5.3.2. CPB Spectrum Analysis

Special cases of a CPB spectrum analysis discussed in the section 2.4.1 are the octave and third octave band analysis. The octave and third octave analysis are effective fault detection and will allow separating the gear-meshing components from the signal change caused by a damaged bearing or an unbalanced condition.

The third octave and octave analysis are used when running the experiments on the prototype and on the turbine respectively for the following reasons:

- Since the bands are quite wide, the amount of data is kept to a minimum, although there is still enough information to detect and identify unbalance, misalignment or gear and bearing faults.
- Averaged octave CPB spectrum data can be trended much more easily than FFT data.
- Small changes in running speed do not affect the results substantially.

- More reliable spectral estimates can be obtained in the presence of random, impulsive and non-stationary signals.

5.4. Experimental Results

The experiments are performed on the fan using three different speeds, 720rpm, 870rpm and 1010rpm. These three speeds are provided by the fan's manufacturer, Please note that the speeds mentioned above are valid for new fans with no faults. The fan used for these experiments is old, which can introduce some errors.

The fan has five blades, the maximum frequency of interest is:

$$F_{\max} = 5 \times 16.84Hz = 84.2Hz .$$

The sampling frequency is set to 200Hz for the three speeds. 400 samples are acquired so that the frequency resolution is equal to 0.5 Hz.

During this experiment, the following techniques are tested:

1) Comparison of the time acceleration, power spectrum and the third octave of two accelerometers located at different location.

2) Determination of the number of average needed following the rule of thumb.

3) Order analysis of the power spectrum and the third octave for the three different speed of the fan.

4) Identification of the peaks of the power spectrum at speed level 1 (12 Hz) of the fan.

5) Comparison the acquired data with the baselines and testing of the alerts and alarms criteria in two cases:

- Baselines are the data acquired at speed level 1 (12 Hz) and compared to the data acquired at speed level 3 (16.84 Hz).
- Baselines are the data acquired at speed level 3 and compared to the data acquired

at speed level 1.

5.4.1. Comparison of the Data Acquired from two Accelerometers Located at Different Location

The data are acquired from two accelerometers. The first accelerometer is mounted without mounting disk pad and connected to channel 1. The second accelerometer (with mounting disk pad) is connected to channel 2. The two accelerometers are mounted in different locations, as shown in Figure 14.

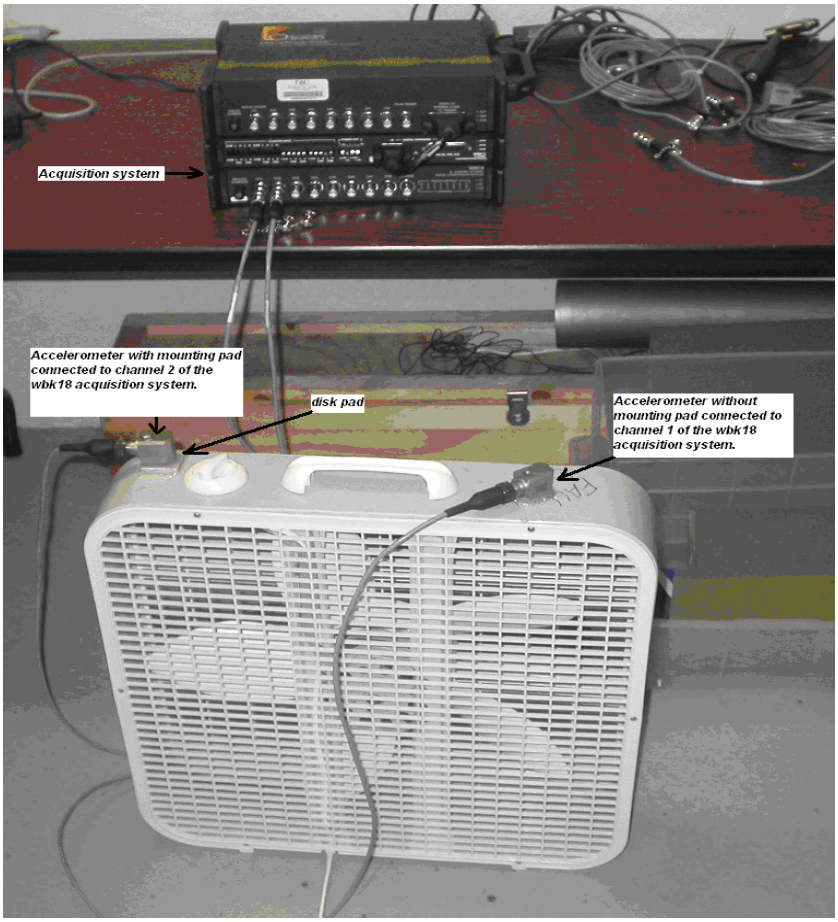

Figure 14: Screen shot of the experimental setup.

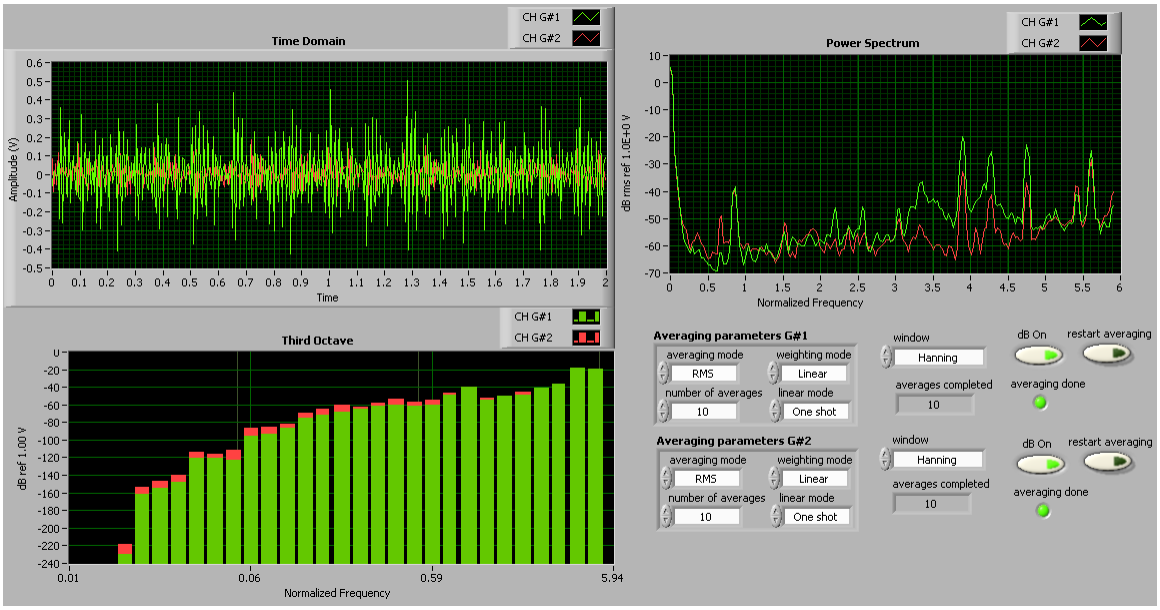

Figure 15: Comparison of two signals: Green signal acquired from sensor 1 and red signal from sensor 2.

In Figure 15: the acceleration level of the sensor 1 “green curve” is higher than the acceleration level of the sensor 2 “red curve”, this is due to the fact that the mounting disk pad add some damping to the surface of the fan, that why the acceleration level is lower.

5.4.2. Determination of Averaging Number

For this operation, only data acquired from accelerometer 1 is used.

First, the number of averages is determined using “rule of thumb” described in section 5.2. Two signals of the same channel 1: the green one with 10 averages and the red one with 1 average are compared, the data for this operation are acquired using the speed level 3 (1010 rpm) of the fan.

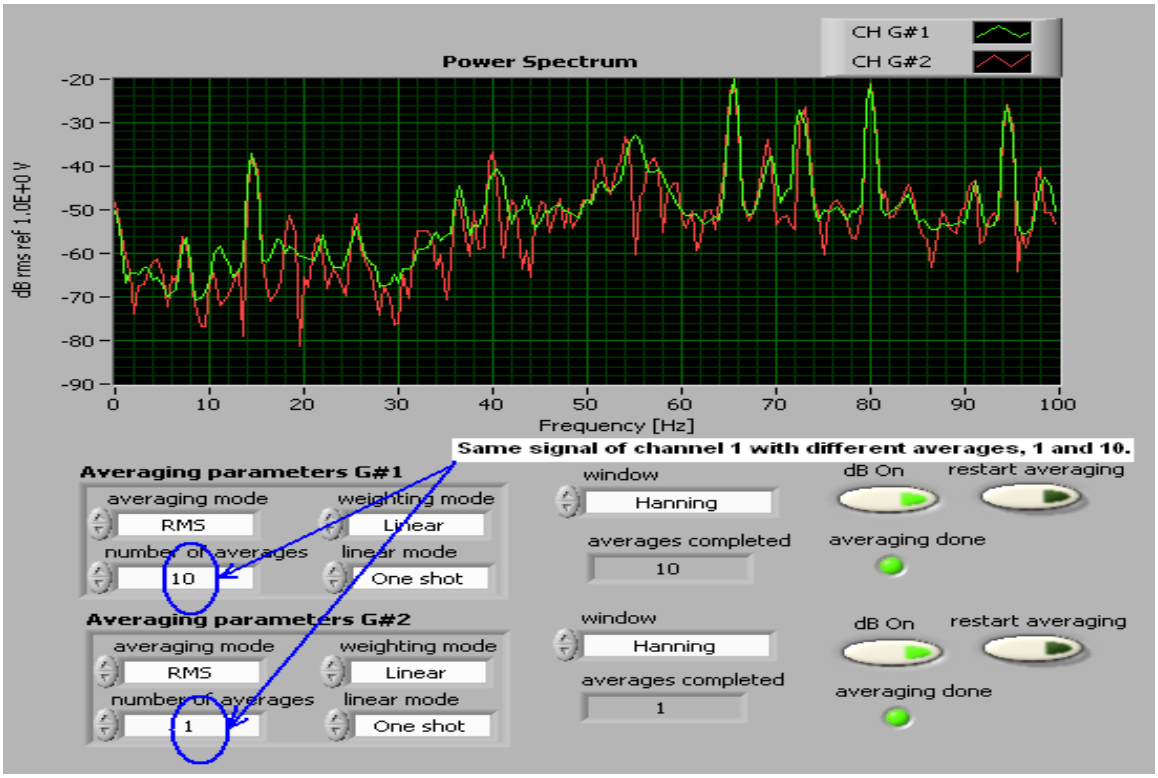

Figure 16: Spectral averaging of the fan vibration measurements (1 or 10 averages).

Figure 16 shows the power spectrum, in dB, of the signal recorded using two different average number (1 and 10). We notice a difference between the signals due to the noise errors. This noise will cancel out by the averaging process, thus, the importance of averaging the signal. In Figure 17, we compare the signals of the same channel 1, the green one with 10 averages, and the red one with 20 averages.

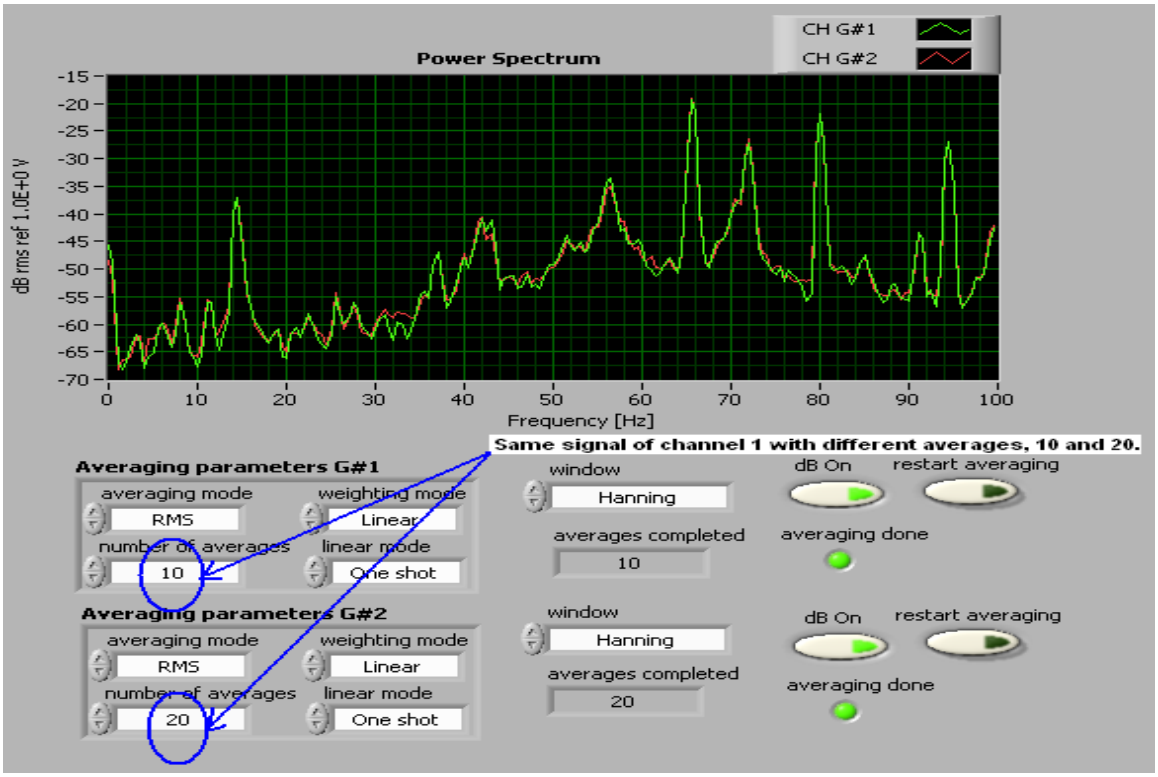

Figure 17: Spectral averaging of the fan vibrations (10 or 20 averages).

The two signals are almost identical, thus we will use the 10 averages for the following experiments.

5.4.3. Order "Normalization" Analysis of the Power Spectrum and Third Octave

Since the encoder cannot be used with the fan, the value of the speed is entered manually to normalize (order) the frequency axis for each iteration. The data are displayed in term of multiples of the rotational speed.

For this operation, the three speeds levels - converted to Hz (12, 14.5 and 16.84Hz) - of the fan are used. Figure 18, 20 and 22 show the normalized power spectrum using the three different speeds of the fan. Figure 19, 21 and 23 show the normalized third octave using the three different speeds of the fan.

Speed level 1 of the fan (12 Hz)

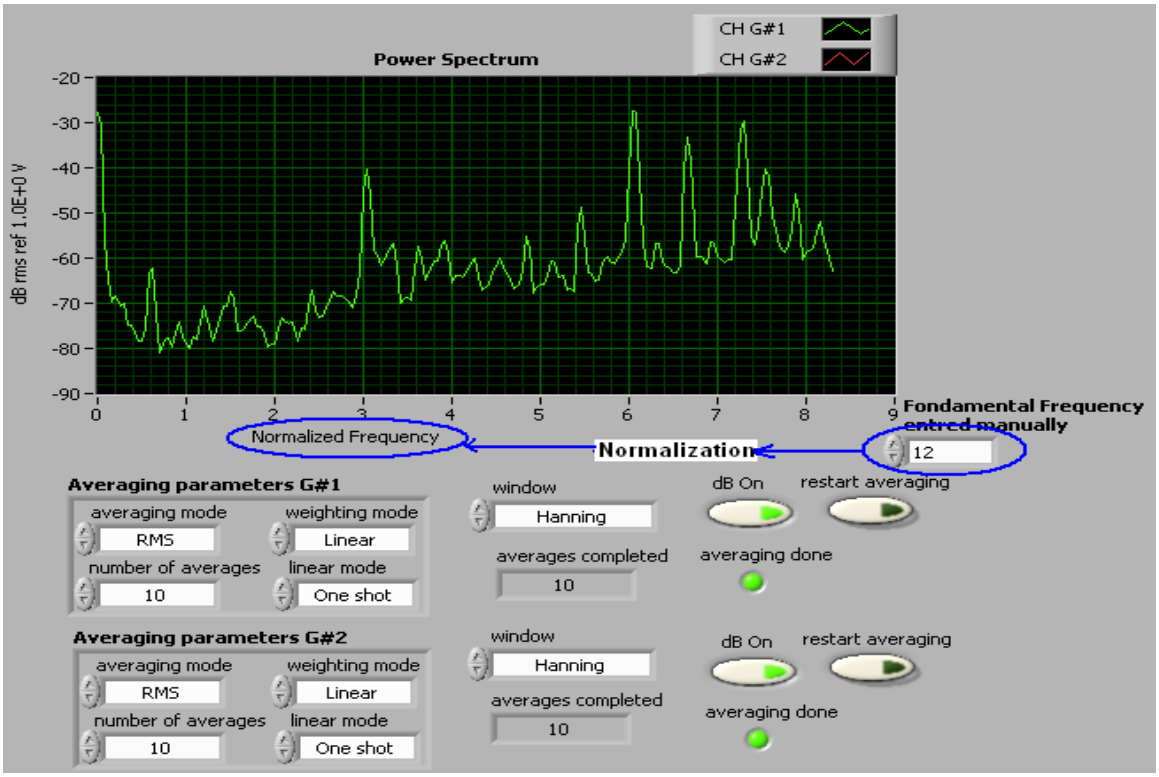

Figure 18: Normalized power spectrum with respect to the rpm (1st speed level of the fan).

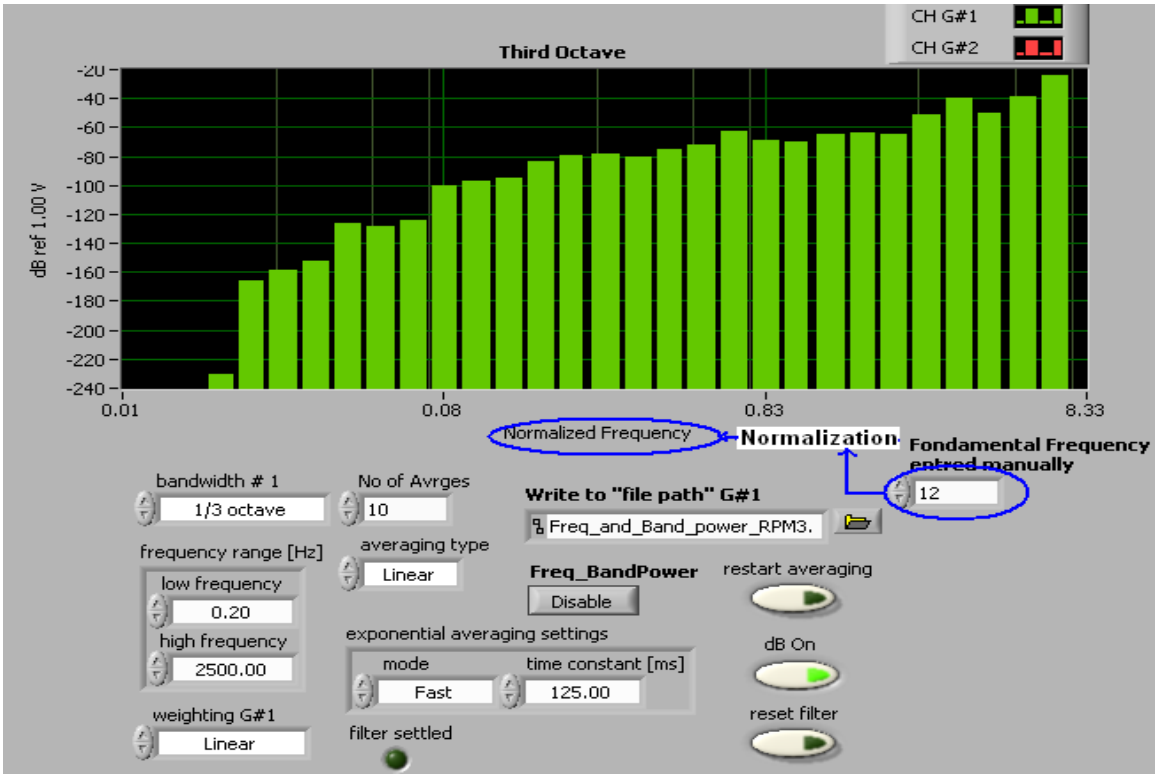

Figure 19: Normalized third octave with respect to the rpm (1st speed level of the fan).

Speed level 2 of the fan (14.5 Hz)

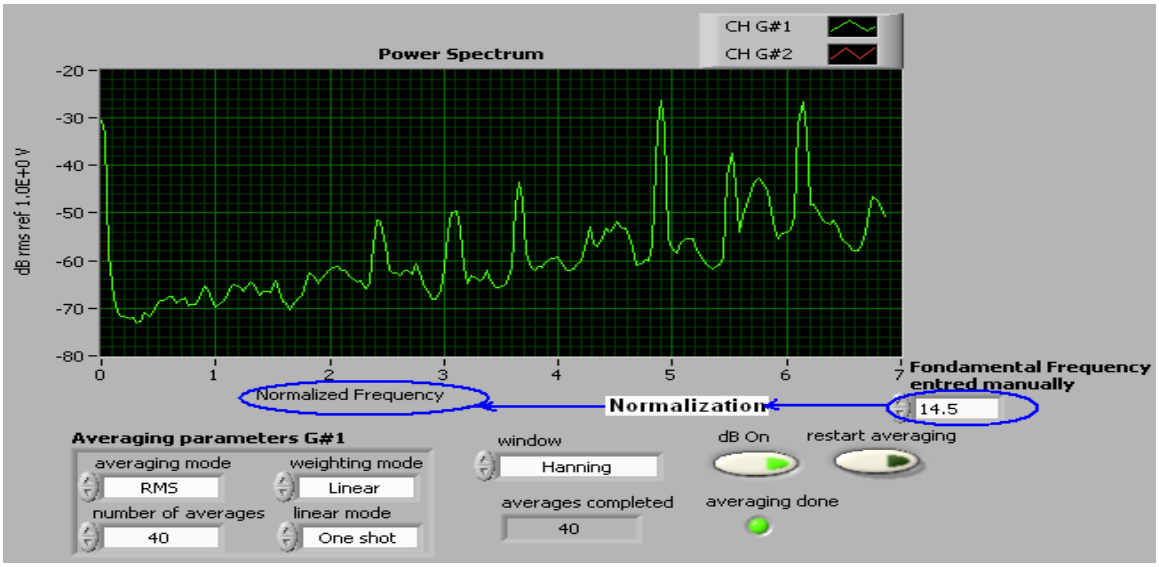

Figure 20: Normalized power spectrum with respect to the rpm (2nd speed level of the fan).

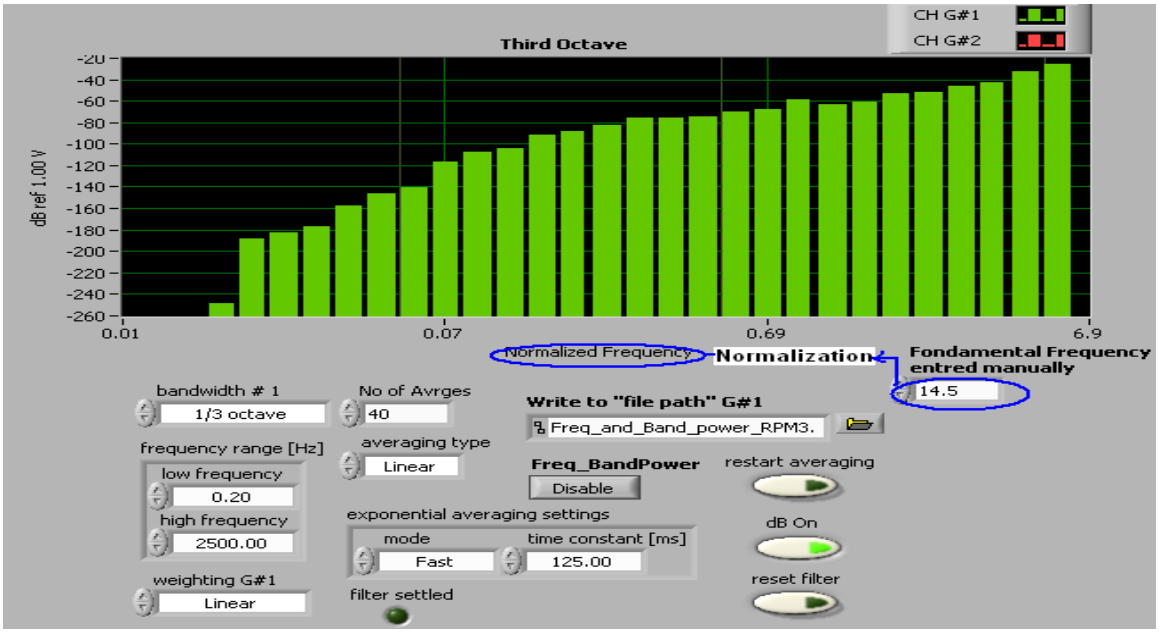

Figure 21: Normalized third octave with respect to the rpm (2nd speed level of the fan).

Speed level 3 of the fan (16.84 Hz)

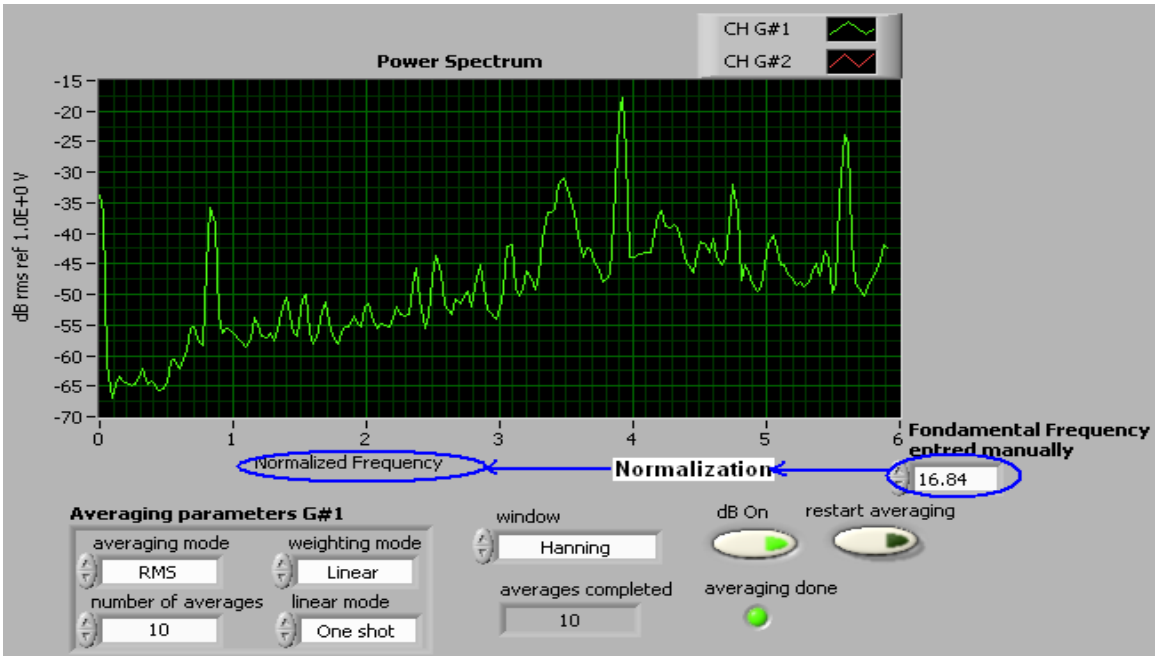

Figure 22: Normalized power spectrum with respect to the rpm (3rd speed level of the fan).

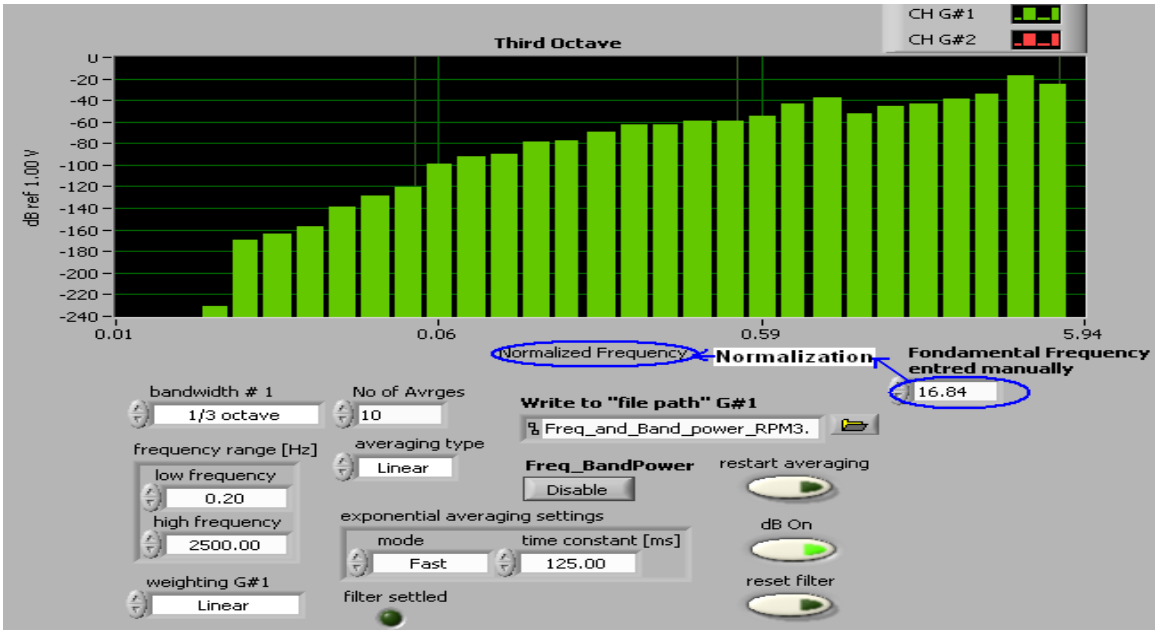

Figure 23: Normalized third octave with respect to the rpm (3rd speed level of the fan).

5.4.4. Identification of the Peaks of the Power Spectrum

The data are acquired from the sensor 1 at speed level 1 (12 Hz) of the fan.

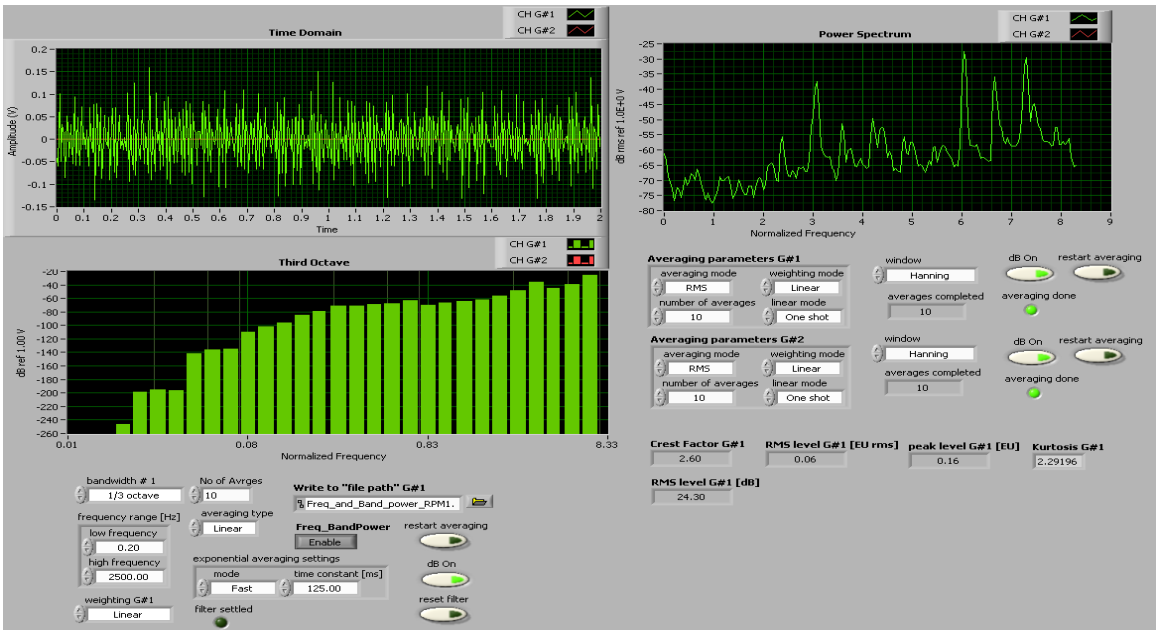

Figure 24: Time acceleration, power spectrum, third octave, crest factor,
RMS level and kurtosis acquired from accelerometer 1 using speed level 1 of the fan.

Figure 25 below shows clearly the fundamental frequency and harmonics of the acceleration 1.

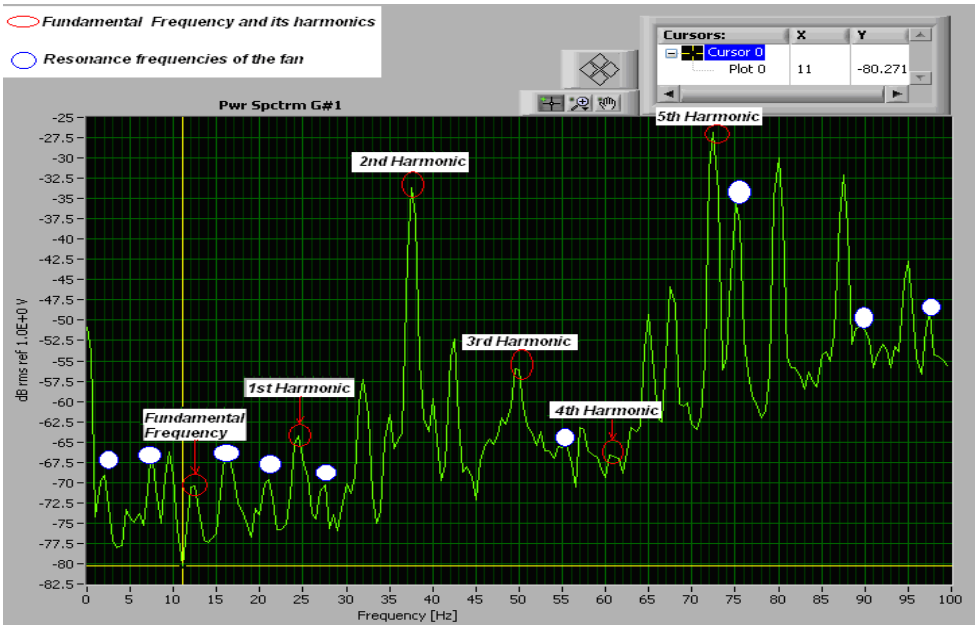

Figure 25: Power spectrum of the acceleration measured at sensor 1.

The resonance frequencies of the fan are clearly shown in Figure 25. The resonance testing on the fan was performed using LabVIEW program and the results are provided in the section 5.4.6.

5.4.5. Comparison with the Data Acquired with the Baselines

The acquired data are compared to the baseline added with a constant mask (tolerance level). For the fan, the trending of the 1/3 octave is used for each band to separate the rotational frequencies from the resonance frequencies.

For the ocean turbine, the octave data will be used and the speed regime will be divided in such manner the rotational frequency stay within the band as speed changes.

The masks for threshold limits chosen for different parameters are:

Alerts - third octave: 5 dB, RMS: 0.1 dB, crest factor: 0.04 and kurtosis: 0.1, time waveform: 0.2g.

Alarms - third octave: 10 dB, RMS: 0.2 dB, crest factor: 0.08 and kurtosis: 0.2, time waveform: 0.4g.

The alert buttons are squares for graphs testing, and disks for parameters (single value comparison). Whenever the data exceed the baselines added with constant mask, the alert turns red. When the data are within the limits, the alert button stays green. The time acceleration is compared to the upper and lower limit of 0.2 g, as shown in Figure 26. This technique can be used to detect bearings and gearbox faults [20] but does not give accurate result for unbalance and misalignment anomalies. The frequency component of the faults can be determined from the time spacing between the impacts (f=1/T), then the locations and types of faults can be determined. However, due to the presence of lot of noise, high frequency application, etc… This method is not very accurate and it should be used with combination of the spectral techniques to enhance and confirm their information.

Test 1: baselines are the data acquired at speed level 1

In this test, the data acquired at speed level 1 is assumed to be the baselines. Data acquired at speed level 3 are compared with the baselines.

Since the vibration at speed level 3 is generally higher than the vibration at speed level 1 "baselines", the alerts and alarms buttons are turned on "red" as shown in Figure 27.

In Figure 26 we clearly see that the third octave and time waveform exceed the thresholds limits, thus the alerts and alarms buttons are turned on "red" for all the indicators except the kurtosis because there is no transient effect introduced during the measurement.

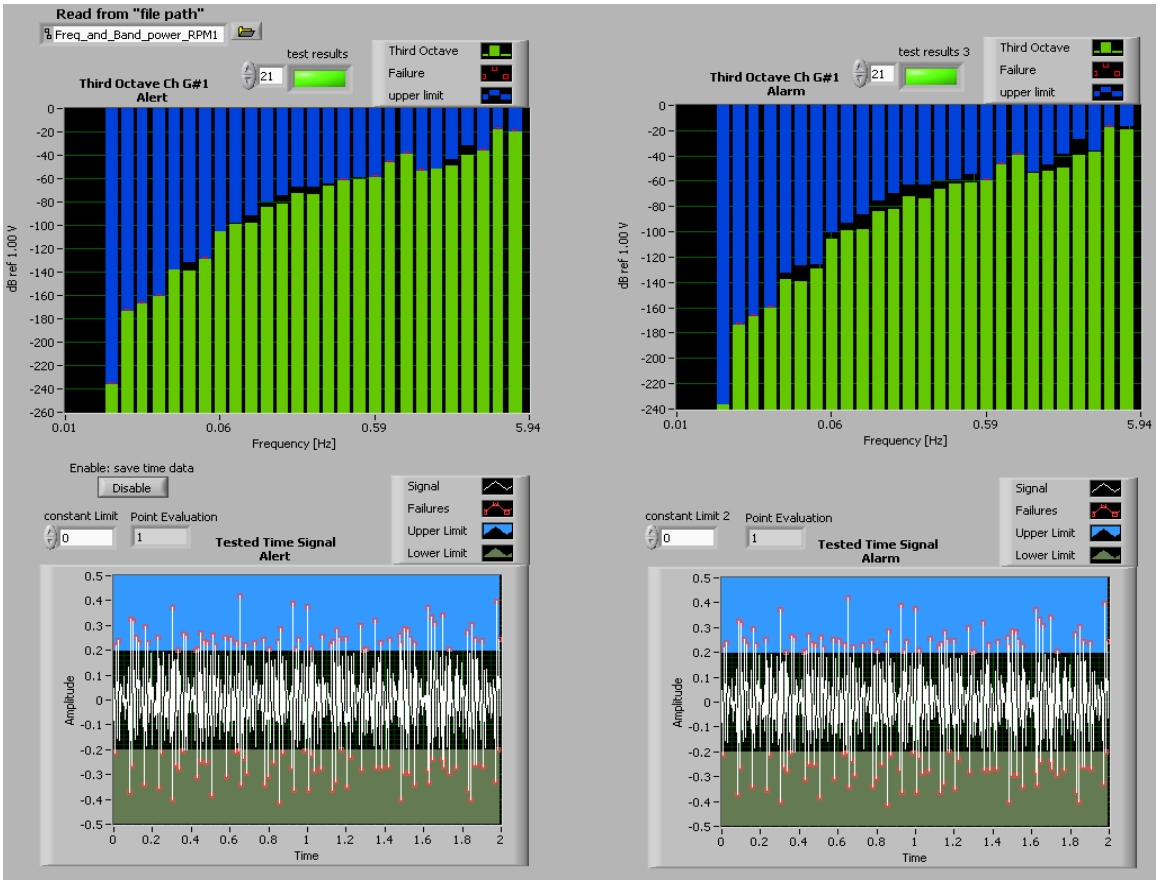

Figure 26: Acquired and compared to the baselines (alert and alarm criteria).

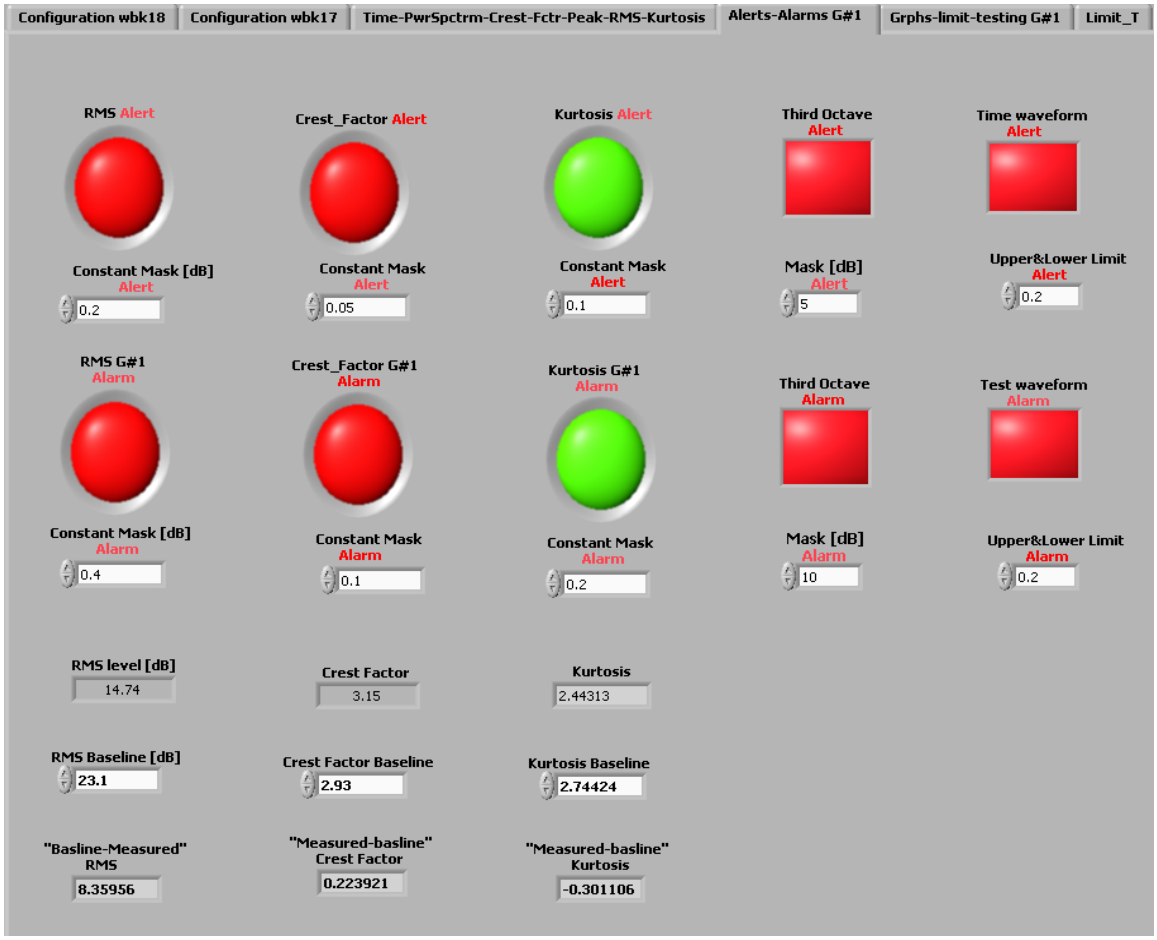

Figure 27: Alert, Alarms and indicators of the acquired data.

The difference between the measured and baseline of the RMS, crest factor and kurtosis are calculated.

Test 2: baselines are the data acquired at speed level 3

The baselines are taken to be the data acquired when the fan is running at speed level 3, this data are stored in a file and is compared with the data acquired at level speed 1 (lower than 3).

Since the vibration at speed level 3 is higher than the vibration at speed level 1, time acceleration, third octave, RMS value, crest factor and kurtosis value did not exceed the thresholds limits and the alerts and alarms buttons stayed off "green".

Figure 28 shows the third octave and time waveform compared with their baselines. Alerts and alarms of all indicators in Figure 29 are off "green".

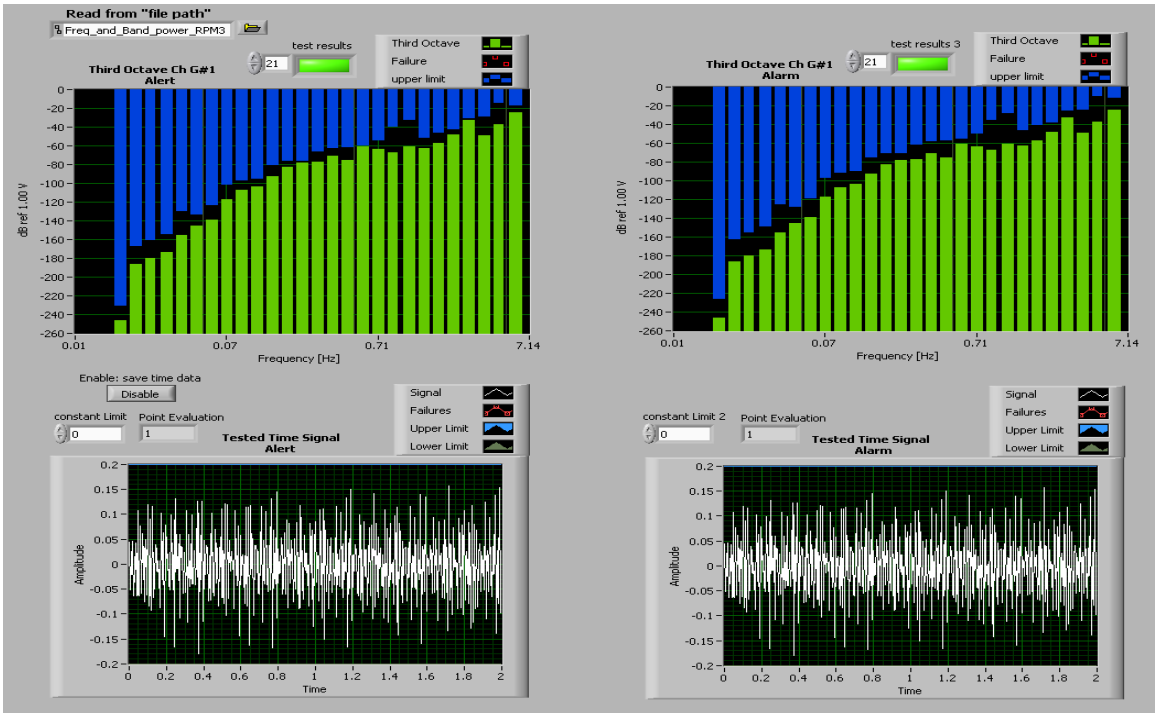

Figure 28: Acquired and compared to the baselines (alert and alarm criteria).

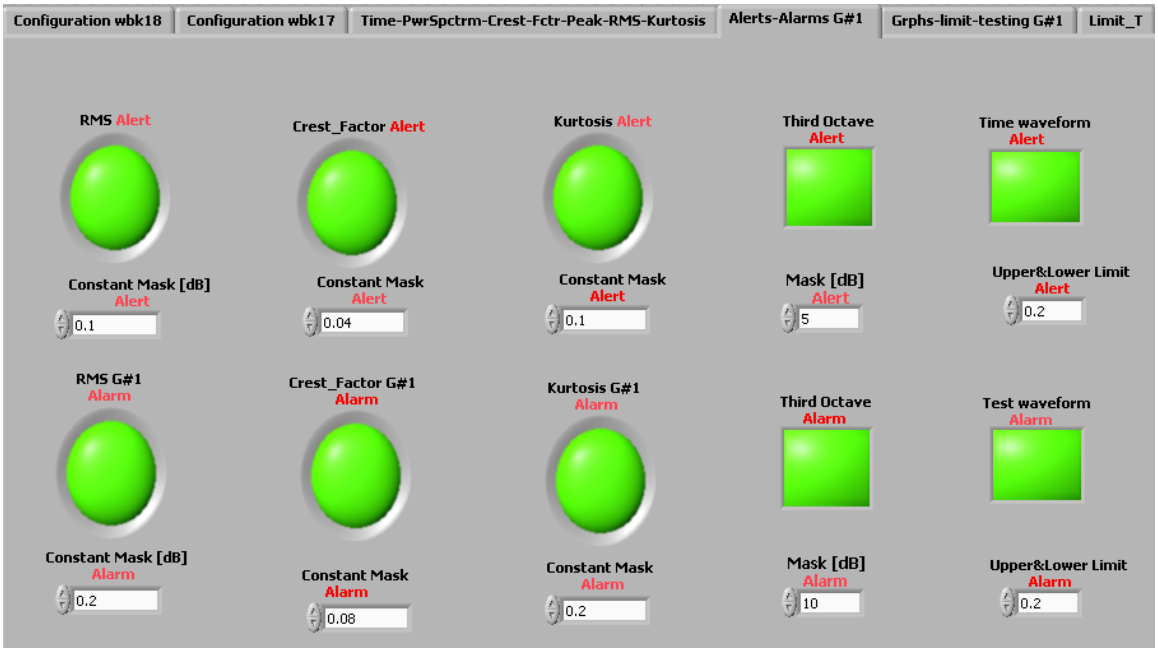

Figure 29: Alerts and Alarms buttons.

5.4.6. Resonance Testing on the "Fan" System using LabVIEW Program

The resonance testing on the fan system is performed using the same procedures in section 6.1. 500 points (50 before triggering and 450 after) are collected giving a frequency resolution of 1Hz. The sampling rate is 500 Hz.

An impact hammer is connected to channel 1 of the data acquisition system and its signal is used to trigger the data collection. The accelerometer is connected to channel 2. Figure 30 and 31 show the screenshot of the time history of impact hammer and its response.

The exponential window is set to 10%, which indicates the remaining level of the applied exponential window at the end of the signal. The impact hammer hits the fan three times at different location while the reference accelerometer is placed at one location on the cylinder. The high pass filter is set to 0.1 Hz. The low pass filter used has 8 poles and a cut-off frequency of 250 Hz. The FRF is calculated using the H1 method, which is the ratio of cross power spectrum between stimulus (impact hammer), response (accelerometer) and auto power spectrum of stimulus. The sensitivity of the accelerometer and the hammer is set to 100 mV/g and 10 mV/g respectively.

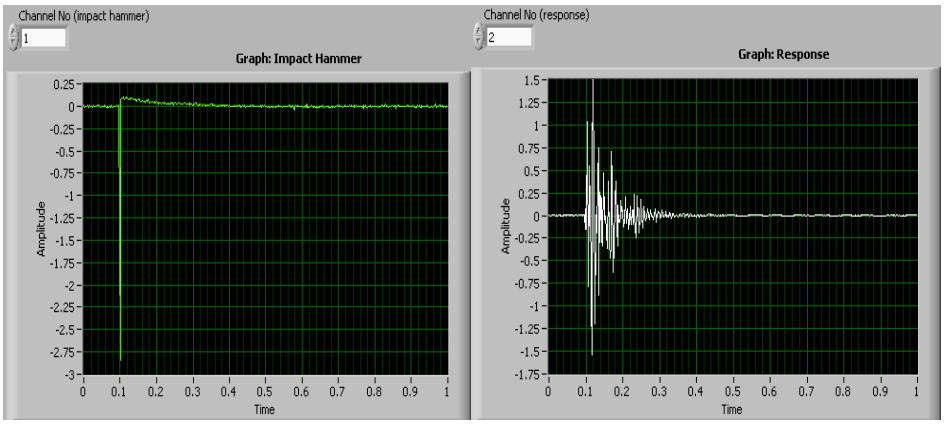

Figure 30: Time history of the impact hammer (left) and its response (right).

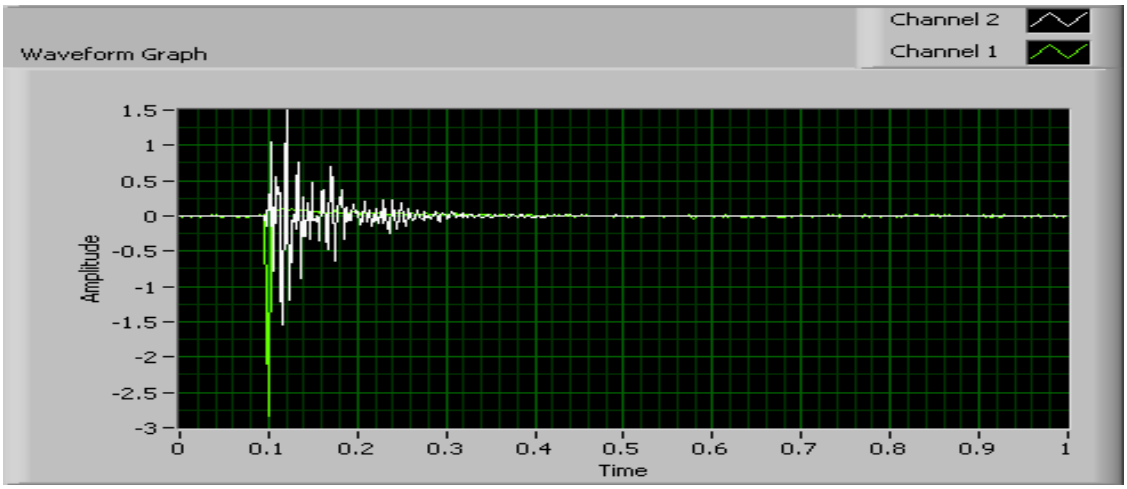

Figure 31: Both the excitation (green signal) and the response (white signal) in time domain.

Figure 32 below show the FRF response for the three hammer impact and theist average.

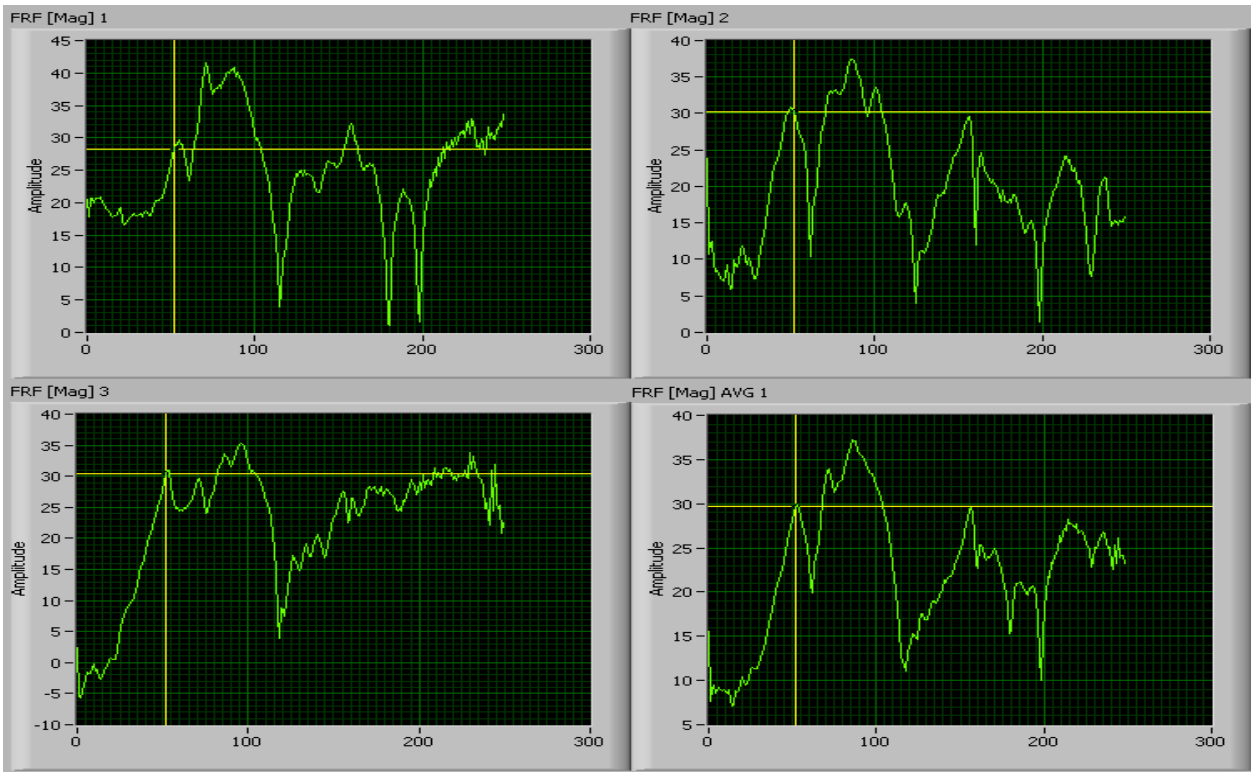

Figure 32: Magnitude FRF of the three measurements and its average.

Due to the complexity of the fan structure, the FRF graph below shows several structural resonance frequencies, this gave rise to significant noise during the experiment in the previous section.

According to Figure 32, the natural frequencies less than 100 Hz are:

Mode	Frequency [Hz]
1	3
2	7
3	16
4	21
5	27
6	55
7	75
8	90
9	97

Table 6: Natural frequencies less than 100 Hz measured experimentally.

6. MODAL ANALYSIS IN AIR ON A SMALL-SCALE CYLINDER

Modal analysis is the process of determining the modal parameters (resonance frequencies and mode shapes …) of systems by means of experimental, numerical or theoretical approach. This information can be used to improve understanding the dynamic comportment of the systems for condition monitoring purpose.

In order to validate the modeling and measurement set-up, a simple cylinder is first analyzed. This cylinder approximates a small scale model of the actual ocean turbine cylinder.

The objectives of this modal testing are:

1) To conduct a modal test on the cylinder and extract the natural frequencies from the processed data.

2) To develop a FE model for the cylinder and perform the modal analysis to obtain the natural frequencies and mode shapes.

3) The comparison between the numerical and experimental results and calculates the error between the two approaches.

The resonance testing is conducted on the cylinder hanged by bungee cords, using an impact hammer and an accelerometer. Appropriate signal processing was performed, using LabVIEW program written for this purpose, on the acquired data to obtain the Frequency Response Functions (FRF) and their averages.

The modal analysis is performed in ANSYS and the resonance frequencies and modes shapes of the cylinder were evaluated. The FE model results were used in planning the modal tests to determine the best impact, best suspension, and the best accelerometer locations, this test planning is important in acquiring a good quality of data.

The experimental and numerical results of the first mode of the cylinder were compared and it was found that the difference of the results between the two approaches is 0.95 %.

Finally, the modal analysis of the same cylinder with different added masses is performed in order to determine how the mass affect the modes of the cylinder.

6.1. Resonance Testing on the Cylinder and Validation with Numerical Result using FE Modeling on ANSYS

The accelerometer 784A is placed at 6 inches from the edge of the cylinder (Figure 30). 9 tests were performed. Three different locations were chosen and three averages of the FRF were made for each location. The details of the test planning and setup are provided in detail in the next section.

6.1.1. Test Planning and Setup

The test is conducted on the cylinder supported with bungee cords (Figure 33), in practice the free support is not possible to realize, the suspension using bungee cords will add some damping to the cylinder, and this suspension effect will introduce some errors. The 784A light accelerometer (45g), of sensitivity 100mV/g and frequency range of 2-10000 Hz, is used. The hammer (283g) is used without the added mass since the cylinder is not heavy. A rubber tip is used to excite the cylinder, since the maximum frequency of excitation needed is only 500 Hz.

Figure 33 : Accelerometer's location on the cylinder.

6.1.2. Data Acquisition and Analysis

The LabVIEW program developed for modal analysis purpose is used to acquire and analyze the data from the impact hammer and accelerometer. Three averages in three different location of the impact hammer are made.

Nine sets of data are acquired. This program computes the Frequency Response Function (FRF) and FRF averaged in real time. A sampling rate of 2500 Hz and 660 points (60 before triggering and 600 after) were collected giving a frequency resolution of 3.79 Hz. This resolution means that if we have two modes that are within 3.79 Hz will not be shown, the total time should be increased if interested in two modes that are close each other.

An impact hammer is connected to channel 1 of the data acquisition system and its signal is used to trigger the data collection. The accelerometer 784A is connected to channel 2.

Figure 34 and Figure 35 show the screenshot of the time history of impact hammer and its response.

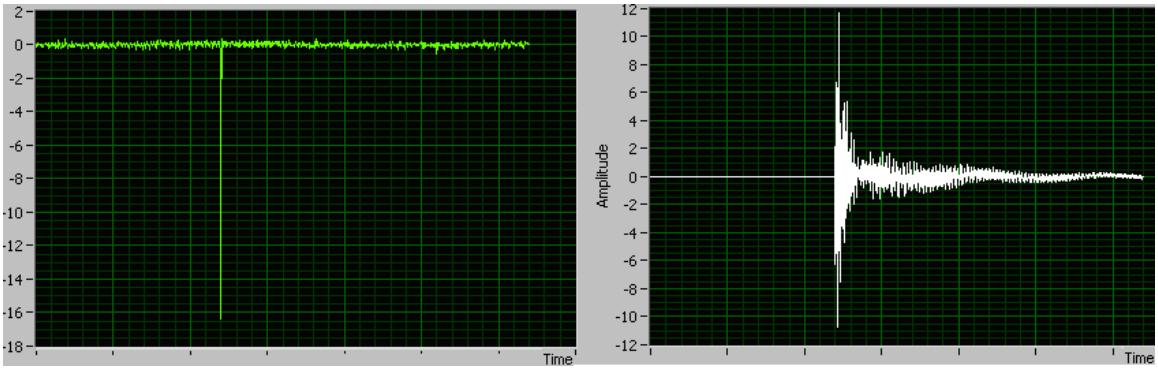

Figure 34: Time history of the impact hammer (left) and its response (right).

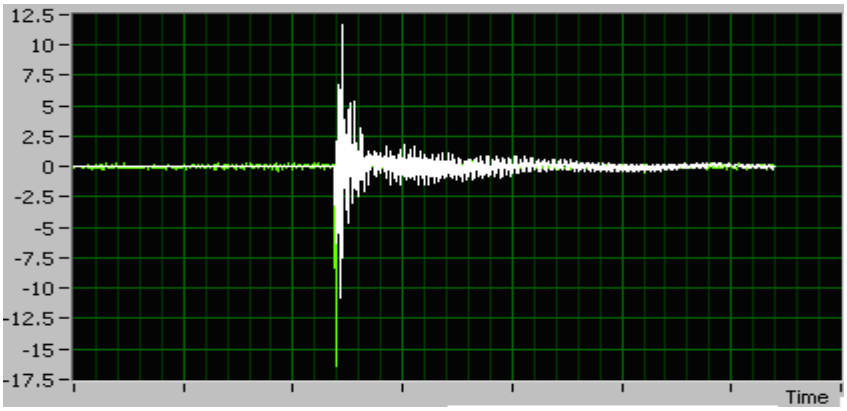

Figure 35: Both the excitation (green signal) and the response (white signal) in time domain.

The threshold for trigger of impact hammer is set to 0.01 V and 300 points of pre-trigger was collected to completely acquire the impact signal. The force window was set to 80%, which means that the duration of the force window is 80% of the total duration of the stimulus signal. The exponential window is set to 10%, which indicates the remaining level of the applied exponential window at the end of the signal. The impact hammer hits the cylinder three times at each location while the reference accelerometer is placed at one location on the cylinder. The high pass filter is set to 0.1 Hz. The low pass filter

used has 8 poles and a cut-off frequency of 1000 Hz. The FRF is calculated using the H1 method, which is the ratio of cross power spectrum between stimulus (impact hammer), response (accelerometer) and auto power spectrum of stimulus.

The sensitivity of the 784A accelerometer and the hammer is set to 100mV/g and 10mV/g respectively.

Figure 36 (a) to (i) show the FRF response for each hammer impact.

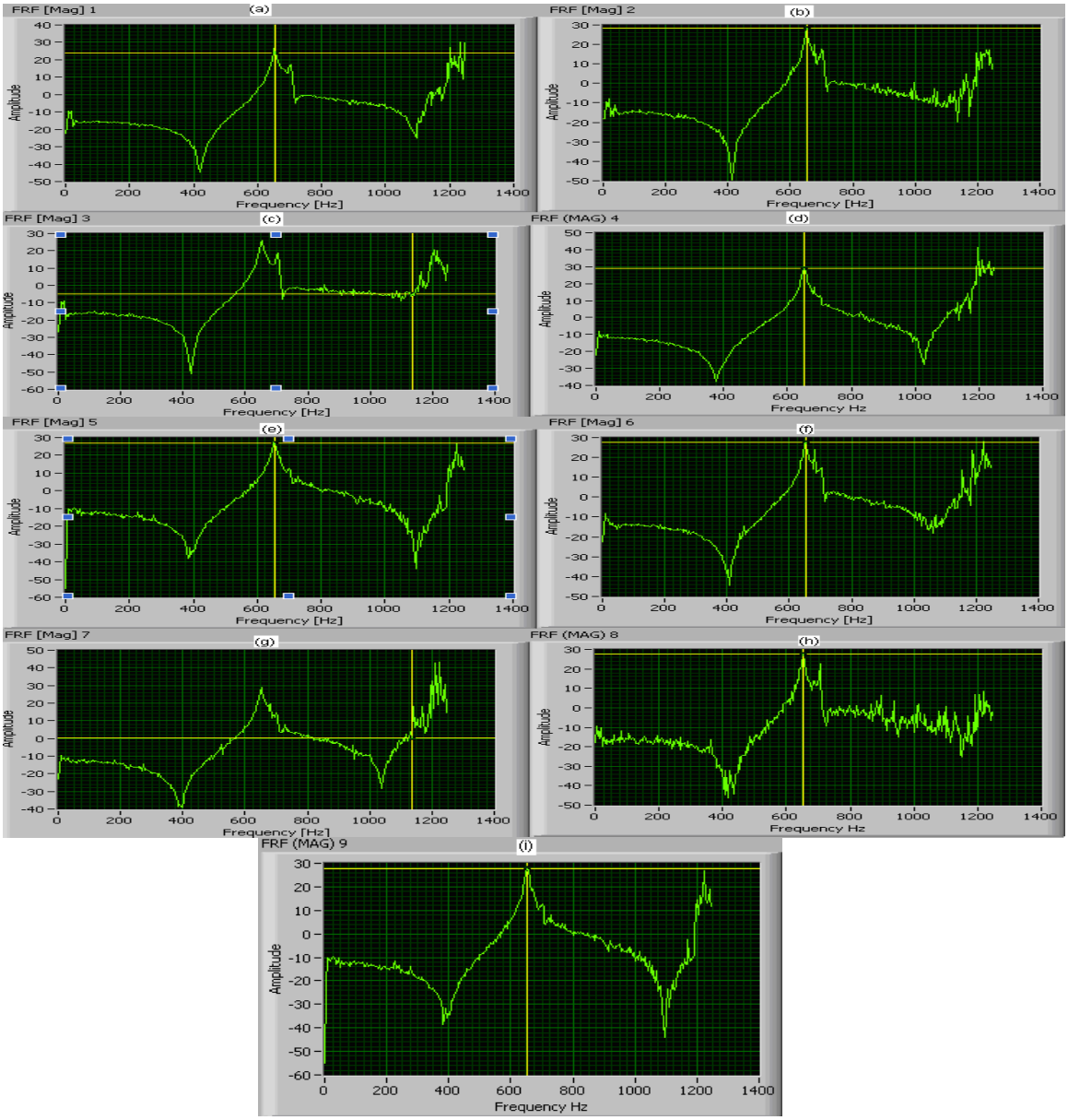

Figure 36: (a) to (i) FRF of hammer impacts 1 to 9.

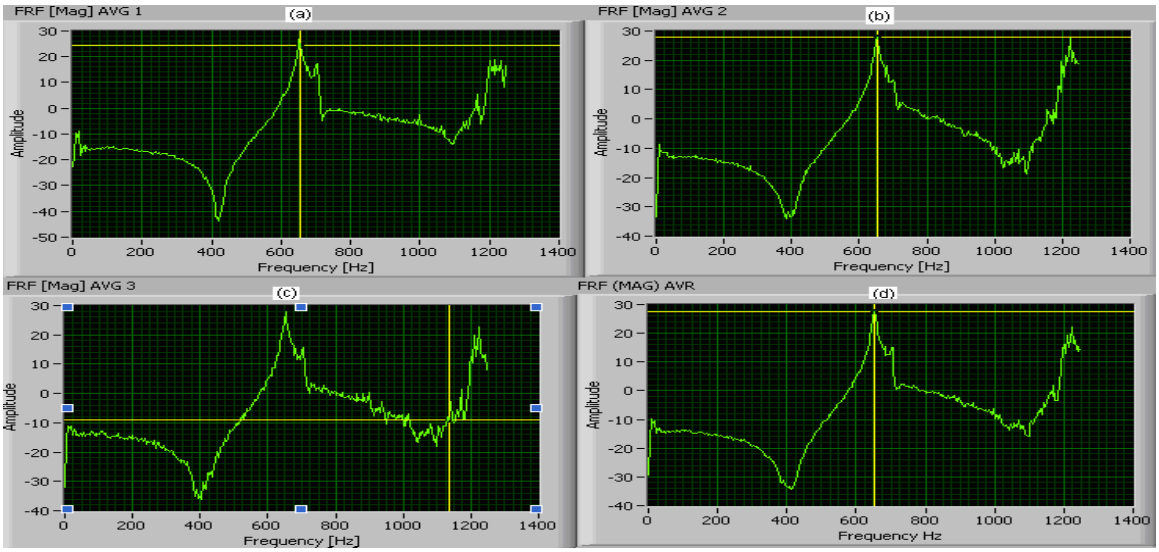

Figure 37: Averaged Magnitude of the FRF for measurements 1 to 9.

According to Figure 37, the first natural frequency of 651.88 Hz is identified.

Mode	Frequency [Hz]
1.	651.88

Table 7: First natural frequency measured experimentally.

6.1.3. Finite Element Analysis

The following table indicates the natural frequency of the first mode of the cylinder and the maximum and minimum deformation for this mode in inch.

Results	
Frequency	658.14 Hz
Minimum	1.708 in
Maximum	12.616 in

Table 8: Natural frequency and maximum and minimum deformation of the cylinder for the first mode.

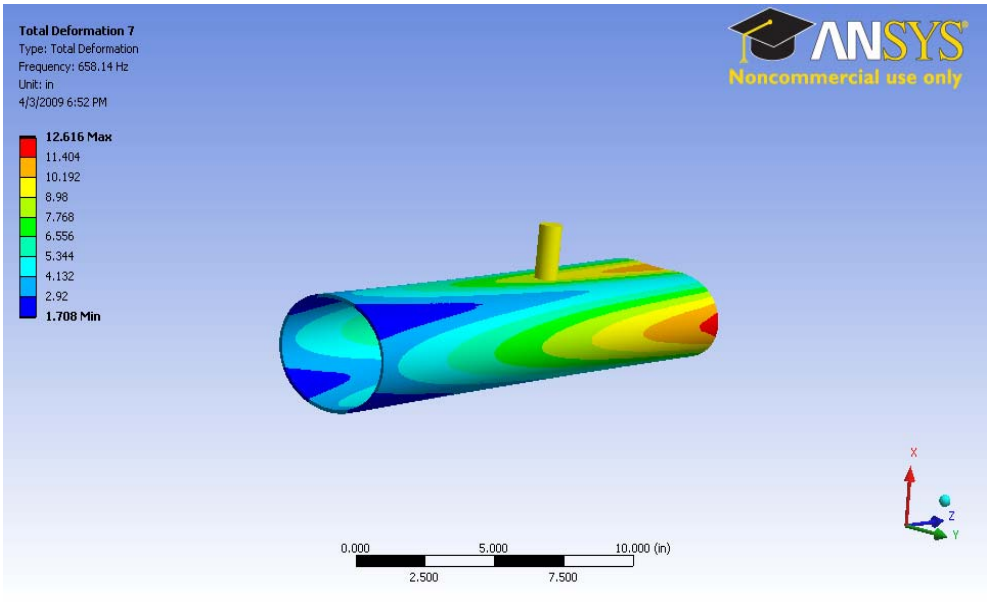

Figure 38: Mode shape of the first mode of the cylinder.

6.1.4. Comparison between Numerical and Experimental Results

The error between the FEM and experimental results is due to the suspension effect using bungee cord. Indeed the bungee cords have added some damping to the cylinder that was not taken into account in FEM modeling.

FE Model Frequencies	Experimental Frequencies	Relative error [(FEM-EXP)/FEM]*100%
658.14	651.88	0.95 %

Table 9: First resonance frequency for the experimental and FEM and the relative error between the two approaches.

6.2. Resonance Testing on the Shaft

The same procedures applied to the cylinder in section 6.1 will be applied to the shaft to extract the natural frequencies, when the turbine equipment becomes available. The FE

results can be used to properly plan the test setup including determination of the best locations for impact hammer excitation and best locations for accelerometer. The details of the test planning and setup are provided in detail in section 6.1.

Modal test data acquired from the test must be processed and analyzed using the LabVIEW program developed for this purpose. The sensor locations will be selected by using the results of the FE Modeling of the shaft in section 7.1 and by following these criteria:

1) Avoiding the nodal lines of modes since there would be no energy transfer from the point of impact at node locations to all other degrees of freedoms of the cylinder.

2) Picking a location with low average velocity for all the modes will eliminate the problem of "double-hits" of impact hammer.

Measurement locations should be chosen such that mode shapes are independent, which means that two accelerometers should not pick up the vibration signals that are caused by only one shape.

For the shaft, the frequency range of interest will be from 0 to 5000Hz. According to sampling theorem, the sampling frequency should be larger than 25 kHz.

Two AC-104 accelerometers (Sensitivity of 100mV/g and frequency range of 1-10000 Hz) will be used to acquire the structure's response. The accelerometers will be attached to the structure using a permanent stud.

The size of impact hammer should be chosen so that it is heavy enough to produce sufficient energy into the structure to excite all the modes of interest without damaging the cylinder. To do so, an additional mass (122g) is added to the hammer, so that the hammer has a total mass of 412.3g.

A steel tip will be used to excite the shaft, since the maximum frequency of excitation needed is 5000 Hz.

6.3. Effect of the Added Mass on the Modes of the Cylinder

The modeling has been performed on the cylinder without any added mass, and with accelerometers of different masses (30g, 45g, 145g), and comparison of the result of these four different cases.

6.3.1. Modal Analysis of the Cylinder without any Added Mass

Table 10 shows the geometry, dimension and material properties of the cylinder without any accelerometer mounted on it. Table 11 presents its nine first natural frequencies.

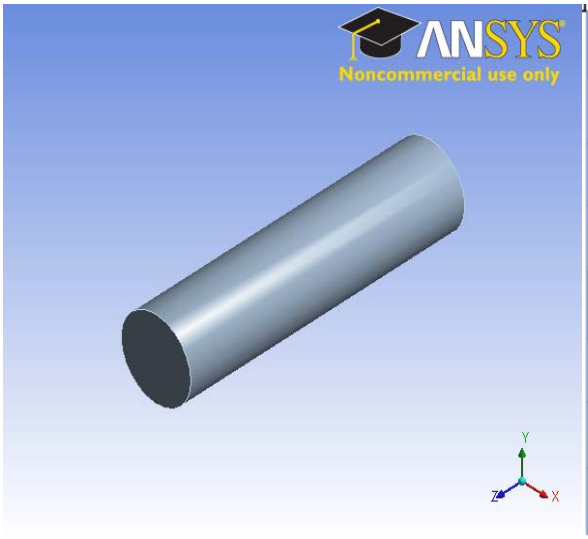

Geometry	
L	17.252 in
D	4.504 in
d	0.125 in
Material Properties	
Young's Modulus	1.e+007 psi
Poisson's Ratio	0.33
Density	0.101 lbm/in³

Table 10: Geometry, Dimensions and material properties of the cylinder.

Mode	Frequency [Hz]
1.	730.42
2.	734.52
3.	1111.8
4.	1114.4
5.	2097.2
6.	2119.7
7.	2268.9
8.	2269.
9.	2326.9

Table 11: First nine resonance frequencies of the cylinder without any added mass.

Figure 39 shows the mode shapes of the first two modes of the shaft.

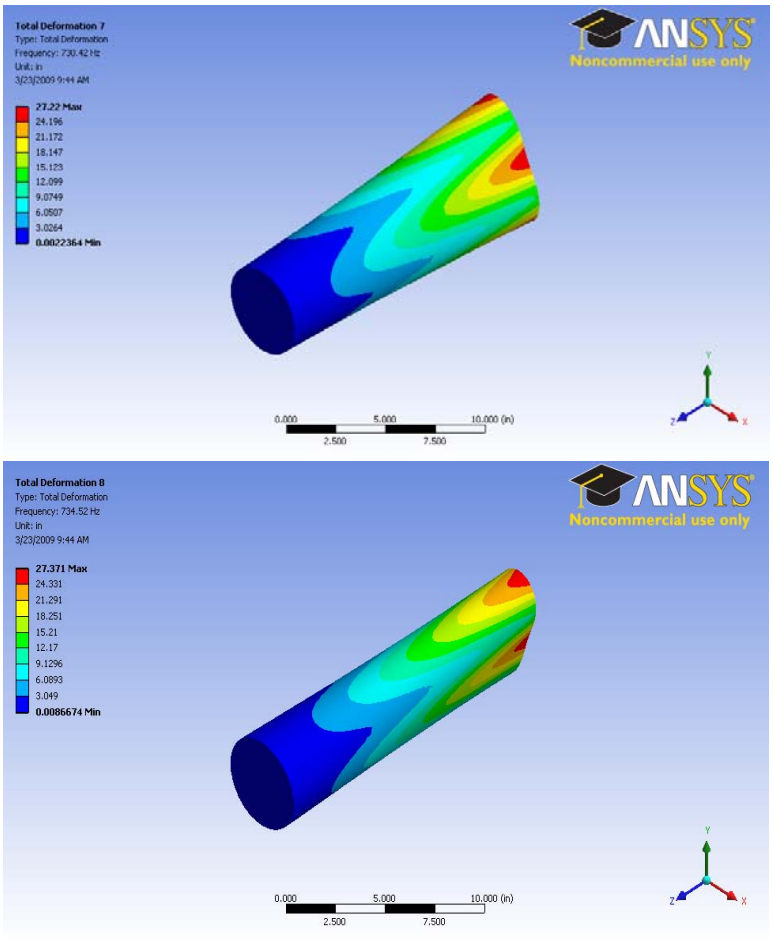

Figure 39: First two mode shapes of the model cylinder.

6.3.2. Modal Analysis of the Cylinder taking into Account the Mass of the Accelerometer 726 (30g)

Figure 40 shows the geometry of the cylinder with the accelerometer 726 mounted on it, and Table 12 presents its nine first natural frequencies.

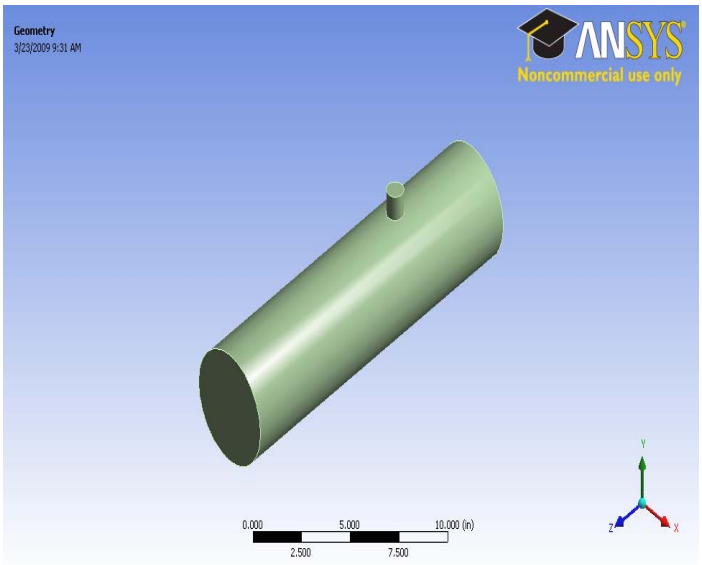

Figure 40: Geometry of the cylinder with 30g accelerometer installed.

Mode	Frequency [Hz]
1.	685.36
2.	700.73
3.	1064.
4.	1071.4
5.	1946.3
6.	1994.6
7.	2135.1
8.	2157.2
9.	2241.7

Table 12: First nine resonance frequencies of the cylinder with 30g accelerometer installed.

Figure 41 shows the mode shapes of the first two modes of the shaft.

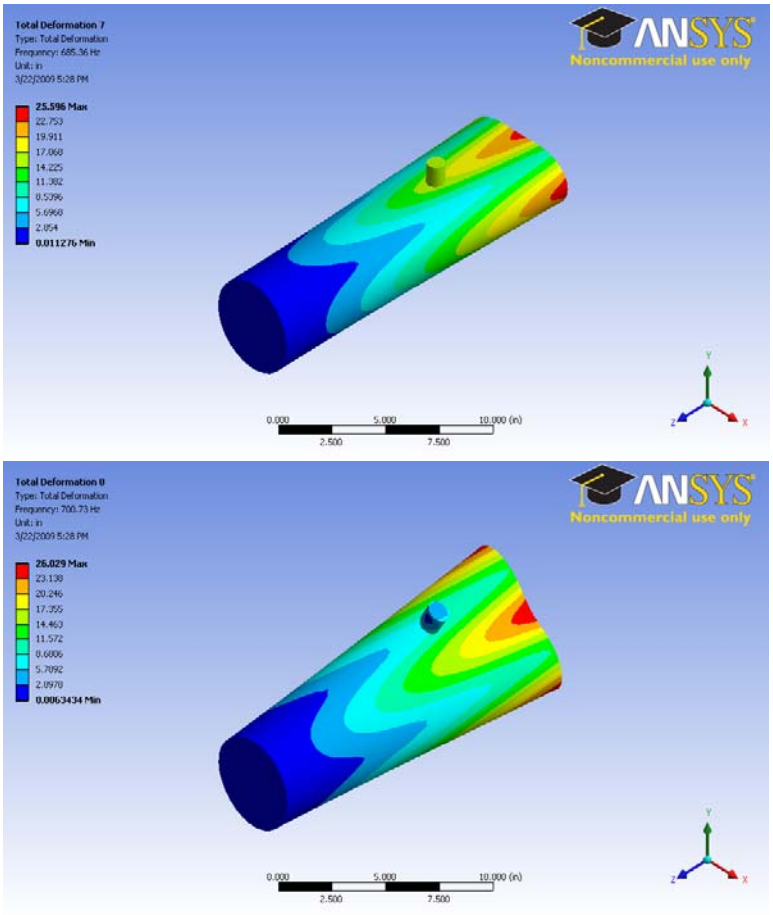

Figure 41: First two mode shapes of the cylinder with 30g accelerometer installed.

6.3.3. Modal Analysis of the Cylinder taking into account the Mass of the Accelerometer 784A (45g)

Figure 42 shows the geometry of the cylinder with the accelerometer 784A mounted on it. Table 13 presents its nine first natural frequencies.

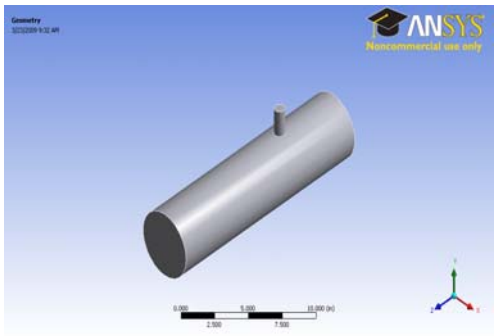

Figure 42: Geometry of the cylinder with a 45g accelerometer installed.

Mode	Frequency [Hz]
1.	675.87
2.	692.91
3.	1052.4
4.	1064.9
5.	1392.3
6.	1895.1
7.	1991.5
8.	2052.6
9.	2163.7

Table 13: First nine resonance frequencies of the cylinder with 45g accelerometer installed.

Figure 43 shows the mode shapes of the first two modes of the shaft.

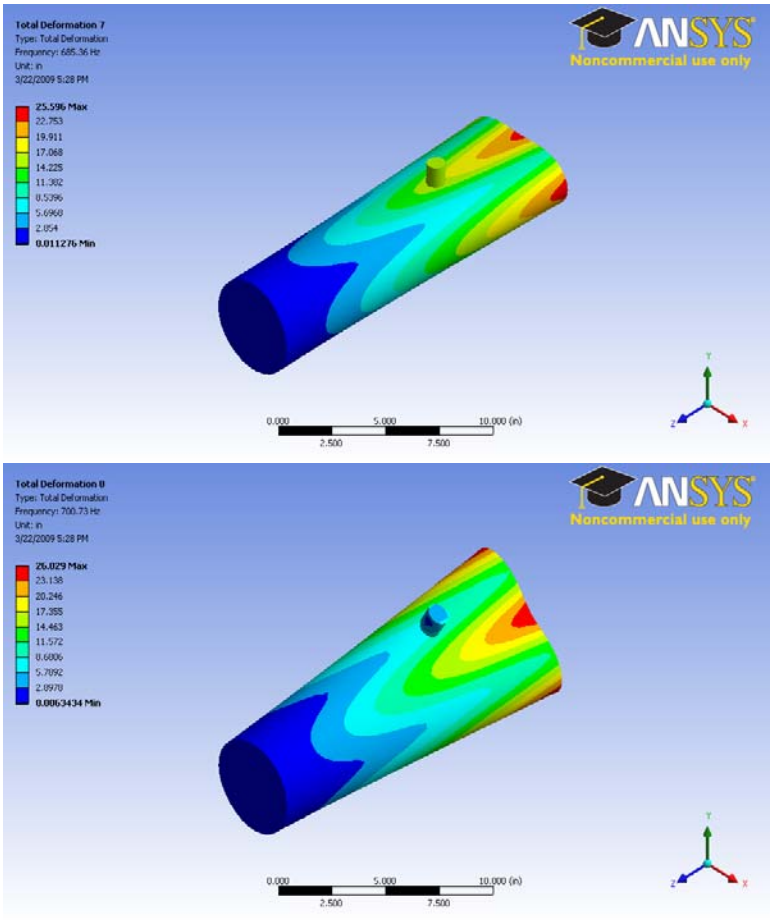

Figure 43: First two mode shapes of the cylinder with a 45g accelerometer installed.

6.3.4. Modal Analysis of the Cylinder taking into account the Mass of the CTC Accelerometer (145g)

Figure 44 shows the geometry of the cylinder with the accelerometer 784A mounted on it. Table 14 presents its nine first natural frequencies.

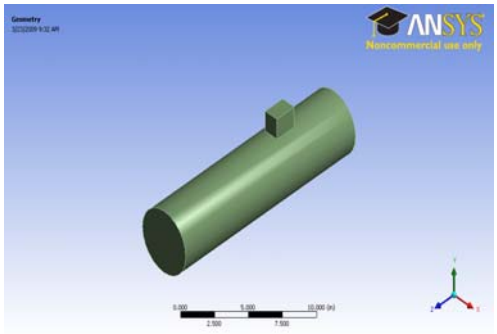

Figure 44: Geometry of the cylinder with a 145g accelerometer installed.

Mode	Frequency [Hz]
1.	633.83
2.	685.92
3.	1030.5
4.	1062.6
5.	1225.2
6.	1691.4
7.	1929.9
8.	2049.5
9.	2175.2

Table 14: First nine resonance frequencies of the cylinder with 145g accelerometer installed.

Figure 45 shows the mode shapes of the first two modes of the shaft.

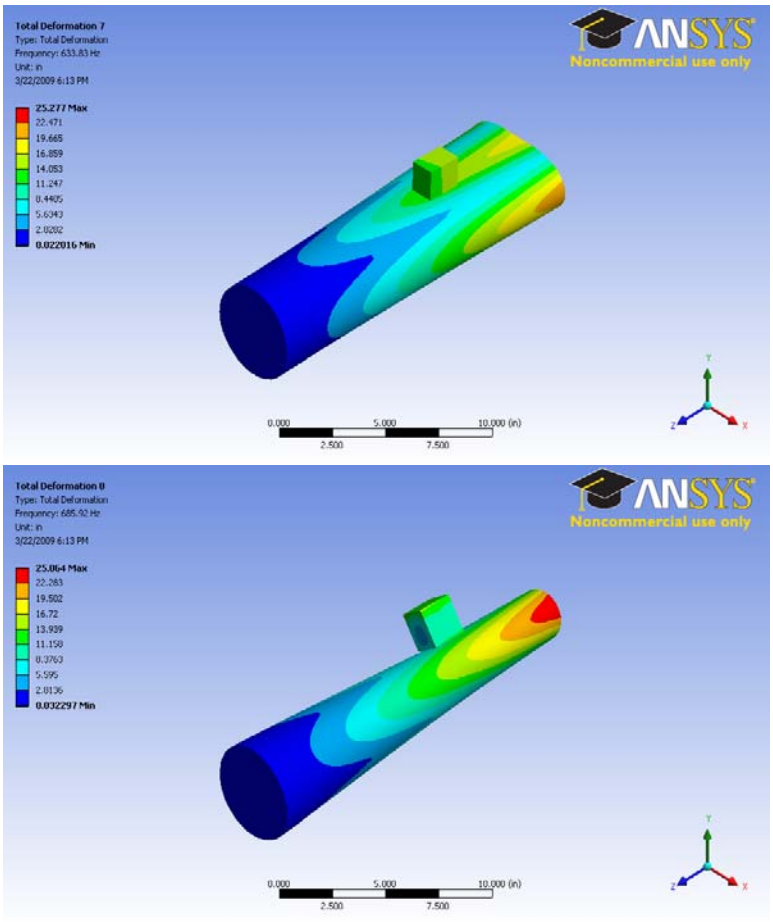

Figure 45: First two mode shapes of the cylinder with a 145g accelerometer installed.

6.3.5. Comparison between the Result for the four cases (effect of different added mass)

Natural Freq Without added mass	Natural Freq With 726 Acc (30g)	Natural Freq With 784A Acc (45g)	Natural Freq With CTC Acc (145g)
730.42	685.36	675.87	633.83
734.52	700.73	692.91	685.92
1111.8	1064.	1052.4	1030.5
1114.4	1071.4	1064.9	1062.6
2097.2	1946.3	1392.3	1225.2
2119.7	1994.6	1895.1	1691.4
2268.9	2135.1	1991.5	1929.9
2269.	2157.2	2052.6	2049.5

Table 15: Summary of the first nine resonance frequencies of the cylinder in 4 different cases.

Table 15 shows that the first resonance frequency without added mass is 730.42 Hz, when we loaded the cylinder by using more heavier accelerometer, the resonance frequency went down to 685.36 Hz, 675.87 Hz and 633.83 Hz for 30g, 45g and 145g accelerometer respectively.

We concluded that the addition of extra mass to the cylinder lower the resonance frequencies of the cylinder. Added mass has a larger effect on high frequency than on low frequency.

7. FE MODELING OF THE 20 KW TURBINE USING ANSYS

The simulation on ANSYS Workbench of the turbine and its sub-components is performed under the assumption of steady state conditions. The modal analysis using the IGES file of the shaft is performed and the resonances frequencies are identified. The flexible dynamic analysis is performed on the entire turbine to determine the dynamic response due to the harmonic loads on the gearbox and the bearings.

7.1. Modal Analysis of the Shaft in ANSYS and Comparison with Theoretical Results

The modal analysis is used to determine the vibration characteristics (natural frequencies and mode shapes) of the shaft. The modal analysis is performed on the imported “iges” file of the shaft originally generated in solidworks.

If the shaft runs at twice the critical speed, it will produce a large sub-synchronous response; this sub-synchronous response is not related to any fault of the system and can be easily mistaken for instability. Thus, the importance of performing the modal analysis on the shaft to determine their resonance frequencies [15].

First, the modal analysis is performed while taking into account the presence of the two needle bearings and the thrust bearings. The needle bearings load and thrust bearings load are modeled as radial and axial displacement constraint, respectively. Second, the modal analysis is performed on the shaft alone, free at each end.

For this analysis only the linear behavior is valid. Damping and load are ignored for this type of analysis. In the second phase of this section the numerical results of the modal analysis are compared to theoretical ones. When calculating theoretically the modes, the shaft is modeled as a beam. This approximation is expected to produce only small discrepancies as compared with the measured modes.

The difference between theoretical and numerical results is due to the fact that the shaft is not a beam but has different sections and different shape. The results of the modal analysis show three different types of the modes of the shaft: torsional, bending and axial as shown in Figure 46.

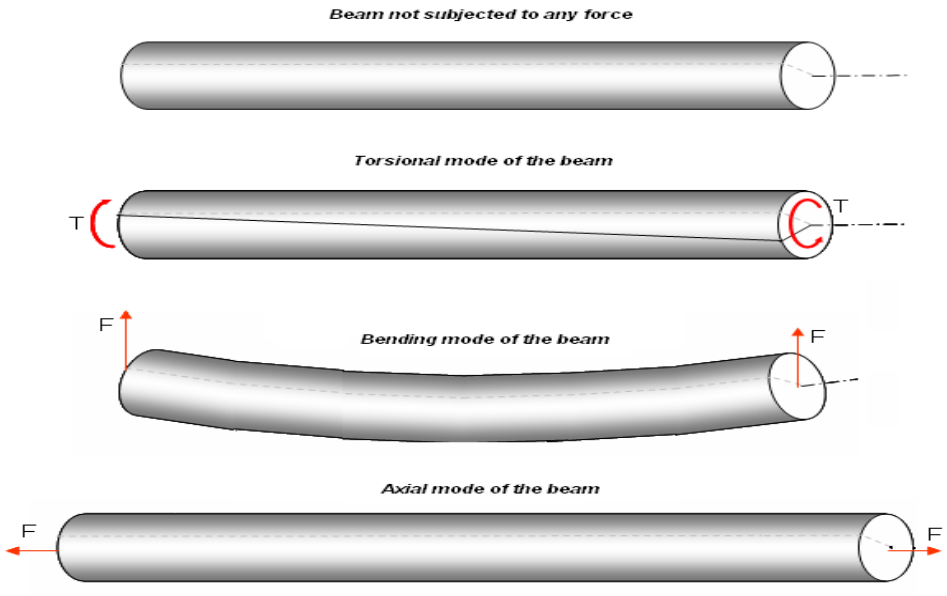

Figure 46: Definition of different mode type of the shaft.

7.1.1. Modal Analysis of the Shaft taking into account the Needle and Thrust Bearings

The modal analysis was performed on the shaft taking into account the needle bearings load as shown in Figure 47.

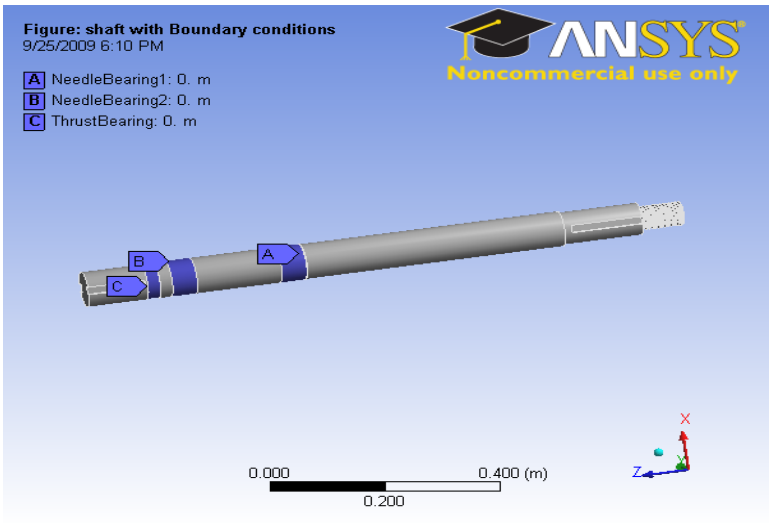

Figure 47: Shaft taking into account the needle and thrust bearings.

Table 16 indicates the frequency, the mode type, the minimum and the maximum deformation at each calculated mode. Note that the minimum and maximum deformation are expressed in meter unit and is equal to the maximum angular deformation times the radius of the shaft.

Mode	Mode type	Frequency [Hz]	Minimum	Maximum
1.	1st Bending Mode	123.65	5.5991e-006 m	0.48403 m
2.		123.67	5.0706e-006 m	0.48305 m
3.	2nd Bending Mode	691.42	5.226e-005 m	0.60971 m
4.		697.43	3.7839e-006 m	0.59133 m
5.	1st Axial Mode	1495.4	1.7656e-003 m	0.26933 m
6.	1st Torsional Mode	1651.9	2.508e-004 m	0.35682 m
7.	.. Bending Mode	1704.3	4.6035e-005 m	0.73122 m
8.		1760.0	1.8514e-005 m	0.69778 m
9.		3034.4	2.1855e-004 m	0.78561 m
10.		3068.0	5.0185e-005 m	0.95915 m
11.		3130.6	8.3301e-005 m	0.8174 m
12.	2nd Torsional Mode	3233.7	5.0388e-005 m	0.43177 m
13.	.. Bending Mode	3235.8	4.685e-005 m	0.93557 m
14.	.. Axial Mode	4296.4	2.5113e-003 m	0.31594 m
15.	3rd Torsional Mode	4556.0	1.751e-004 m	0.51624 m
16.	.. Bending Mode	4577.9	3.0826e-005 m	0.88017 m
17.		4639.9	9.7498e-005 m	0.91674 m
18.	4th Torsional Mode	5874.7	9.4313e-005 m	0.53918 m
19.	.. Bending Mode	5989.3	1.4493e-003 m	0.50754 m
20.		6009.3	1.167e-003 m	0.50292 m
21.		6404.5	5.6733e-004 m	0.67437 m
22.		6457.5	4.2493e-004 m	0.70295 m
23.	.. Axial Mode	6903.5	4.3658e-003 m	0.39313 m
24.	5th Torsional Mode	7298.1	4.4488e-005 m	0.57595 m
25.	.. Bending Mode	8195.4	4.6221e-004 m	0.7286 m
26.		8281.3	3.4422e-004 m	0.57703 m
27.		8300.1	1.218e-003 m	0.57566 m
28.		8379.3	1.3027e-004 m	0.69968 m
29.	6th Torsional Mode	8676.5	1.2084e-004 m	0.88601 m

Table 16: Resonance frequencies, modes type, minimum and maximum deformations for the first 29 calculated modes.

Figure 48 shows the mode shapes of the first six torsional mode of the shaft. These resonance frequencies will be correlated with the peaks shown in the spectrum when performing the Vibration condition monitoring on the turbine, so we make sure these peaks does not correspond to some other faults but to this resonance phenomena.

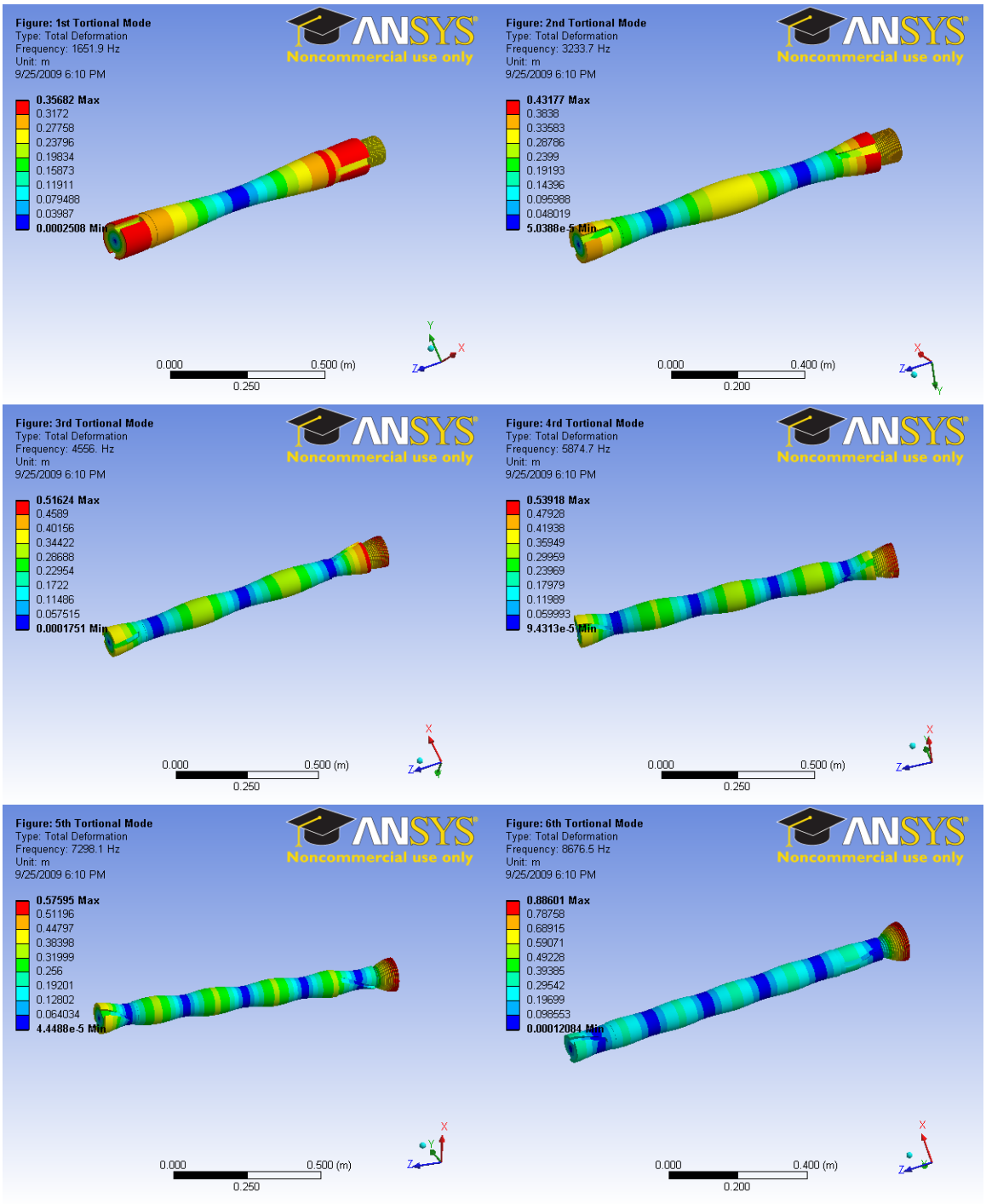

Figure 48: First six Torsional mode shapes of the shafts taking into account the needle and thrust bearings.

7.1.2. Modal Analysis of the free Supported Shaft

In this section, the modal analysis is performed on the free supported shaft without taking into account the bearing loads.

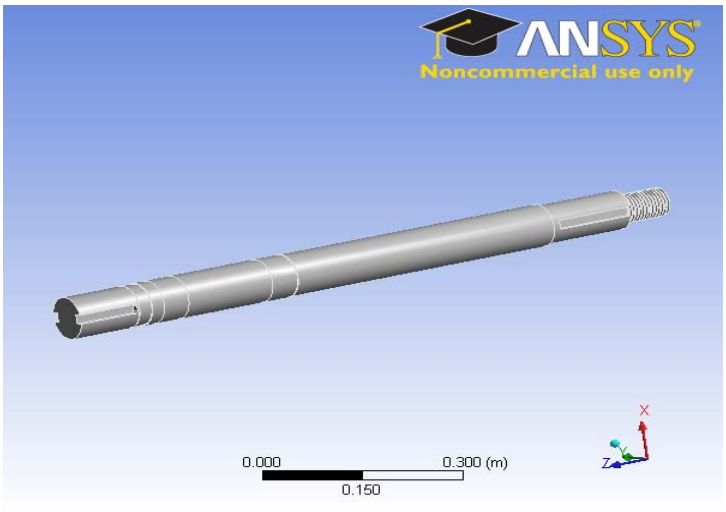

Figure 49: Free supported shaft.

The following table indicates the frequency, the mode type, the minimum and the maximum deformation at each calculated mode.

Mode	Mode type	Frequency [Hz] using "ANSYS"	Frequency [Hz] using "Theoretical Method"	Minimum	Maximum
1.	1st Bending Mode	323.38		6.0842e-004 m	0.44489 m
2.		323.75		2.15e-004 m	0.43977 m
3.	2nd Bending Mode	837.27		1.2722e-003 m	0.52084 m
4.		844.12		3.0804e-004 m	0.49838 m
5.	3rd Bending Mode	1521.3		1.3231e-003 m	0.58984 m
6.		1551.7		2.0654e-004 m	0.55557 m
7.	1st Torsional Mode	1651.7	1739	5.4963e-005 m	0.35674 m
8.	4th Bending Mode	2350.1		1.5468e-003 m	0.62936 m
9.		2411.4		1.464e-003 m	0.61816 m
10.	1st Axial Mode	2547.5		2.0766e-003 m	0.26538 m
11.	2nd Torsional Mode	3232.7	3478	3.9711e-005 m	0.43162 m
12.	5th Bending Mode	3317.7		8.5066e-004 m	0.66736 m
13.		3392.		6.6063e-004 m	0.69706 m
14.	6th Bending Mode	4365.2		2.9443e-004 m	0.72401 m
15.		4434.2		7.3316e-004 m	0.76435 m
16.	3rd Torsional Mode	4553.2	5217	1.1115e-004 m	0.49625 m
17.	2nd Axial Mode	5011.5		1.4116e-003 m	0.31758 m
18.	7th Bending Mode	5461.6		6.3976e-004 m	0.72957 m
19.		5538.7		2.1677e-003 m	0.73993 m
20.	4rd Tortional Mode	5869.3	6956	1.4844e-004 m	0.5378 m
21.	8th Bending Mode	6655.3		1.5015e-003 m	0.65125 m
22.		6761.2		1.3802e-003 m	0.64854 m
23.	3rd Axial Mode	7264.1		2.0471e-003 m	0.36872 m
24.	5th Tortional Mode	7289.3	8695	1.0082e-004 m	0.57473 m
25.	9th Bending Mode	7965.3		1.3888e-003 m	0.57829 m
26.		8084.4		5.7009e-004 m	0.58669 m
27.	6th Tortional Mode	8669.	10435	1.4466e-004 m	0.88283 m
28.	10th Bending Mode	9351.8		2.7738e-004 m	0.56037 m
29.		9457.2		5.2754e-004 m	0.56443 m
30.	4th Axial Mode	9510.8		2.9186e-003 m	0.40761 m

Table 17: Resonance frequencies, modes type, minimum and maximum deformations for the first 30 calculated modes.

The equation used to compute the natural frequencies of the shaft for torsional modes is:

$$\omega_n = \frac{i \times \pi \times \sqrt{G}}{l \times \sqrt{\rho}}. \tag{7.1}$$

Where i is the mode number, G is the shear modulus, l is the length of the shaft and ρ is the mass per unit volume.

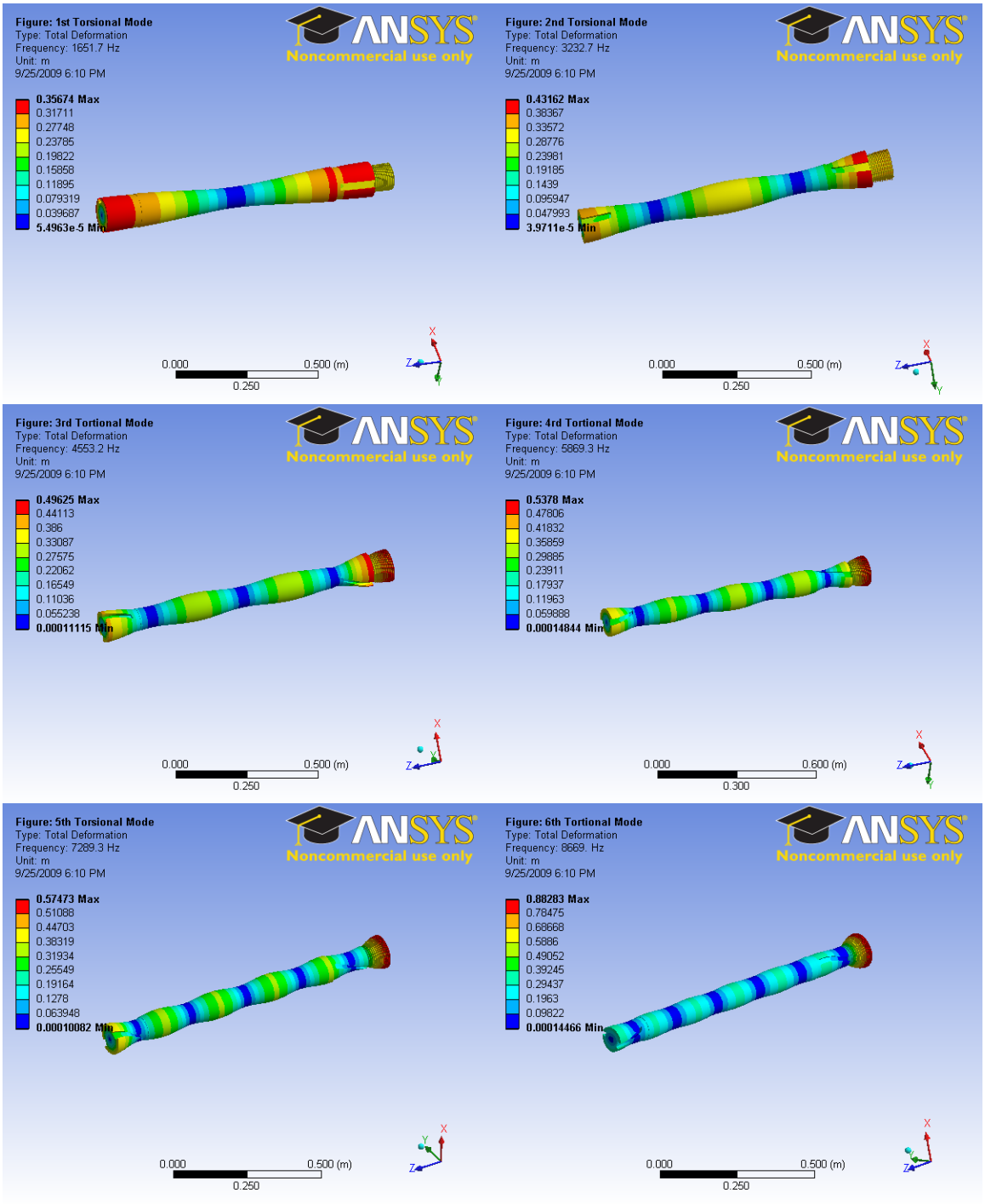

Figure 50: First six Torsional mode shapes of the free supported shafts.

7.2. Dynamic Response in Steady State Condition

The assembly in Figure 51 modeled on ANSYS is composed of different parts including the motor shell, the shaft housing, the inner end cap, outer end and the end cap.

Flexible Dynamic Analysis is used to determine the dynamic response of the turbine under the action of the gearbox and the bearing loads. The gearbox load is simulated as a rotating punctual point load on the circumference inside the motor shell. There are two types of the bearing load that apply on the shaft housing:

- The needle bearing load simulated as a radial surface load rotating on the surface band inside the shaft housing.
- The thrust bearings load simulated as axial surface load rotating on the surface band inside the shaft housing.

This analysis is used to determine the time-varying accelerations in specific locations (where the accelerometers are located) as it responds to these harmonic loads. The damping ratio caused by the bearings is assumed to be 0.1.

Geometry and material properties of the turbine:

The material properties are summarized in Table 18:

Structural	
Material	Structural steel
Young's Modulus	2.e+011 Pa
Poisson's Ratio	0.3
Density	7850. kg/m³

Table 18: Geometry and material properties of the turbine.

The geometry of the turbine including the shaft housing and the end cups is shown in Figure 51:

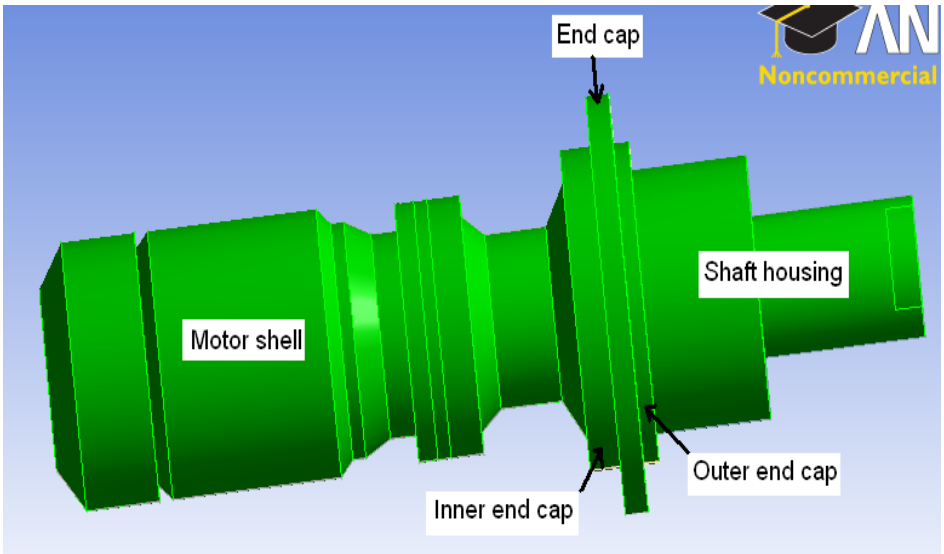

Figure 51: Geometry of the 20 kW turbine shaft, gearbox, and power plant housing.

Loads and constraints:

The gearbox load is simulated as a rotating punctual point load on the circumference inside the motor shell. Its mathematical expression is:

$$P(Pascal) = 3000 \times \left|\sin(2\pi f \times 25 \times t + \theta)\right|,\ 0 \le \theta \le 2\pi\,. \qquad (7.1)$$

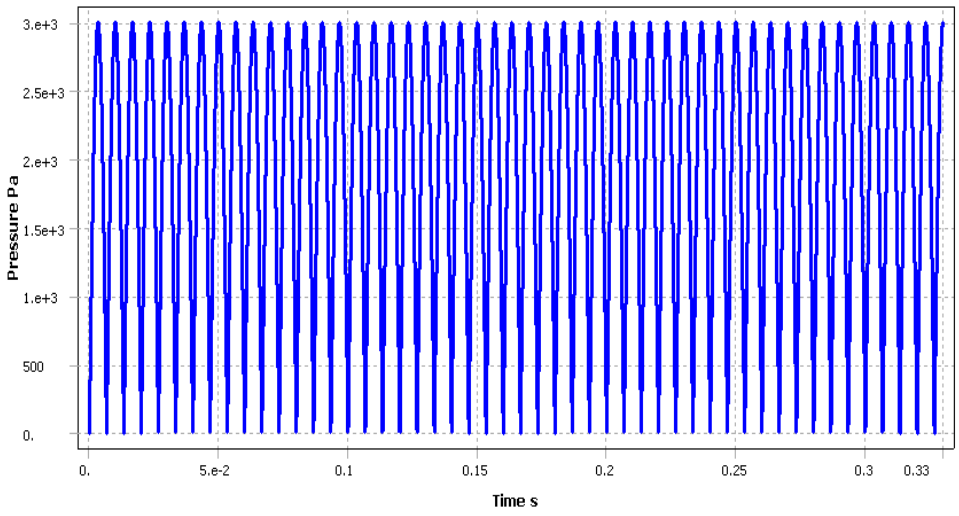

Figure 52: Harmonic gearbox load vs. Time.

The needle bearing and thrust bearing loads simulated as radial and axial surface load rotating on the surface band inside the shaft housing. Its mathematical expression is:

$$P(Pascal) = 3000 \times \left|\sin(2\pi ft + \theta)\right|,\ 0 \le \theta \le 2\pi\,. \tag{7.2}$$

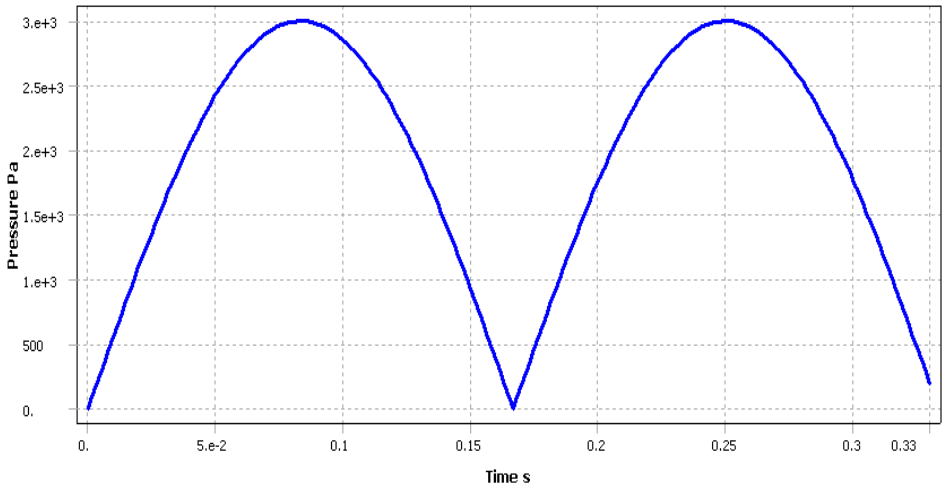

Figure 53: Harmonic bearing load vs. Time.

All those loads and constrains are shown in Figure 54 below:

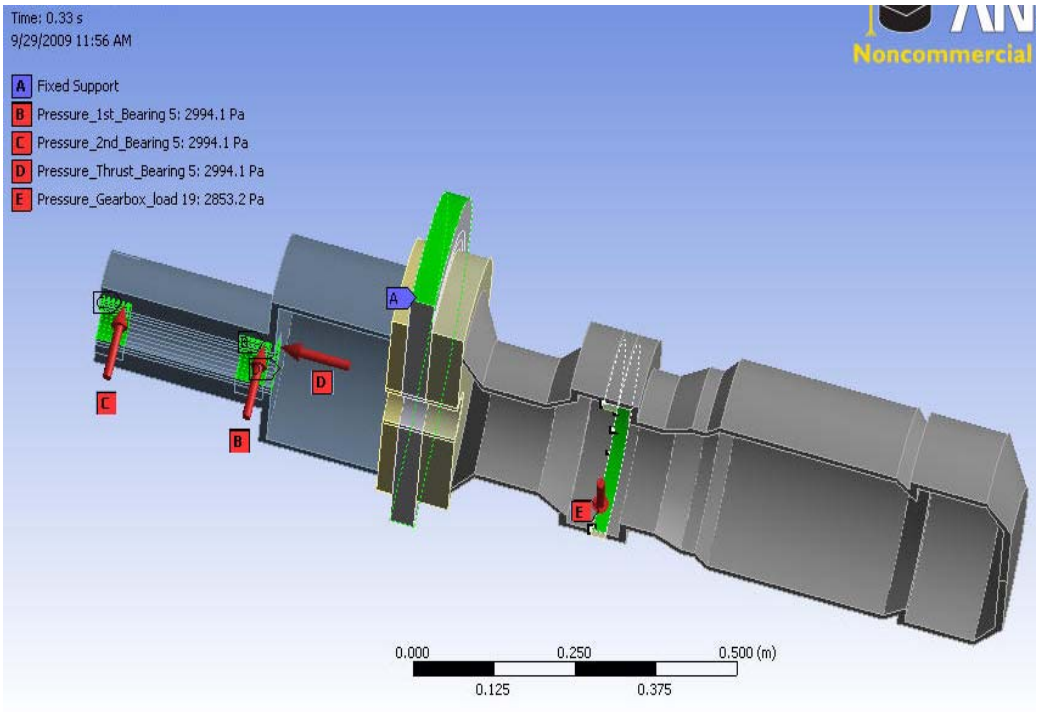

Figure 54: Loads and constraints on the 20 KW turbine shaft, gearbox and power plant housing.

First, the acceleration due to the bearings load is calculated at the location of the six low and high frequency accelerometers shown in the Figure 55 and 56.

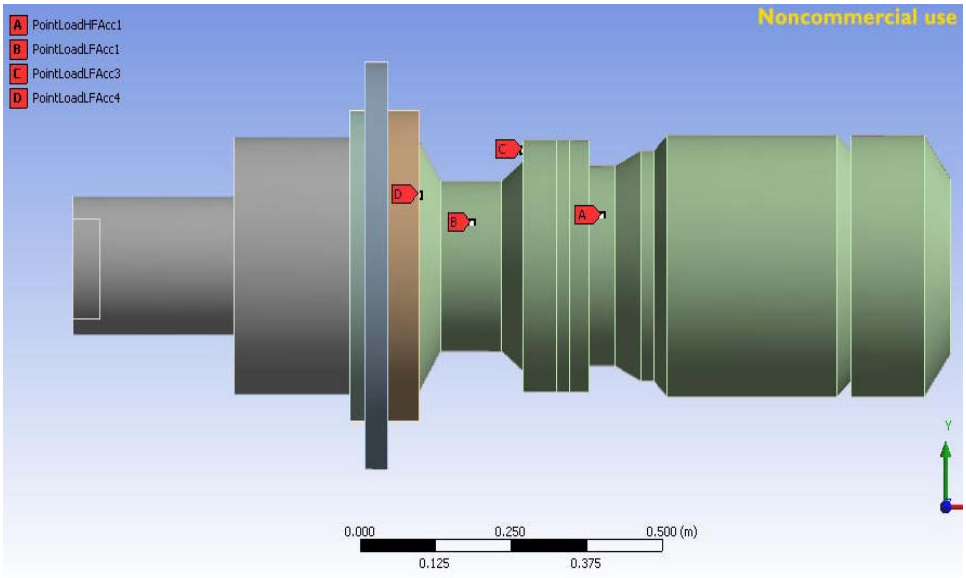

Figure 55: Locations of the high frequency accelerometer 1 and low frequency accelerometers 1, 3 and 4.

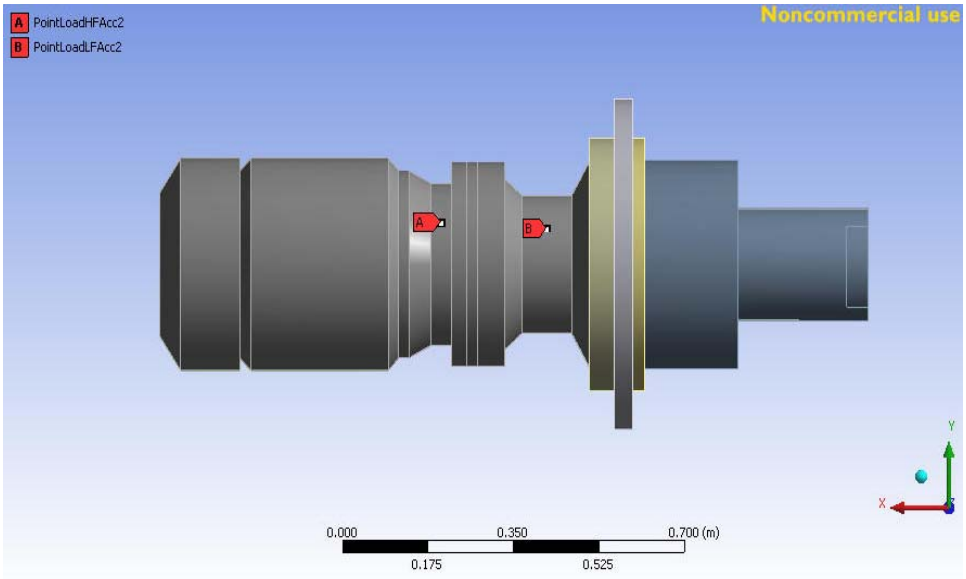

Figure 56: Location of high-frequency accelerometer 2 and low frequency accelerometer 2.

Figure 57 shows the magnitude of the radial acceleration of the assembly at time 0.33s shown.

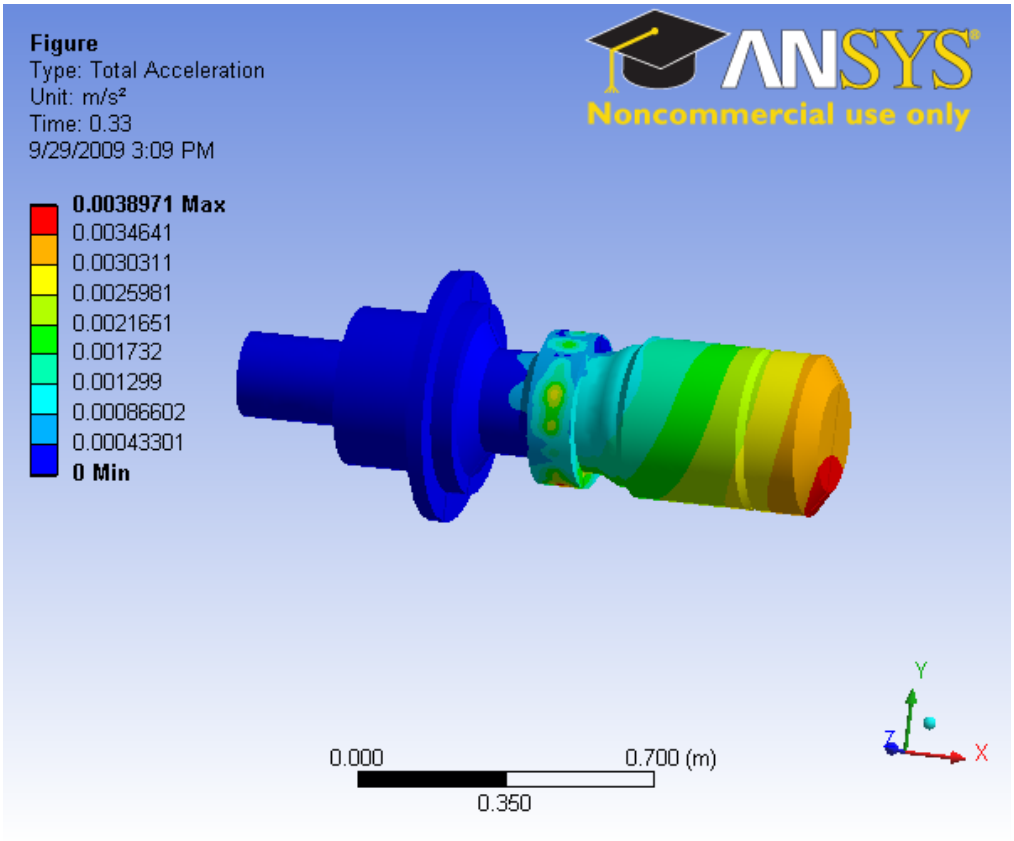

Figure 57: Radial Acceleration magnitude distribution on the assembly at time 0.33s.

Figure 58 below shows the directional radial acceleration of the assembly at time 0.33s.

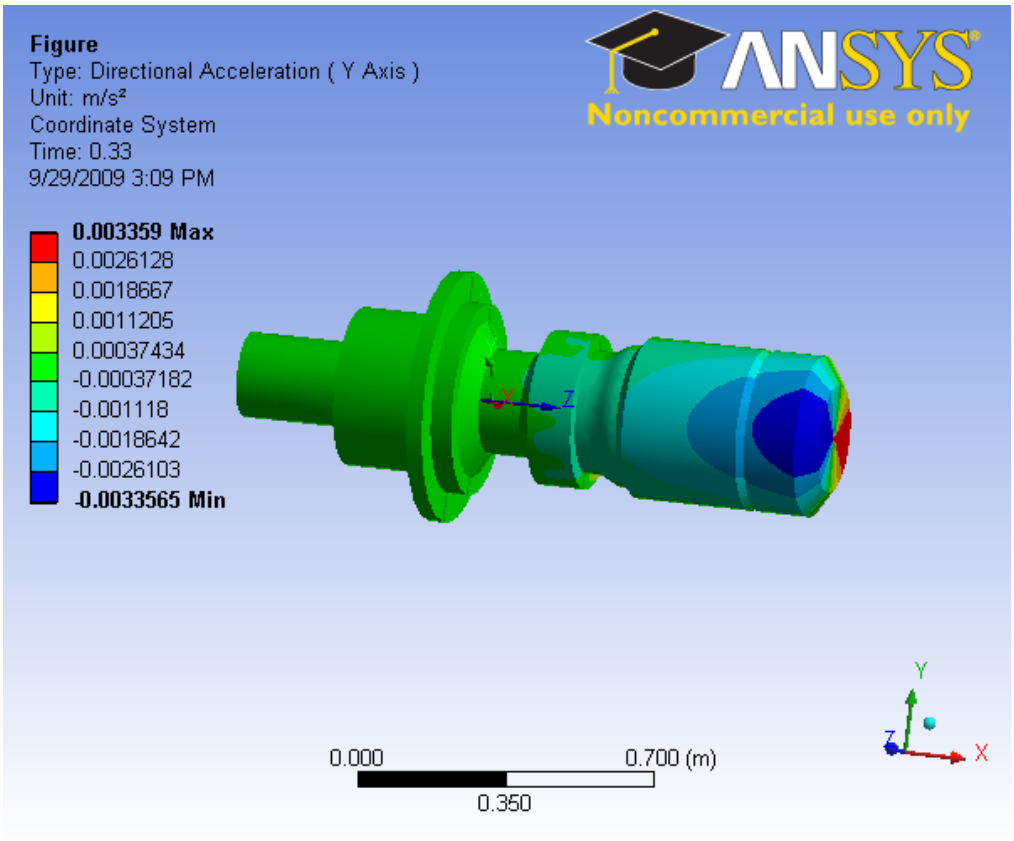

Figure 58: Directional Radial acceleration distribution on the body of the turbine at time 0.33s.

Figure 59 below shows the instantaneous radial acceleration versus time at location of high frequency accelerometer 1.

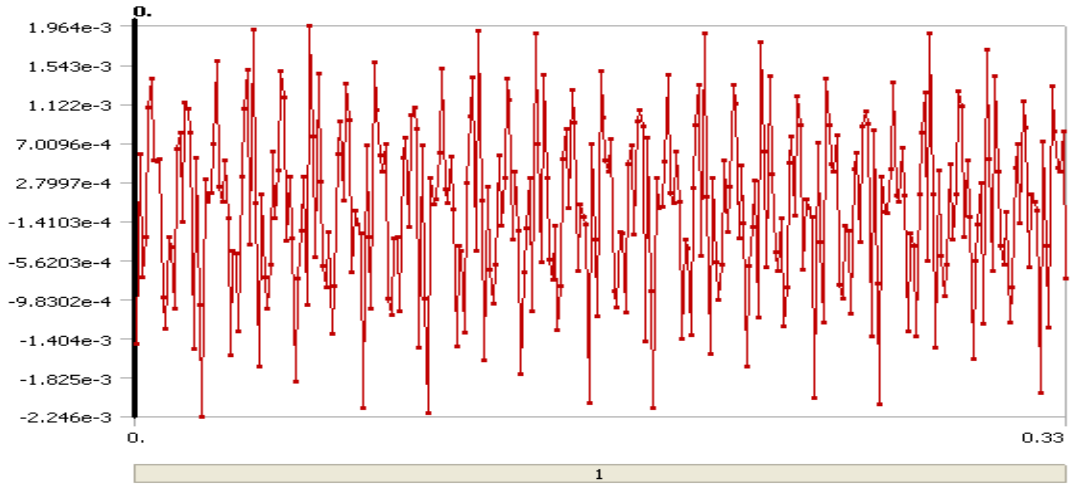

Figure 59: Radial acceleration [m/s^2] vs. time (second) at location of high frequency accelerometer 1.

Figure 60 shows the instantaneous radial acceleration versus time at location of high frequency accelerometer 2.

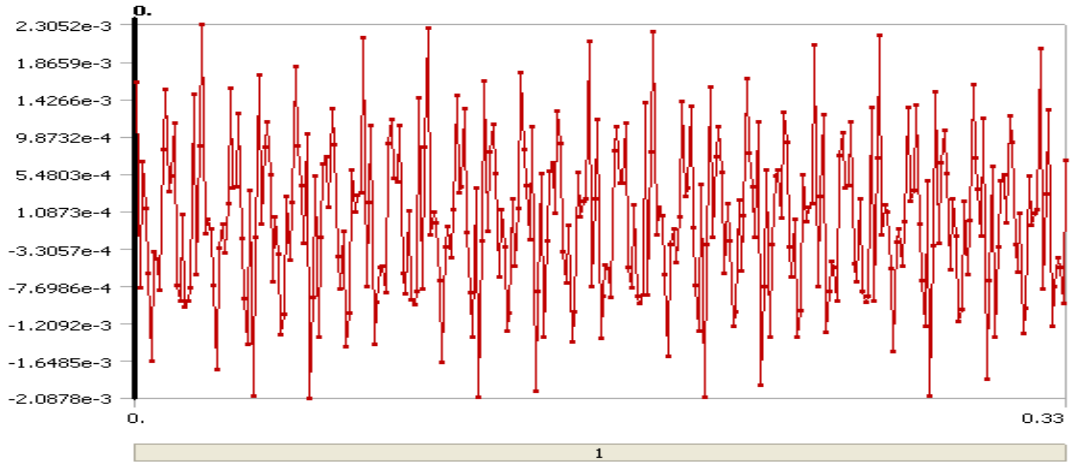

Figure 60: Radial acceleration [m/s^2] vs. time (second) at location of high frequency accelerometer 2.

Figure 61 below shows the instantaneous radial acceleration versus time at location of low frequency accelerometer 1.

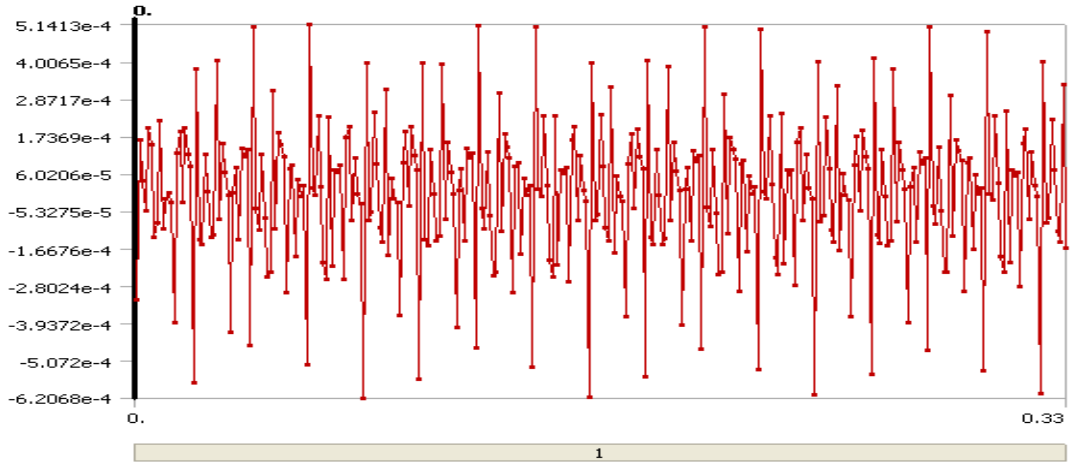

Figure 61: Radial acceleration [m/s^2] vs. time at location (second) of low frequency accelerometer 1.

Figure 62 shows the radial acceleration versus time at location of the low frequency accelerometer 2.

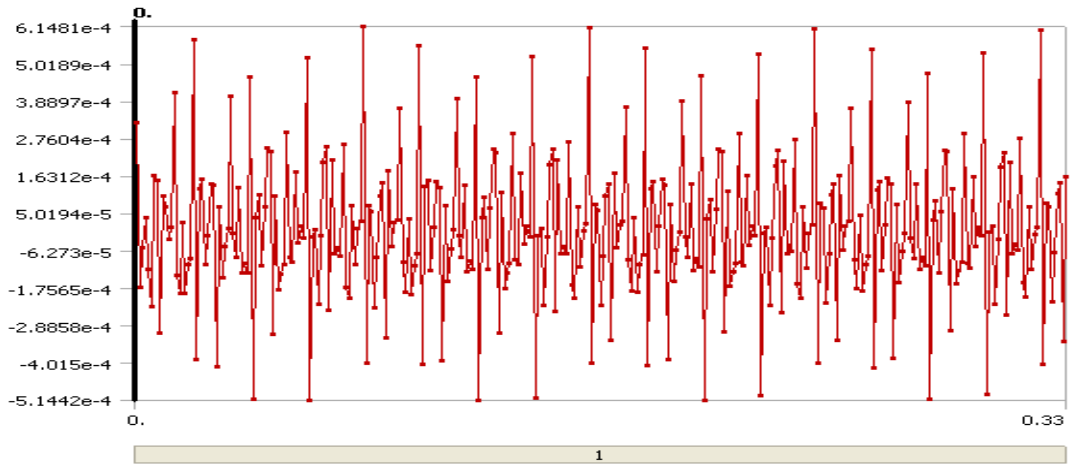

Figure 62: Radial acceleration [m/s^2] vs. time at location (second) of low frequency accelerometer 2.

Figure 63 shows the axial acceleration versus time at location of low frequency accelerometer 3.

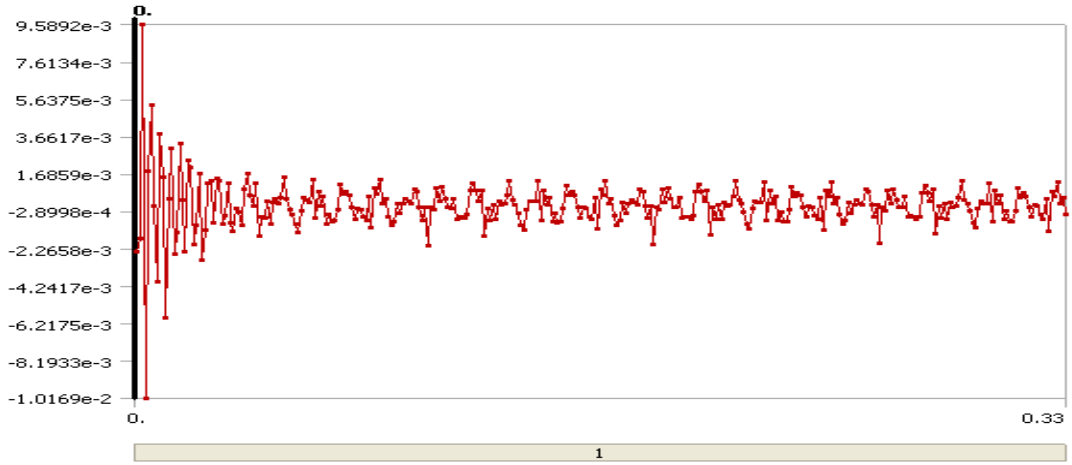

Figure 63: Axial acceleration [m/s^2] vs. time (second) at location of low frequency accelerometer 3.

Figure 64 shows the axial acceleration versus time at location of the low frequency accelerometer 4.

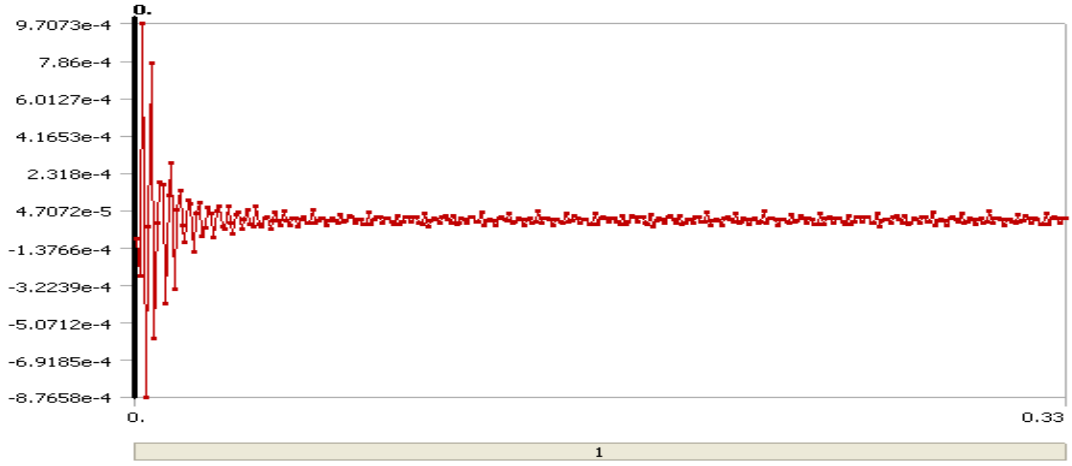

Figure 64: Axial acceleration [m/s^2] vs. time (second) at location of low frequency accelerometer 4.

8. CONCLUSION

Based on the literature survey presented in chapter 2, vibration analysis is proven to be amongst the most powerful, reliable and practical method among other techniques for condition monitoring of rotating machines. For this purpose, a LabVIEW program has been developed and implemented with more advanced and sophisticated techniques for faults detection and diagnostic.

This program contains features (filtering and spectral analysis) to identify the machine signature without interfering noise that may cause false alarms. Finding the resonance frequencies of the sub-components of the system is the most important step for vibration condition monitoring. The LabVIEW program has been developed for this purpose and allows performing the resonance testing on any structure.

A modal experiment was performed on a small scale cylinder of the turbine and a fan, using the LabVIEW program developed for this purpose. The Finite Element Modeling of the small-scale cylinder was performed to verify the experimental results. The relative error between the two approaches was found to be 0.95%. The modal testing results of the fan were used in the vibration experiment to correlate the peaks related to its resonances frequencies.

The experiment was performed on the fan to demonstrate the faults detection and diagnostic techniques implemented on the LabVIEW program. Crest factor, kurtosis value and RMS level commonly used as vibration condition monitoring features in time domain data analysis were tested during the experiment. The crest factor is a measure of the impulsiveness of the vibration signal, kurtosis is used to detect any transient effect – shocks, impulse noise and short events - in the vibration signal, and RMS value is used for general monitoring purpose.

The peaks on the power spectrum were clearly identified and correlated to the fundamental frequency, its harmonics and to the resonance frequencies of the system. The ordering technique was also tested by setting the value of the fan rotating speed manually (since the encoder cannot be used with the fan). The power spectrum and the third octave were displayed as a function of multiples of the rotational speed. This technique is important when trending the data acquired from a non-stationary rotating machines.

The minimum number of measurement averages necessary was found: ten averages are sufficient to eliminate the noise present in the fan measurements.

The alerts and alarms were tested for each technique mentioned above, and the alerts turned red whenever the vibration signal exceeded the threshold limits. The baseline was associated with the vibration data acquired when the fan is running at minimum speed (12 Hz). When the fan was run at speed level 3 (16.84 Hz), the indicators mentioned above (including the time and third octave signals) exceeded the threshold limits, triggering and alarm.

The finite element modeling in ANSYS of the 20 KW ocean turbine was also performed, and the vibration signals in different locations were estimated. Accelerometers should be placed at these locations once the 20 kW ocean turbine is ready.

8.1. Future Work

A certain number of tasks remain before the vibration-based machine condition monitoring method proposed here is complete:

The next task of work that should be performed is:

- How Condition Monitoring should be used in relation to maintenance planning and operation should be determined. In other terms, one should determine when to do inspection, and at what degradation levels one should renew or replace the component under consideration or correct the fault that is causing this degradation.
- The dynamic simulations on ANSYS should be used to estimate the vibration signals while faults (imbalance, misalignment, bearing and gearbox faults) are presents in the system. How theses faults can propagate within and across sub-systems and lead to potential failure modes. The severity of the faults should also be identified.
- The vibration response should be determined when using the mechanical brake of the 20 kW ocean turbine, using FEM modeling in ANSYS.
- The resonance testing on the shaft using the LabVIEW program should be performed to validate the finite element modeling results presented in this thesis.

9. NOMENCLATURE

Symbols and Abbreviations

Variable name	Description
STFT	Short Time Fourier Transform
TFA	Time-Frequency analysis
FEM	Finite Element Modeling
RMS	Root Mean Square
CPB	Constant Percentage Band
RPM	Round per minute
RPS	Round per second
FFT	Fast Fourier Transform
PSD	Power spectral density
PS	Power Spectrogram
GUI	Graphic User Interface
FT-OT	Fourier Transform based order tracking
AD-OT	Angle domain sampling based order trucking
VKF-OT	Vold-Kalman filter based order tracking
C	Cepstrum
τ	quefrency
t'	Variable of integration
$s(t)$	Time signal
$w(t)$	Time window
$F(f)$	Power Spectrum
ξ	Fourier Transform Operator
F_{max}	Maximum frequency of interest
F_s	Sampling frequency
df	Frequency resolution

Variable name	Description
N	Number of revolution
n	Number of samples
σ	Variance
dB	Decibel
kW	Kilowatt
w	Angular Velocity
T_s	Scan Period
n_s	Rotational speed of the sun
n_p	Rotational speed of the planet carrier
n_t	Number of teeth
s	Shaft speed
n_r	Number of rolling elements
f_{gmf}	Gear-mesh frequency
D_r	Diameter of the ring wheel
D_s	Diameter of the sun
D	Roller diameter
G	Shear modulus of the shaft
i	Number of the tortional mode
ρ	Mass per unit volume of the shaft
l	Length of the shaft
d	Pitch diameter
log	Logarithmic operator

Figure 65: Description of all variables used in the thesis.

10. APPENDIX-A

This appendix provides some additional technical details for the vibration monitoring hardware and software.

10.1. Encoder Mode Options

In the encoder mode X1, only one rising or falling edge of signal A is detected. In the encoder mode X2, rising and falling edge of signal A is detected. In the encoder mode X4, rising and falling edge of both signal A and B is detected.

10.2. AC/DC Input Coupling

AC coupling can be used to reject the unwanted DC offsets, for example to prevent DC offsets from reaching the comparator. DC coupling is used when both AC and DC components are to be presented as input to the comparator.

10.3. Analog Filtering

Single-pole, low-pass filter with three programmable cut-off frequencies 100 kHz, 20 kHz, and 30 Hz is available to reject low-level noise that may interfere with the comparator.

10.4. Comparator

The threshold of the comparator can be set anywhere from –12.5V to +12.5V.

Ringing on the square wave caused by the noise or amplitude modulated noise may cause extraneous switching of the comparator, causing false counts to be measured. Ideally, the comparator threshold should be set so that the comparator switches at the point of fastest slew rate on the input waveform.

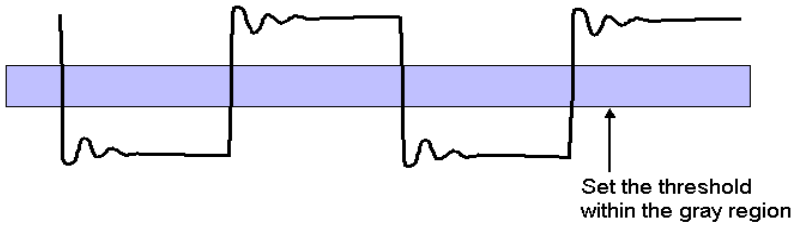

Figure 66: Setting the Comparator Threshold.

10.5. Debounce Module

16 programmable debounce times from 500 ns to 25.5 ms for each channel is available.

The debounce time determines how fast the signal can change and still be recognized.

There are three debounce modes “trigger after stable” and “trigger before stable” and bypass.

10.6. Trigger After Stable Mode

The output of the debounce module will not change state until a period of stability has been achieved. This means that the input has an edge and then must be stable for a period of time equal to the debounce time in order for that edge to be accepted. This mode

rejects glitches and disturbances due to the vibration of the encoder and only passing state transitions after a required period of stability (debounce time). The debounce time should be set short enough to accept the desired input pulse but longer than the period of the undesired disturbance. Some experimentation is required to find the appropriate debounce time for our application. The debounce time in Figure 67 is T1.

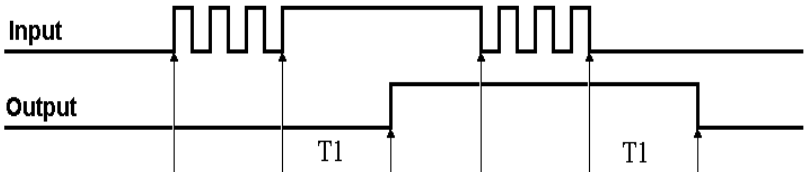

Figure 67: Trigger after Stable Mode of the debounce module.

10.7. Trigger Before Stable Mode

The output of the debounce module immediately changes state, but will not change state again until a period of stability has passed. For this reason the mode can be used to detect glitches. The debounce time in Figure 68 is T1.

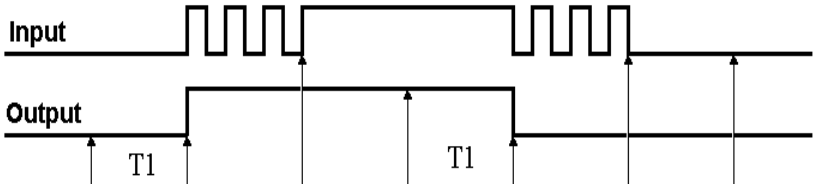

Figure 68: Trigger before Stable Mode of the debounce module.

10.8. Averaging Number

Used for period counting method and has four set of averaging numbers: 1, 10,100, and 1000.

BIBLIOGRAPHY

[1] Frank Fahy, “Sound and structural vibration, radiation, Transmission and response”, Academic Press 2001.

[2] Michael Peter Norton, Denis G. Karczub, “Fundamentals of Noise and Vibration Analysis for Engineers”, Cambridge, U.K., New York: Cambridge University Press, 2003.

[3] Connection Technology Center, Inc. New York, “Accelerometer’s for wind turbine”, https://ctconline.com/pdf/pubTechPapers/17-Accelerometers%20for%20Wind%20 Turbines.pdf.

[4] James R. Rasmussen, Brian Howard, “Condition monitoring for hydro machinery“, http://www.gepower.com/prod_serv/products/oc/en/orbit/downloads/2q04condmonhydro mach.pdf.

[5] Agnes Muszynska, “Vibrational Diagnostics of Rotating Machinery Malfunction”, International Journal of Rotating Machinery 1995, Vol. 1, No. 3-4, pp. 237-266 (Jan. 1994).

[6] Pratesh Jayaswal, A. K.Wadhwani, and K. B.Mulchandani, “Machine Fault Signature Analysis”, International Journal of Rotating Machinery Volume 2008, Article ID 583982. (Jan. 2008).

[7] Ray Beebe, “Condition monitoring of steam turbines by performance analysis”, Journal of Quality in Maintenance Engineering, Vol. 9 No. 2, 2003 pp.102-112.

[8] Dr. T. J. Chalko, Dr. D. X. Li, “Modeling Turbine Vibration in Terms of its Load Variation”, International Journal of Rotating Machinery 1995, Vol. 1, No. 3-4, pp. 293-299.

[9] Ulrich Sudmersen, Fortec-Forschungstechnik Gmbh, “Vibration Monitoring for Process Control and Optimization in Production Lines”. http://www.ndt.net/article/ecndt2006/doc/We.4.8.2.pdf.

[10] Wilfried Reimche, Ulrich Südmersen, Oliver Pietsch, Christian Scheer, Fiedrich-Wilhelm Bach, “Basics Of Vibration Monitoring For Fault Detection And Process Control”, http://www.aaende.org.ar/sitio/biblioteca/material/T-039.pdf.

[11] Mohamed Farhat & Paul Bourdon, Jean_Louis Gagne & Louise Remillard, "Improving Hydro Turbine Profitability by Monitoring Cavitation Aggressiveness", conference and exposition, Vancouver, QC, Canada March 29-31, 1999.

[12] Angelo M 1987, "Vibration Monitoring of Machines", Technical Review No. 1, Bruel and Kjaer.

[13] Glew C.A.W. & Watson D.C, 1970, "Vibration Analysis as a Maintenance Tool at Sea", Institute of Marine Engineers.

[14] Glew C.A.W. 1974, "The Effectiveness of Vibration as a Maintenance Tool", Institute of Marine Engineers, Canada.

[15] Tranter J. 1989, "The Fundamentals of, and the Application of Computers to, Condition Monitoring and Predictive Maintenance", Proceedings of 1st conference IMMDC Las Vegas, Nevada, USA.

[16] Ndubuisi Ekekwe, "Peter Kazanzides. 2007, Incremental Encoder Based Position and Velocity Measurements VLSI Chip with Serial Peripheral Interface", IEEE.

[17] Archambault R. 1989, "Getting More Out of Vibration Signals", Proceedings of 1st Conference /MMDC Las Vegas, Nevada, USA.

[18] Acta Metallurgica Slovaca, 2004, "Angular Vibration Measurements of the power Driwing Systems".
http://www.ams.tuke.sk/data/ams_online/2004/number3/mag12/mag12.pdf

[19] Lubomir Smutny, Jiri Tuma2, Radim Farana, "Calibration of sensors for angular vibration measurements, XVIII IMEKO WORLD CONGRESS", Metrology for a Sustainable Development September, 17 – 22, 2006, Rio de Janeiro, Brazil
http://www.imeko.org/publications/wc-2006/PWC-2006-TC22-002u.pdf

[20] Courrech J. & Gaudet M.1987, "Envelope analysis - the key to rolling-element bearing diagnosis", Bruel & Kjaer, Application Note.

[21] Berry J.E. 1990, "How to Specify Machinery Vibration Spectral Alarms", Sound & Vibration, September 1990.

[22] Randal, R. B., "Cepstrum analysis and gearbox fault diagnosis", Bruel and Kjoer Publications, Application Note 233.

[23] Caryn, M. R., "A method for sensorless on-line vibration monitoring of induction machines", IEEE, Transaction on Industry Applications, Vol. 3, N.6.

[24] Grade, S., Herlufsen, H., konstantin-Hansen, H. and Vold, H., "characteristics of Vold-Kalman Order Tracking filter", Bruel and kjoer technical review, 1999.

[25] Blough, J. R., “A survey of DSP methods for rotating machinery analysis, what is needed, what is available”, Journal of Sound and Vibration 262, 2003, pp707-720.

[26] Hewlett Packard. Application Note 243-1: Dynamic signal analyzer application, Palo Alto, 1983.

[27] Albright M. F. and Qian Sh., “A comparison of the newly proposed Gabor order tracking technique vs. other order tracking methods”, SAE paper, No. 2001-01-1471, 2001.

[28] Troy V. Nguyen, Harold W. Nelson, “A System Approach to Machinery Condition Monitoring and Diagnostic”. http://www.dtic.mil/ndia/2001systems/nguyen.pdf.

[29] GE Wind Energy, LLC, “Advanced Wind Turbine Program Next Generation Turbine Development Project” http://www.nrel.gov/docs/fy06osti/38752.pdf.

[30] D. Corbus, A.C. Hansen and J. Minnema, “Effect of Blade Torsion on Modeling Results for the Small Wind Research Turbine (SWRT)“. http://www.nrel.gov/docs/fy06osti/39000.pdf.

[31] Ehrich, F.F., “Sub-harmonic Vibration of Rotors in Bearing Clearance”, American Society of Mechanical Engineers Journal of Engineering for Power 88 (1966).

[32] A.El-Shafei, “Fan Diagnosis in the field”. ISO/TC108/SC2/WG10/N065.

[33] Wenxian Yang, P. J. Tavner and Michael Wilkinson, “Condition Monitoring and Fault Diagnosis of a Wind Turbine with a Synchronous Generator using Wavelet Transforms”, IET Power Electronics, Machines and Drives (PEMD2008), 2-4 April, York, UK, 2008.

[34] D. M. Yang, A. F. Stronach, and P. MacConnell, “The application of advanced signal processing techniques to induction motor bearing condition monitoring”, Meccanica, vol. 38, no. 2, pp. 297–308, 2003.

[35] M.J. Schulz, Cincinnati, Ohio, M.J. Sundaresan, North Carolina, “Smart Sensor System for Structural Condition Monitoring of Wind Turbines”. http://www.nrel.gov/docs/fy06osti/40089.pdf.

[36] Caselitz P., Giebhardt J., “Rotor condition monitoring for improved operational safety of offshore wind energy converters”, Journal of Solar Energy Engineering, May 2005, Vol. 127, pages (253-261).

[37] Paresh Girdhar, C. Scheffer, “Machinery Vibration Analysis & Predictive Maintenance”, Elsevier 2004.

[38] Victor Wowk, “Machinery Vibration: Balancing”, New York: McGraw-Hill, c1995.

[39] Steve Goldman, P.E. “Vibration Spectrum Analysis”, 2nd edition, New York: Industrial Press, c1999.

[40] Robert B. McMillan, PE, CEM, “Rotating Machinery: Practical Solutions to Unbalance and Misalignment”, Lilburn, Ga.: Fairmont Press; New York: Marcel Dekker, c2004.

[41] Robert C. Eisenmann, Sr., P.E., Robert C. Eisenmann, Jr., “Machinery Malfunction Diagnosis and correction: Vibration Analysis and Troubleshooting for the Process Industries”, Upper Saddle River, N.J. : Prentice Hall PTR, c1998.

[42] ISO 13373-1, Condition monitoring and diagnostics of machines - Vibration condition monitoring - Part 1: General procedures.

[43] ISO 13373-2, Condition monitoring and diagnostics of machines - Vibration condition monitoring - Part 2: Processing, analysis and presentation of vibration data

[44] Sedat Karabay, Ibrahim Uzman, “Importance of early detection of maintenance problems in rotating machines in management of plants: case studies drom wire and tyre plants”. Elsevier 2008.

[45] Boashash, B., Black, P. J., “An Efficient Real Time Implementation of the WingerVille Distribution”, IEEE Trans. on Acoustics, Speech, and Signal Processing, Vol. ASSP35, No.11, November 1987.

[46] Shin, Y. S., Jeon, J. J., “Wigner-Ville Time-Frequency Distribution and its Application to Machinery Condition Monitoring”, Journal of Shock and Vibration, Vol.1, Issue 1, 1993/1994.

[47] Nandi, S. and Toliyat, H. A., “Fault diagnosis of electrical machines- a review”, IEEE International Conference on Electric Machines and Drives, pp. 219-221, 1999.

[48] Ray s Beebe, “Predictive Maintenance of Pumps using Condition Monitoring”, Elsevier 2004.

[49] J.C. Sloan, T.M. Khoshgoftaar, P. Beaujean, F. Driscoll, “Ocean Turbines – a Reliability Assessment,” International Journal of Reliability, Quality and Safety Engineering, in press (2009).

[50] P. P. Beaujean, T. M. Khoshgoftaar, J. C. Sloan, N. Xiros, D. Vendittis, “Monitoring Ocean Turbines: a Reliability Assessment” , Proceedings of the 15th ISSAT International Conference on Reliability and Quality in Design, August 2009, San Francisco, California.

[51] N. I. Xiros, “Robust control of diesel ship propulsion”. Springer 2002.

[52] GE Energy. (www.bently.com)

[53] Brüel & Kjær Vibro (www.bkvibro.com)

[54] Sensicast Systems, Inc. (www.sensicast.com)

[55] DLI Engineering Corporation. (http://www.dliengineering.com)

[56] Motornostix. (www.motornostix.com)

[57] Center for intelligent maintenance systems. (www.imscenter.net)